WIND AND WAVES

Investigation of an optimization approach to parameter estimation

Promotoren :
Prof. J. BERLAMONT
Prof. E. SMETS

Proefschrift voorgedragen tot
het behalen van het doctoraat
in de toegepaste wetenschappen

door

Jaak MONBALIU

Mei 1992

KATHOLIEKE UNIVERSITEIT LEUVEN
FACULTEIT TOEGEPASTE WETENSCHAPPEN
DEPARTEMENT BURGERLIJKE BOUWKUNDE
LABORATORIUM voor HYDRAULICA
de Croylaan 2, B-3001 Leuven (Heverlee)

WIND AND WAVES

Investigation of an optimization
approach to parameter estimation

Jury :
Prof. J. Delrue, voorzitter
Prof. J. Berlamont, promotor
Prof. E. Smets, promotor
Prof. V. Ferdinande
Dr. G. Komen
Prof. M. Rijckaert
Prof. E. Van den Bulck

U.D.C. 551.466

Proefschrift voorgedragen tot
het behalen van het doctoraat
in de toegepaste wetenschappen

door

Jaak MONBALIU

Mei 1992

Dankwoord

Veel heb ik te danken aan prof. J. Berlamont. Niet alleen bood hij mij aan om assistent te worden voor het postgraduaat programma in Irrigation Engineering, hij kwam ook op het idee om mijn ervaring op het gebied van wind en windbelasting uit te breiden naar de interaktie met water. Vooral zijn grenzeloos vertrouwen, zelfs in moeilijke dagen, stel ik ten zeerste op prijs.

Prof. E. Smets moet ik bedanken voor het kritisch nalezen van het manuscript en voor de talrijke referenties die hij trouw op vrijdag heeft meegebracht.

Dank ook aan prof. E. Van den Bulck. Zijn suggesties bij het voorstellen van de resultaten van het optimaliseringsvraagstuk hebben de leesbaarheid van deze verhandeling aanmerkelijk verbeterd.

Vele anderen hebben heel wat bijgedragen tot de inhoud van deze verhandeling. Ik wil daarbij speciaal K. en S. Hasselmann van het Max-Planck Institut für Meteorologie in Hamburg (Duitsland) bedanken voor de programma's, voor het gastvrij onthaal tijdens mijn kort verblijf in Hamburg en voor de suggesties bij het tot stand komen van dit werk. Het enthoesiasme en de ideeën van Peter Janssen werken aanstekelijk. Dank om die over te dragen, en dank voor de bemerkingen vanuit Reading. Ook dank aan G. Komen, W. Rosenthal, G. van Vledder, S. Weber, R. Snyder, K. Kahma, M. Donelan en andere WAM-leden voor hun interesse in mijn werk en voor de discussies op de jaarlijkse WAM-meetings. Mijn gedachten zijn ook nooit ver weg van A.G. Davenport en zijn team. Zonder hen had ik nu wellicht heel wat minder hoog van de toren geblazen.

Dichter bij huis mag ik D. van den Eynde, I. Hermans en W. Luo niet vergeten. Hun onderzoek en bijdragen waren heel belangrijk, niet alleen voor dit werk, maar ook voor het verder uitbouwen van onderzoek en toepassingen in het domein van windgolven. Hierbij wil ik ook de medewerkers van de werkgroep 'Getij en Golven' van de Dienst der Kusthavens vernoemen.

De logistieke steun kwam uit verschillende hoeken. D. Verhetsel zorgde voor draagbaar computergebruik. Danny Uten verzorgde de layout van de tekst en heeft mij mee laten genieten van een mooi

ABSTRACT

The atmosphere sees the ocean, with sometimes huge waves, as a much smoother surface, compared to its passage over land where it is slowed down much more, even if obstacles are small compared to the size of ocean waves. A good observer notices right away that waves travel with the wind and consequently do not give much resistance. The details of how much resistance there actually is and its variation with wind speed and parameters defining the wave conditions has been a hot topic for the last 35 years. The correctness of the roughness formulation is a crucial question in the understanding of the air-sea interface. It has major implications in wave modelling, in storm surge modelling and also in modelling of the atmospheric boundary layer above the ocean. Researchers now agree that the roughness is not only a function of the wind speed, but also of the age of the waves. Young wind seas give more drag resistance than old wind seas. Mainly waves at frequencies beyond the peak frequency contribute to the roughness. We propose to use the Donelan constant, representative for the equilibrium range of a wind sea spectrum, as a direct measure for the nondimensionalized roughness of the sea surface.

To obtain a better view and understanding on the working of the source terms in a third generation wind wave model, a framework has been build for tuning unknown parameters in the formulation of the forces involved in wave generation and wave dissipation through whitecapping. In the framework a standard optimization routine from the widely available NAG-Fortran subroutine library is used to minimize a cost function. The cost function is defined as a weighted sum of squares to take advantage of the special structure of this formulation. Measured physical characteristics such as wave energy, and peak frequency of the waves are expressed in function of fetch through the JONSWAP or the Kahma and Calkoen growth curve laws. In the optimization exercise, we try to reproduce the fetch evolution of the total energy by tuning two elected parameters in the wind input and/or dissipation source terms. Such a framework is useful in increasing our understanding of individual source terms.

WIND EN GOLVEN

Onderzoek van een optimaliserings-benadering voor het schatten van parameters in de brontermen

SAMENVATTING

Inleiding

In de loop van de laatste dertig jaar is de modellering van windgolven sterk geëvolueerd. Eerste generatie modellen houden slechts met een gedeelte van de fysica rekening. Modellen van de tweede generatie schetsen de zeetoestand met behulp van een beperkt aantal parameters (maximaal 5 of 6). De zogenoemde derde generatie modellen implementeren de volledige fysica en leggen als zodanig bij het modelleren geen beperkingen meer op aan de uiteindelijke vorm van het spectrum van windgolven.

Het is nu mogelijk om, net als dat gebeurt voor het weer, voor een bepaald gebied voorspellingen te doen over de te verwachten golfhoogte, richting van de golven, enz... De vergelijking met het weer gaat zelfs verder op want voorspellingen op middellange termijn worden ook in Reading aan de European Centre for Medium Range Weather Forecast (ECMWF) uitgevoerd. Het model in Reading is een globaal model. Op een vrij grof berekeningsrooster, worden (vrij goede) voorspellingen gedaan op een globale schaal. Om echter ook lokaal goede voorspellingen te hebben, is het nodig om ook over een regionaal model te beschikken op een fijner berekeningsrooster. De verfijning is noodzakelijk om voldoende rekening te kunnen houden met de lokale kustgeometrie en de lokale bathymetrie. Ook voor de Belgische kust bestaat sinds november 1991 een operationeel fijnmazig model. Het is het HYPAS model, een model van de tweede generatie (Hermans, 1989). Dit

model is bovendien gekoppeld aan een refraktiemodule (Van den
Eynde en Monbaliu, 1989; Van den Eynde et al., 1990 a&b).

Het praktisch en ekonomisch belang van nauwkeurige voorspellingen
van het te verwachten golfklimaat, mag niet onderschat worden.
Het laat toe om de scheepvaart van en naar de Belgische havens
(Antwerpen, Zeebrugge) beter te begeleiden en vooral veiliger te
maken. Op wereldvlak heeft men de mogelijkheid om de vaarroutes
aan te passen. Gevaarlijke stormgebieden met alle risico's
vandien (slachtoffers, schipbreuk, schade aan het milieu, ...)
kunnen vermeden worden. Op brandstof en tijd wordt aanzienlijk
bespaard.

Om golven op te wekken is wind nodig. Om golven te voorspellen,
moet men dus eerst de voorspellingen van de wind kennen.
Wetenschappers die windgolven modelleren, steken maar al te graag
de schuld voor slechte golfvoorspellingen op gebrekkige
windvoorspellingen. Men moet toegeven dat ze zeker gedeeltelijk
gelijk hebben. Recentelijk houdt men ook rekening met het effect
van de golven op de wind. Daarbij valt vooral het werk van Peter
Janssen niet te ontkennen. Enkele maanden terug zijn zijn ideeën
aangaande de wisselwerking tussen wind en golven geïmplementeerd
in het WAM-model (het operationeel model in Reading).
Het derde generatie model WAM (WAve Model) is gegroeid uit de
internationale samenwerking van wetenschappers die belangstelling
hebben voor het modelleren van windgolven. De WAM-groep, die
jaarlijks een samenkomst organiseert voor haar leden, werd zo'n
tien jaar geleden opgericht met als doel een derde generatiemodel
te ontwikkelen en dit te implementeren op zowel regionale als
globale schaal. Daarenboven wilde ze ook een meer grondige kennis
van de fysica die de grondslag vormt voor de opwekking van
windgolven en zich klaar maken voor het gebruik van
satellietwaarnemingen door het ontwikkelen van data-assimilatie
technieken. Ze is wonderwel in haar opzet geslaagd, zeker wat
betreft de implementatie van het globale en van een aantal
regionale golfmodellen. De individuele brontermen (opwekking en
dissipatie) van energie vormen nu wellicht het meest ongekende

terrein in het modelleren van golven. Het is in die problematiek dat deze verhandeling zich situeert.

Doelstelling van de studie

Aan het begin van de studie werden twee doelstellingen vooropgesteld. Een eerste doelstelling was een beter inzicht te krijgen in de invloed van de golven op de atmosferische grenslaag. Het is fascinerend dat grote golven op de oceaan minder weerstand bieden aan de wind die erover heen blaast, dan voorwerpen die op het vasteland staan, zelfs al zijn die qua afmetingen klein vergeleken met de golven. Een goede waarnemer merkt direkt en terecht op dat dit komt omdat golven meelopen met de wind en daardoor die wind eigenlijk niet tegenhouden. En toch werd er de laatste 35 jaar heel veel over gepubliceerd en is men het nog altijd niet volledig eens hoe groot de weerstand van golven wel is en hoe die varieert met de "ouderdom" van de golven. Ouderdom wordt gedefinieerd als de fazesnelheid van de golf bij de frekwentie van de piek van het energiespectrum, gedeeld door een karakteristieke windsnelheid (wrijvingssnelheid of snelheid op 10 m hoogte). Er zal hier dan ook geprobeerd worden de belangrijke parameters naar voor te brengen. Een goede kennis van de ruwheid van het zeeoppervlak is belangrijk voor veel toepassingen zoals, naast de voorspelling van de golven zelf, de bepaling van stormopzet of van fluxen (verdamping, warmte-afgifte, ...) naar de atmosfeer.

Een tweede doelstelling was een kader op te bouwen om snel waarden toe te kennen aan parameters in de brontermen die kunnen gebruikt worden in derde generatie modellen. Daarbij wordt vooropgesteld dat bepaalde kenmerkende eigenschappen van het golfspectrum, zoals de totale energie of de frekwentie van de spectrale piek, zo goed mogelijk zouden gereproduceerd worden. Liefst zou daarbij gebruik gemaakt worden van standaard beschikbare optimaliseringsprogramma's. Dergelijk kader kan bovendien een handig hulpmiddel zijn om een beter inzicht te krijgen in het gedrag van individuele brontermen.

Beschrijving van het zeeoppervlak

Het wateroppervlak kan gezien worden als een superpositie van een groot aantal lineaire golven met verschillende amplitude. Deze superpositie wordt geschreven in de vorm van het verplaatsingsspectrum

$$\overline{\zeta^2} = \int_0^\infty E(\omega)d\omega = \int_0^\infty F(\overline{k})d\overline{k} \qquad [m^2] \qquad (1)$$

met $E(\omega)$:   frekwentiespectrum ; f is de frekwentie

       $F(\overline{k})$:   golfgetalspectrum waarbij $\overline{k}$ het golfgetal is (een vector)

Het spectrum van windgolven probeert onder invloed van de verschillende effecten die erop inwerken, zijn vorm te behouden (self-similarity) en kan daardoor beschreven worden met een beperkt aantal parameters. Meestal werkt men in het frekwentiedomein. Een aantal formuleringen zijn welgekend. Het JONSWAP spectrum (vgl. (2.14); Hasselmann et al. 1973), heeft een f^{-5}-staart. Het Pierson-Moskowitz (PM) spectrum (vgl. (2.16) ; Pierson en Moskowitz, 1964) is een bijzonder geval van het JONSWAP spectrum en beschrijft het zeeoppervlak bij volgroeide zeegang. Het Toba spectrum aangepast door Battjes (vgl. (2.18); Toba, 1973 en Battjes et al. 1987) en het Donelan spectrum (vgl. (2.19); Donelan, 1985) hebben een f^{-4}-staart. Het Toba spectrum wordt daarbij nog gekenmerkt door de wrijvingsnelheid u_* in de lucht, terwijl het Donelan spectrum de frekwentie van de piek van het energiespectrum gebruikt. Het valt daarbij op dat voor jonge windgolven, de bovenvermelde spectra heel goed op elkaar gelijken. Voor volgroeide zeegang daarentegen, gelijken enkel het Donelan spectrum en een aangepast Toba spectrum op een PM-spectrum (zie Figuren 2.a tot 2.d).

De evolutie van het golfoppervlak onder invloed van wind

Om vat te krijgen op de evolutie van het spectrum van windgolven onder invloed van wind, is op het eind van de jaren zestig een grote meetcampagne opgezet vóór de kust van het eiland Sylt (grens Duitsland en Denemarken). Dit resulteerde in 1973 tot het JONSWAP rapport (Hasselmann et al., 1973). Belangrijk in dit rapport was de formulering van het JONSWAP spectrum, samen met de uitwerking van de groeicurven voor de parameters die dit spectrum beschreven (vgln. (2.41)). Deze groeicurven werden dimensieloos gemaakt met behulp van de gemeten windsnelheid op 10 meter hoogte. Ook anderen hebben experimenten gedaan om de evolutie van het spectrum te bekijken, o.a. Kahma (1981) in de Botnische Golf, en Donelan (1985) in het Ontariomeer. Kahma en Calkoen (1991) vonden het merkwaardig dat de groeicurven voor de energie tussen de verschillende experimenten vrij grote verschillen vertoonden. Daarom brachten ze de data van bovenvernoemde experimenten bijeen en heranalyseerden deze. Dit resulteerde in nieuwe groeicurven. Daarbij werd ook getracht ze dimensieloos te maken door middel van de wrijvingssnelheid (vgln. (2.49)). De wrijvingssnelheid werd bepaald uit metingen van de snelheid op 10 m hoogte, aan de hand van de Wu relatie (Wu (1982); vgl. (2.33)). Ideaal zou hun analyse nog eens moeten worden overgedaan met niet alleen een windsnelheidsafhankelijke maar ook een golfouderdomsafhankelijke omzetting van u_{10} naar u_*. Het is eigenlijk nog altijd niet duidelijk welke karakteristieke snelheid moet genomen worden om gemeten golfgrootheden dimensieloos te maken. Wel is duidelijk dat het ofwel de windsnelheid buiten de grenslaag moet zijn (u_∞), ofwel de wrijvingsnelheid die een maat is voor de schuifspanning op het wateroppervlak. Er is intuïtief een voorkeur voor de wrijvingssnelheid u_*. Harde bewijzen daarvoor bestaan echter niet (Janssen et al. 1987).

Beschrijving van de atmosferische grenslaag

Het snelheidsprofiel in de atmosferische grenslaag boven het zeeoppervlak, kan beschreven worden met een logaritmisch profiel (vgl. (2.28) ; Panofsky and Dutton, 1984). Kenmerkend voor een logaritmisch profiel zijn de wrijvingsnelheid u_*, die een maat is voor de schuifspanning die de lucht uitoefent op het wateroppervlak, en de ruwheidslengte z_0, die weergeeft hoeveel weerstand het oppervlak biedt aan die schuifspanning.

In de loop der jaren zijn er verschillende ideeën voor de ruwheidslengte van het wateroppervlak voorgesteld. Charnock stelde in 1955 dat de ruwheidslengte enkel afhankelijk was van de wrijvingsnelheid en bekwam met behulp van dimensie-analyse :

$$z_o = \alpha_{Ch} \frac{u_*^2}{g} \tag{2}$$

Verscheidene onderzoekers (Wu, Garratt, ...) hebben die idee bevestigd en dan ook waarden toegekend aan de Charnock-constante α_{Ch}. Benaderend kan de vergelijking (2) ook geschreven worden als een lineaire functie van de snelheid op 10 m hoogte. In Tabel 2.2 kan men een aantal van die uitdrukkingen terugvinden.

Geleidelijk aan is men echter tot het besef gekomen dat ook de ouderdom van de golven een belangrijke rol speelt in de bepaling van de ruwheidslengte z_0. Jonge golven voelen namelijk veel ruwer aan en geven dan ook een grotere ruwheidslengte, dan golven die ouder zijn. Dit komt natuurlijk omdat bij oudere golven, de voornaamste golven en het voornaamste deel van de energie in het zeeoppervlak getransporteerd worden met een snelheid die ongeveer even groot is als de windsnelheid. Een aantal onderzoekers stelde dan ook dat de ruwheidslengte als volgt kan bepaald worden (vergelijking (2.39) :

$$z_o^* = \mu \left(\frac{c_p}{u_*}\right)^n \tag{3}$$

Maat et al. (1991) geven waarden van 0.7 aan μ en -1 aan n.

Hsu's formule (vgl. (2.36); Hsu (1974)) kan omgerekend worden en men bekomt een waarde van 0.14 voor μ en van -0.5 voor n (vgl. (2.58)).

Is er een verband tussen het spectrum van de golven en de atmosferische grenslaag erboven ?

Intuïtief voelt men aan dat er een verband moet bestaan tussen de parameters die de geometrische samenstelling van het wateroppervlak beschrijven en diegenen die de ruwheid samenvatten die de lucht ondervindt. De weerstand die de lucht ondervindt, is vooral te wijten aan golven die zich aanzienlijk trager voortplanten dan de windsnelheid, met name die golven met een frekwentie hoger dan de piekfrekwentie. Deze golven bevinden zich in een soort evenwichtstoestand die zich laat vertalen in de zogenaamde Phillips-constante α_P in het JONSWAP-spectrum, een Donelan-constante α_D in het Donelan-spectrum en een Toba-constante α_D in het Toba-spectrum. Het valt daarbij op dat wanneer men het Toba-spectrum gelijkstelt aan het Donelan-spectrum in het hoogfrekwente gedeelte, men een afhankelijkheid krijgt van de Donelan-constante α_D, die identiek is aan wat Maat et al. (1991) vonden voor de afhankelijkheid van de ruwheidslengte met betrekking tot de ouderdom der golven. Men zou daaruit kunnen besluiten dat de Donelan-constante α_D rechtstreeks de ruwheid weergeeft van het zeeoppervlak (vgl. (2.55)):

$$C^{u} \; \alpha_D = z_o^*$$ (4)

Deze stelling werd getoetst aan een beperkt aantal meetgegevens van het HEXMAX experiment (Katsaros et al. 1987; Smith et al. 1990). Deze data werden bereidwillig ter beschikking gesteld door het HEXOS-team. In de Figuren 2.6, 2.7 en 2.8 kunnen deze data teruggevonden worden. De stelling dat de Donelan-constante een rechtstreekse maat is voor de ruwheidslengte, kan via deze metingen niet weerlegd worden. Het past de metingen zelfs goed. De spreiding op de meetresultaten is echter vrij groot. Dit is

niet het gevolg van de kwaliteit van de metingen zelf, maar van de afleidingen die gebeuren met deze metingen. Zo wordt bijvoorbeeld de ruwheidslengte z_0 niet rechtstreeks gemeten, maar bepaald aan de hand van een logaritmisch snelheidsprofiel waar de gemeten waarden voor de snelheid op 10 m hoogte en voor de wrijvingssnelheid ingevuld worden (vgl. (2.56)). Daar men te maken heeft met een exponentiële functie, wordt een relatief kleine meetfout van bijvoorbeeld 10 % op de wrijvingssnelheid, uiteindelijk een grote afwijking op de ruwheidslengte z_0 (een factor 2 tot 3).

De energietransportvergelijking voor graviteitsgolven

De energie die men terugvindt in de golven van de zee zijn het gevolg van de verschillende processen die erop inwerken. In deze studie zijn we enkel geïnteresseerd in golven opgewekt door wind en er zal dan ook aangenomen worden dat de kracht van de wind de enige bron van energie is. Energie kan verloren gaan door breking van de golven (branding en schuimkopjes), en door middel van wrijving op de bodem.

Door de aanname dat het wateroppervlak bestaat uit de superpositie van een groot aantal lineaire (=sinusoïdale) golven, worden hogere orde termen verwaarloosd. Hasselmann (1962, 1963a en 1963b) heeft theoretisch aangetoond dat een aantal combinaties van golven, energie onderling kan uitwisselen. Deze niet lineaire wisselwerking, ook wel resonante wisselwerking genoemd, tussen golven heeft geen energieverlies noch energiewinst tot gevolg.

Bovenvermelde processen, met name, de inwerking van de wind, het verlies van golfenergie door breking of door bodemwrijving en de niet lineaire wisselwerking tussen verschillende golfcomponenten vormen de basis voor de huidige kennis aangaande de energiebalans van golven opgewekt door wind.

In diep water, waar de waterdiepte voldoende groot is zodat de bodemwrijving en andere diepte-effecten zoals refractie kunnen verwaarloosd worden, wordt de energietransportvergelijking in de x-richting gegeven door (vergelijking (3.2)) :

$$\frac{\partial E}{\partial t} + c_{gx} \frac{\partial E}{\partial x} = S_{tot} = S_{nl} + S_{in} + S_{diss} \tag{5}$$

In woorden betekent dit dat wat in de tijd gewonnen wordt aan energie, en dit per eenheid van oppervlakte en per eenheid van gewicht, gelijk is aan wat erin gebracht wordt door de wind (S_{in}), wat verloren gaat door breking (S_{diss}) en wat uitgewisseld wordt door de resonante wisselwerking (S_{nl}), verminderd met de energiehoeveelheid die weggevoerd wordt aan een snelheid die gelijk is aan de groepsnelheid (c_{gx}).

Men kan ook een impulsbalans opstellen. Maximaal kan de winst aan impuls of momentum gelijk zijn aan de schuifspanning veroorzaakt door de wind. Merk op dat momentum hier uitgedrukt wordt per eenheid van oppervlakte en per eenheid van tijd. Hasselmann et al. (1973), toonden aan dat ongeveer 5 % van die schuifspanning uiteindelijk door advectie weggevoerd wordt (vergelijking (3.4)).

De brontermen

Het effect van de wind op de golven en het daarmee gepaard gaande groeiproces worden voornamelijk door twee mechanismen verklaard. Een eerste mechanimse is het Phillips-mechanisme (Phillips (1957)). De wind wordt voorgesteld als bestaande uit wervels, die worden meegevoerd. Kleine wervels worden dicht bij het wateroppervlak meegevoerd met een kleine snelheid. Hoe groter de wervels, hoe hoger die zich in de atmosferische grenslaag bevinden en hoe sneller die worden getransporteerd (zie Figuur (3.1.a)). De wervels creëren een drukverdeling op het wateroppervlak. De golflengten van deze drukverdeling kunnen samen vallen met de golflengten van het wateroppervlak. Men krijgt dan een soort resonantie-effekt. Als deze drukschommelingen nu zouden voortbewegen star verbonden aan het wateroppervlak, zou men een voortdurende toevoer van energie krijgen en een exponentiële groei van de golven. Dit is niet het geval en uiteindelijk krijgt men slechts een lineaire groei van de golfenergie in functie van de tijd. Het Phillips-mechanisme is het voornaamste proces voor de initiële groei van windgolven.

Een tweede mechanisme is het zogenoemde Miles-mechanisme. Doordat er een gradient is van de snelheid ('shear flow') in de atmosferische grenslaag, krijgt men op de loefzijde van het golfoppervlak een verhoogde druk (stroomlijnen dichter bij elkaar) en op de lijzijde een verminderde druk (stroomlijnen verder uit elkaar), zie Figuur (3.1.b). De golven groeien en worden steiler. Doordat de golven steiler worden, wordt het mechanisme versterkt, zodat er sprake is van een instabiliteit. Wiskundig formuleert zich dat in een exponentiële groei. Meestal wordt enkel het Miles-mechanisme weerhouden in wiskundige modellen, zodat de wind toevoer kan geschreven worden als (vergelijking (3.12)) :

$$S_{in} = \frac{\partial E(f,\theta)}{\partial t} = b\ E(f,\theta) = \mu\omega\ E(f,\theta) \tag{6}$$

Een aantal formuleringen voor de koppelingscoëfficiënt μ zijn in de literatuur gegeven. Men kan ze onderverdelen in twee categorieën, met name diegenen die lineair zijn in een karakteristieke snelheid (aangeduid als het Snyder type naar de metingen van Snyder et al. (1981)) en diegene die kwadratisch zijn, aangeduid als het Stewart type (Stewart (1974)).

- type 1 (het Snyder type; vergelijking (3.24)) :

$$S_{in}(f,\theta) = 0.25\ a_1 \frac{\rho_a}{\rho_w}(a_2 \frac{28u_*}{c}\cos\theta - 1)\ \omega\ E(f,\theta) \tag{7}$$

- type 2 (het Stewart type; vergelijking (3.25)) :

$$S_{in}(f,\theta) = 0.04\ \frac{\rho_a}{\rho_w}\ a_3[(a_4\frac{28u_*}{c})^2 - a_5(a_4\frac{28u_*}{c})]\ \cos\theta\ \omega\ E(f,\theta) \tag{8}$$

De coëfficiënten a_1 tot en met a_4 hebben in de literatuur een waarde 1, maar zullen hier als parameters beschouwd worden. De parameter a_5 heeft in deze studie altijd een waarde 1. Dit is een keuze om de werking van de wind teniet te doen wanneer de golven zich voortplanten met een snelheid gelijk aan de windsnelheid. Merk ook op dat hier gekozen werd voor de wrijvingssnelheid als karakteristieke snelheid; dit is in overeenstemming met het idee

xiii

dat de wrijvingssnelheid de drijvende kracht is op het wateroppervlak (Komen et al., 1984 ; Janssen et al., 1987). Alhoewel de koppeling tussen een atmosferisch model en een model voor zeegolvenvoortplanting buiten het bestek van deze studie valt, moet de quasi-lineaire theorie van Janssen (1982; 1989; 1991) voor de opwekking van golven zeker vermeld worden. Zijn theorie geeft aan in welke mate de input van de wind gevoelig is aan de ouderdom van de golven.

Voor de dissipatie van golfenergie door breking zijn de ideeën van Hasselmann (1974) overgenomen. Dit resulteert in een bronterm die evenredig is met het energiespectrum en evenredig met het kwadraat van de frekwentie (vgl. (3.26)). De evenredigheidsfactor hangt enkel af van het golfgetal en geïntegreerde spectrale groothheden zoals de gemiddelde steilheid van de golven. Komen et al. (1984) werkten deze bronterm in meer detail uit (vgl. (3.27)) :

$$S_{diss}(f,\theta) = -c_1 \, \bar{\omega} \, (\frac{\omega}{\bar{\omega}})^n (\frac{\hat{\alpha}}{\hat{\alpha}_{PM}})^m \, E(f,\theta) \tag{9}$$

De coëfficiënt c_1 beinvloedt het algemeen niveau van de demping, de coëfficiënt n verschuift de demping t.o.v. de piek van het spectrum en de coëfficiënt m geeft de afhankelijkheid van de demping t.o.v. de steilheid van de golven weer. De coëfficiënten c_1, m en n werden in deze studie als parameters beschouwd. Na de studie van Komen et al. (1984), kregen ze waarden van respectievelijk $3.33 \, 10^{-5}$, 2 en 2.

Tenslotte is er nog de resonante wisselwerking van de golven. De theorie werd uitgewerkt door Hasselmann (1962, 1963a en 1963b). Stellen van vier golven kunnen onder bepaalde voorwaarden energie uitwisselen. Deze resonantievoorwaarden zijn gegeven in vergelijking (3.28). De hoeveelheid energie die uitgewisseld wordt, is gegeven in vergelijking (3.29). Het is een vrij ingewikkelde integraal, die ook veel rekentijd vraagt om opgelost te worden. Daarom zal ook het 'discrete interaction approximation' algoritme van Hasselmann et al.(1985) gebruikt worden om de rekentijd te beperken.

Het rekenprogramma ONEDMOD

Met het rekenprogramma ONEDMOD, ontwikkeld door S. Hasselmann van de Max-Planck Institut für Meteorologie in Hamburg (Duitsland), wordt de energietransportvergelijking in diep water opgelost. De oplossing gebeurt ofwel in het tijdsdomein (duration limited) ofwel in de ruimte (fetch limited). Het model inkorporeert alle fysica die normaal aanwezig is in modellen van de derde generatie. De beperking in tijd of ruimte laat echter toe om met relatief geringe rekentijden, het effekt van de verschillende brontermen te bestuderen.

Het rekenschema is een eerste orde schema met eindige differenties met aanpasbare integratiestap. Wanneer de energiegroei in een iteratiestap een bepaalde limiet overschrijdt, wordt de integratiestap gehalveerd.

Het integratiegebied wordt beperkt in het frekwentiedomein tot 2.5 maal de piekfrekwentie. Het energieniveau van het spectrum bij frekwenties die hoger liggen, wordt bepaald door een f^{-5}-staart te bevestigen aan de hoogst berekende frekwentie.

Omdat in de brontermen van de energietoevoer door wind, enkel de exponentiële term werd beschouwd, is een zeker energieniveau noodzakelijk om het programma te kunnen laten lopen. Dit gebeurt door een initieel spectrum op te geven. Dit spectrum wordt gegenereerd door het programma FRSPEC (Van Vledder en Weber, 1988).

De wrijvingssnelheid, een maat voor de schuifspanning uitgeoefend op het wateroppervlak, wordt gebruikt als drijvende kracht. Wanneer men echter het programma laat lopen met verschillende wrijvingssnelheden, dan bekomt men niet dezelfde dimensieloze resultaten. Dit wordt geïllustreerd in de Figuren 4.6, 4.7 en 4.8.

De evolutie van het spectrum, samen met de evolutie van de brontermen wordt geïllustreerd in de Figuren 4.9 tot en met 4.12. Voor jonge en groeiende golven, ziet men dat er energie input bij en overdracht naar frekwenties lager dan de piekfrekwentie is. Daardoor schuift de piekfrekwentie naar lagere frekwenties. Bij volgroeide zeegang daarentegen is er geen netto energietoevoer.

De overdracht van energie door de resonante wisselwerkingen en
de toevoer van de wind, worden tenietgedaan door de breking van
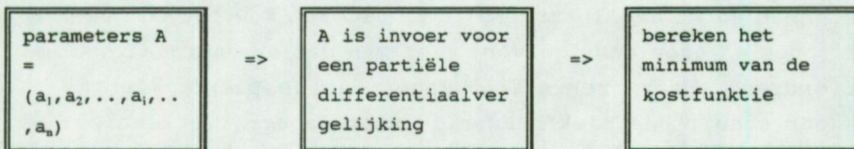de golven.
Het programma ONEDMOD is ook uitgebreid om naar de balans van het
momentum te kijken. Daarbij valt vooral op dat er bij evenwicht
zowat 20 % meer momentum input is dan er gedissipeerd wordt. De
verklaring daarvoor ligt in de sterke numerieke dissipatie van
het gebruikte schema met eindige differenties (Dijkhuis, 1990)
en mogelijks in de opgelegde staart bij de hogere frekwenties
(Janssen, 1992 ; persoonlijke mededeling).

De optimaliseringsbenadering

Het criterium om waarden toe te kennen aan bepaalde parameters
in de brontermen (vgln. (7), (8) en (9)), bestaat erin dat het
verschil tussen gemeten waarden en waarden die men kan vinden
door berekeningen zo klein mogelijk moet zijn. Daarbij werd er
vanuit gegaan dat een gewogen kleinste kwadraten benadering, een
goede keuze is. Daarom wordt de volgende kostfunktie voorgesteld
(vgl. (5.1)):

$$
SUMSQ = \frac{1}{W} \sum_{i=1}^{N} [w_{1,i}(\frac{E_{i,cal}^* - E_{i,meas}^*}{E_{i,meas}^*})^2
$$

$$
+ w_{2,i}(\frac{f_{p\ i,cal}^* - f_{p\ i,meas}^*}{f_{p\ i,meas}^*})^2 + w_{3,i}(\frac{\alpha_{i,cal} - \alpha_{i,meas}}{\alpha_{i,meas}})^2]
$$

(10)

Voor de gemeten (measured) waarden, zullen de gemeten groeicurven
genomen worden (zie verder). De berekende (calculated) waarden
zijn de resultaten van het oplossen van de energietransport-
vergelijking (vgl. (5)). Het probleem kan dan ook als volgt
samengevat worden :

parameters A = $(a_1, a_2, .., a_i, ..$ $, a_n)$	=>	A is invoer voor een partiële differentiaalver gelijking	=>	bereken het minimum van de kostfunktie

Om een idee te krijgen van het gedrag van de kostfunktie, is een aantal gevoeligheidstests uitgevoerd waarbij slechts één parameter varieert. De kostfunktie werd gedefinieerd in het groeiende gedeelte van de JONSWAP groeicurve (zie Hoofdstuk 6). Voor de wind input werd het Snyder-type gekozen (vgl. (7) met $a_1 = 1$ en $a_2 = 1$). De dissipatieterm is gegeven in vgl. (9) ($c_1 = 3.33 \cdot 10^{-5}$; m $=2$; n $= 2$). De parameters nemen de hier opgegeven waarden aan, uitgenomen de parameter die varieert. De resultaten van deze tests werden samengebracht in de Figuren 5.1 tot en met 5.21. Daarbij vallen volgende bevindingen op. De kostfunktie waarin enkel de verschillen in de energiehoeveelheden in het spectrum meetellen, is het meest gevoelig. De hoger tussen haakjes opgegeven waarden voor de bronterm parameters (de waarden vooropgesteld door Komen et al. (1984)), zijn zowat optimaal voor elke parameter afzonderlijk. De minimale waarden voor een kostfunktie gedefinieerd om de totale energie van het golfspectrum te verkrijgen, liggen bij andere parameterwaarden dan voor een kostfunktie om enkel de piekfrekwentie of de Phillips-constante α_p optimaal te benaderen. De kostfunktie is ongevoelig voor veranderingen in de parameter n van de dissipatieterm. Grotere waarden (> 2.5) van de parameter n, leveren echter aanzienlijke problemen op voor het berekenen van de Phillips-constante. De kostfunktie is ook niet erg gevoelig aan veranderingen in de dissipatie-parameter c_1, zeker niet in de buurt van zijn optimale waarde. Bij dat alles valt nog op, dat de verandering van de groeicurven door de verandering in de waarde van om het even welke parameter, qua vorm ongeveer dezelfde blijft. Een bijkomende moeilijkheid is het feit dat kleine verschillen in een welbepaalde parameter leiden tot willekeurige schommelingen (grootte-orde 10^{-3}) in de kostfunktie (zie Figuur 5.21). Dit is enerzijds te wijten aan het numeriek schema (aanpasbare integratiestap, staart voor de hoge frekwenties,...) en anderzijds aan het discrete domein van richtingen en frekwenties waarin gewerkt wordt.

Beschikbare routines

Op de IBM-3090 van het rekencentrum van de K.U.Leuven, is de mathematische subroutine bibliotheek NAG beschikbaar. Naast vele andere routines, is er ook een aantal beschikbaar die een optimalisering via een kleinste kwadraten benadering aanpakken. Schematisch kan men via het diagramma in Figuur 5.22 beslissen welke routines daarvoor in aanmerking komen. Uiteindelijk hebben we gekozen voor de routine E04FCF, omdat deze routine een aantal opties had om het optimaliseringsproces van dichtbij te volgen. De routine E04FCF is gebaseerd op de Gill-Murray methode (zie Gill en Murray (1976), Gill et al. (1981), en Scales (1985)). Deze methode maakt gebruik van het feit dat bij een kleinste kwadraten methode de Hessiaan, de matrix met partiële afgeleiden van de tweede orde, kan benaderd worden met een uitdrukking in de Jacobiaan die enkel partiële afgeleiden van de eerste orde nodig heeft. Dit heeft een aanzienlijk rekenvoordeel tot gevolg.

Gebruik van het optimaliseringsprogramma

Bij het gebruik van de opgestelde optimaliseringsprogramma's zijn volgende zaken belangrijk :

1) het gebruik van schaalfaktoren voor de te optimaliseren parameters
2) het gebruik van aanpasbare parameters in de NAG-subroutine bibliotheek
3) het interpreteren van de NAG convergentiecriteria

Het gebruik van schaalfaktoren voor de parameters is noodzakelijk omdat de eerste partiële afgeleiden numeriek moeten benaderd worden via de NAG-subroutine E04FCF. Deze afgeleiden worden via een voorwaartse stap berekend. Die stap is een absolute stap van de grootte-orde 10^{-8} op de IBM-3090. Hoger is reeds vermeld dat kleine veranderingen in de parameters aanleiding geven tot schommelingen in de kostfunktie. Daarom moet men er zeker van zijn dat de absolute stap voor het berekenen van de afgeleiden,

een betekenisvol verschil geeft in de waarde van de kostfunktie. In de praktijk komt het erop neer dat die absolute stap enkele tot zelfs twintig procent bedraagt t.o.v. de parameterwaarde. Het gebruik van de door NAG-bijgeleverde parameters, kunnen wij uit ervaring als volgt samenvatten. De parameter ETA, die aangeeft hoeveel moeite men zich wil getroosten om het minimum in de huidige zoekrichting te bepalen, moet een tamelijk grote waarde (= weinig moeite) toegemeten krijgen. Daardoor wordt bij voorkeur de zoekrichting opnieuw berekend. Het maximaal aantal keren (MAXCAL) dat de kostfunktie mag berekend worden, wordt best aan de lage kant gezet (20 tot 50 maal het aantal optimaliseringsparameters). Dit vermijdt rekentijdverspilling. De NAG-routines hebben hun eigen convergentiecriteria (zie Figuur(5.27)). Met een oordeelkundig gebruik van de NAG-tolerantieparameter XTOL en een goede keuze voor de schaalfaktor van de kostfunktie, kan aan deze criteria voldaan worden. Het is ook mogelijk om zelf een convergentiecriterium in te bouwen en het programma via de foutmelder IFAIL stop te zetten. Aangewezen keuzes voor de schaalfaktoren en voor de NAG-parameters, kunnen in Figuur 5.28 gevonden worden. Daarbij moeten wij nog vermelden dat het soms gebeurt dat er geen convergentie optreedt, omdat het optimaliseringsprogramma niet in staat is bij een nieuwe zoekrichting, de minimale kostfunktie uit de vorige iteratie te verbeteren. Het optimaliseringsprogramma interpreteert dit als een discontinuïteit en wil daaroverheen springen. Door onze keuze van schaalfaktoren wordt die sprong, relatief gezien, veel te groot (= veel groter dan onze parameterwaarden). Meestal zijn dan echter de gevonden waarden voor de parameters en de gevonden waarde voor de kostfunktie in de vorige iteratie, goede resultaten.

Numerieke experimenten

Voor de numerieke experimenten werden als brontermen met mogelijks variabele parameters, de windtoevoer formulering van

het Snyder type (vgl. (7)) en van het Stewart type (vgl. (8))
weerhouden, samen met de dissipatie-formulering volgens Komen et
al. (1984), zie vgl. (9). De variabele parameters zijn a_1 tot en
met a_4 voor de wind-brontermen, en c_1 en m voor de
dissipatie-bronterm. De parameter n in de dissipatie-bronterm,
werd buiten beschouwing gelaten wegens de ongevoeligheid van de
kostfunktie voor een variatie in die parameter (zie hoger).
Als 'correcte' groeicurven zijn de JONSWAP en de Kahma en Calkoen
curven gekozen, beide dimensieloos gemaakt met de
wrijvingssnelheid u_*.

Ze worden gegeven door :
- JONSWAP (vgl. (6.4) of (2.43)) :

$$E_* = 1.6 \ 10^{-4} \ x_*$$
$$f_p^* = 1.082 \ x_*^{-.33}$$
$$\alpha_p = 0.35 \ x_*^{-.22}$$

(11)

$$E_* = \frac{Eg^2}{u_*^4} \qquad f_p^* = \frac{f_p u_*}{g} \qquad x_* = \frac{xg}{u_*^2}$$

- Kahma en Calkoen (vgl. (6.5) of (2.50)) :

$$E_* = 2.4 \ 10^{-3} \ x_*^{0.78}$$
$$f_p^* = 0.358 \ x_*^{-0.244}$$

(12)

In al de numerieke experimenten zal enkel getracht worden de
groeicurve voor de energie te benaderen. De kostfunktie waarbij
enkel rekening gehouden wordt met de energiewaarden, is namelijk
het meest gevoelig (zie hoger). Daarenboven worden slechts twee
parameters tegelijkertijd aan het optimaliseringsproces
onderworpen. De mogelijke kombinaties die werden bekeken zijn de
volgende :
1) één van de wind-bronterm parameters (a_1, a_2, a_3 of a_4)
   gekombineerd met de parameter die het algemeen niveau van de
   dissipatie weergeeft (c_1),
2) de parameter die het algemeen niveau van de dissipatie
   weergeeft (c_1), gekombineerd met de parameter die de
   afhankelijkheid van de steilheid van de golven weergeeft (m).

xx

Daarenboven zal nog een onderscheid gemaakt worden naargelang het gedeelte van de groeicurve die we wensen optimaal te reproduceren. Een eerste mogelijkheid is dat enkel het gedeelte van de groeicurve waarin de zeegolven nog groeien belangrijk geacht wordt. Volgens de JONSWAP groeicurven is dit gebied bij benadering te situeren in het dimensieloze strijklengte (fetch) tussen 10^5 en 10^7. Een tweede mogelijkheid bestaat erin zowel het groeiend gedeelte als volgroeide zeegang optimaal weer te geven. Voor volgroeide zeegang stellen Komen et al. (1984) volgende eigenschappen voor (de notatie PM slaat op het feit dat deze waarden gebaseerd zijn op de metingen van Pierson en Moskowitz (1964)) :

$x_*^{PM} = 1.2 \ 10^8$; $E_{PM}^* = 1.1 \ 10^3$; $f_{PM}^* = 5.6 \ 10^{-3}$; $\alpha_p^{PM} = 0.0081$

Tussen het groeiend gedeelte en volgroeide zeegang, bevindt zich een overgangsgebied. In de numerieke experimenten, is dit vertaald door aan het overgangsgebied geen gewicht toe te kennen. De strijklengtewaarden die gekozen werden om metingen en berekeningen te vergelijken kunnen teruggevonden in Tabel 6.1.

In de Tabellen 6.2 tot en met 6.5, werden de numerieke experimenten samengevat. Voor een aantal van de parameterwaarden die met het optimaliseringsprogramma bekomen werden, zijn de groeicurven getekend. Ook werd voor sommige van de oplossingen gekeken, hoe de kostfunktie varieert rond de voorgestelde parameterwaarden. Uit dit alles kan men de volgende bemerkingen maken en ook een aantal conclusies trekken.

Een eerste en belangrijke conclusie is het feit dat het voorgestelde optimaliseringsschema inderdaad in staat is om de kostfunktie gevoelig te doen verminderen. Daarbij worden voor de brontermen parameterwaarden gesuggereerd, die groeicurven genereren die nauw aansluiten bij wat vooropgesteld werd.

Wanneer men enkel groeiende zeegang wil simuleren met een ééndimensionaal golvenmodel, dan kan dat leiden tot negatieve waarden voor de dissipatie-parameter c_1. Dit is zeker niet realistisch. Komen et al. (1984), toonden al aan dat een zeker algemeen niveau van dissipatie nodig is om bij volledig ontwikkelde zeegang sterk gereduceerde groei te hebben.

Als we ook de reproduktie van volgroeide zeegang belangrijk
vinden, dan zijn de waarden van de parameters die gevonden worden
via het optimaliseringsprogramma voor de kombinatie JONSWAP
groeicurve en Snyder type wind-bronterm, nagenoeg dezelfde als
diegene die door Komen et al. (1984) werden gekozen op basis van
het gedrag voor volgroeide zeegang. Enkel de kombinatie van de
wind bronterm parameter a_2 en de dissipatie parameter c_1, gaf
uiteenlopende resultaten voor de parameters al naargelang de
startwaarde van die parameters. De gevonden kostfunktie was
daarbij vrijwel identiek (zie Tabel 6.2; runs 5a,5b en 5c).
Daarbij valt vooral op dat de kostfunktie bijna ongevoelig is
voor veranderingen in de dissipatieparameter c_1. In feite geeft
de parameter a_2 in zekere mate ons gebrek aan kennis weer
aangaande de preciese overgang naar volgroeide zeegang. Omdat dit
asymptotisch gebeurt, vertaalt zich dat in een zekere
ongevoeligheid. Verschuiving van dit gebeuren naar hogere
ouderdom van de golven (grotere a_2), gaat gepaard met een
verhoging van het dissipatieniveau c_1. Dit fenomeen doet zich ook
voor wanneer wij proberen de Kahma en Calkoen groeicurven te
reproduceren met deze brontermen (zie Tabel 6.4; runs 5a en 5b).
Zowel de JONSWAP als de Kahma en Calkoen groeicurven, konden
minder goed gereproduceerd worden met het Stewart type als wind
bronterm. We mogen daaruit echter niet direkt besluiten dat het
windtype volgens Stewart fysisch minder goed is dan het windtype
volgens Snyder. Mogelijks is het gekoppelde Stewart type, zoals
beschreven door Janssen (1991; vgl. (3.21)), wel heel goed.
Met het Snyder type wind-bronterm, konden de Kahma en Calkoen
groeicurven, bijna perfekt gegenereerd worden met het gebruikte
golvenmodel. We mogen nogmaals daaruit niet besluiten dat de
Kahma en Calkoen groeicurven beter zijn. Maar als inderdaad
blijkt uit verder onderzoek (zie bemerking hoger over de
golfouderdomsafhankelijke omzetting van u_{10} naar u_*) dat de
energiegroeicurve gevoelig minder stijgt dan lineair met de
strijklengte, gebruiken wij beter andere waarden (dan door Komen
et al.(1984) gepubliceerd) voor de parameters in de brontermen.

Suggesties voor verder onderzoek en praktische toepassingen

De stelling dat de Donelan-constante evenredig is met de dimensieloze ruwheidslengte van het golfoppervlak, moet aan een uitgebreid stel meetgegevens getoetst worden. Eenmaal de HEXMAX-data volledig verwerkt zijn door het HEXOS-team, kan dit gebeuren. Als de bevindingen positief zijn, moet ook uitgekeken worden naar laboratorium metingen en nagegaan worden in hoeverre deze stelling toepasbaar blijft.

De uitbreiding van dit onderzoekswerk naar ondiep water, ligt voor de hand. Het opgezette optimaliseringsschema kan een goed kader zijn om een aantal gangbare brontermen voor bodemdissipatie te evalueren.

De koppeling van een atmosferisch model met een zeegolvenmodel is niet alleen mogelijk, maar bovendien veelbelovend in verband met de verbetering van onze kennis op het gebied van de interaktie tussen lucht en water. Deze kennis is van cruciaal belang om tot nauwkeurige voorspellingen te komen wat betreft uitwisseling van momentum tussen lucht en water, fluxen aan het wateroppervlak (zoals verdamping,...). Deze verhoogde kennis zal ongetwijfeld bijdragen tot verbeterde klimaatmodellen.

Als directe toepassing, moeten we voor de Belgische kust, zeker de implementatie van een regionaal golvenmodel van de derde generatie aanbevelen. Aangezien modellen van de derde generatie het geheel van de fysische bijdragen van het fenomeen windgolven modelleren, zonder 'a priori' een bepaalde vorm voor het spectrum op te leggen, zullen wij binnen afzienbare tijd in staat zijn meer betrouwbare golfvoorspellingen te doen dan wat met het huidige model van de tweede generatie kan bekomen worden. Dit zal zeker het geval zijn met de koppeling tussen een atmosferisch en een zeegolvenmodel, waardoor men nog beter voorspelde windvelden verkrijgt. De ervaring die nu met het huidige tweede generatiemodel voor onze Belgische kust opgedaan wordt, zal van grote waarde zijn. Men zal precies weten waar en in welke omstandigheden, dit model tekort schiet. Bij de implementatie en

kalibratie van een model van de derde generatie, kan daaraan dan extra aandacht besteed worden.

Daarbij zou ook nog moeten gewerkt worden aan de koppeling tussen het golfvoorspellingsmodel en een hydrodynamisch model. De wisselwerking tussen waterdiepte en golfgedrag, zou voor de zeer ondiepe wateren van het Belgisch kustgebied wel eens heel belangrijk kunnen zijn, vooral dan naar stormopzet toe.

TABLE OF CONTENTS

LIST OF TABLES

LIST OF FIGURES

LIST OF SYMBOLS

Roman	Name	Units
a	linear term in wind input	
a_i	coefficients in the wind input term	
A	wave amplitude	[m]
A	parameter array	
b	exponential term in wind input	
c	phase velocity	[m/s]
c_g	propagation velocity of the energy in a wave also called velocity	[m/s]
c_{gx}	x-component of the propagation velocity of the energy in a wave	[m/s]
c_p	phase velocity of the wave at the spectral peak	[m/s]
c_1	overall dissipation level	
CO	coefficient in definition for logarithmic frequency grid	
C_D	drag coefficient	
c_{DN}	neutral drag coefficient	
d	water depth	[m]
D_w	wave diffusion coefficient	[m^2/s]
E	energy in a gravity wave spectrum	[m^2]
E_*	nondimensional energy (friction velocity scaling)	
E_*^{PM}	nondimensial energy of a Pierson-Moskowitz spectrum (friction velocity scaling)	
$\bar{E}$	nondimensional energy (scaling with wind velocity u_{10})	
E(f)	frequency spectrum	[m^2s]
$E_D(f)$	Donelan frequency spectrum	[m^2s]
$E_J(f)$	JONSWAP frequency spectrum	[m^2s]
$E_T(f)$	Toba frequency spectrum	[m^2s]
$E(f,\theta)$	frequency-direction spectrum	[m^2s]
$E(\omega)$	angular frequency spectrum	[m^2 rad s]
$E_{i,cal}^*$	calculated nondimensional energy at fetch x_i	
$E_{i,meas}^*$	measured nondimensional energy at fetch x_i	
f	function	
f	frequency ($\omega/2\pi$) [Hz]	
f_p	frequency of the peak of the spectrum	[Hz]
f_p^*	nondimensional peak frequency (friction velocity scaling)	
$\bar{f}_p$	nondimensional peak frequency (scaling with wind velocity u_{10})	
f_{PM}	peak frequency of a Pierson-Moskowitz spectrum	[Hz]

f_{PM}^{*}	nondimensial peak frequency of a Pierson-Moskowitz spectrum (friction velocity scaling)	
$f_{p\ i,cal}^{*}$	calculated nondimensional peak frequency at fetch x_i	
$f_{p\ i,meas}^{*}$	measured nondimensional peak frequency at fetch x_i	
$F(\overline{k})$	the wavenumber spectrum	$[m^3]$
F	function	
g	acceleration of gravity (= 9.81)	$[m/s^2]$
g	gradient vector	
G	Hessian matrix	
H_p	dominant wave height	$[m]$
H	significant wave height	$[m]$
H_s	significant wave height	$[m]$
J	Jacobian matrix	
k	wavenumber	$[1/m]$
$\overline{k}$	wavenumber vector	
k_x	x-component of the wavenumber vector	$[1/m]$
k_y	y-component of the wavenumber vector	$[1/m]$
l	l is a mixing length	$[m]$
L_p	length of the dominant wave	$[m]$
m	exponent of wave steepness dependency in the dissipation source term	
n	exponent in power law	
n	exponent of frequency dependency in the dissipation source term	
n	coordinate normal to a surface	
n_E	exponent in energy fetch law	
n_f	exponent in peak frequency fetch law	
n_α	exponent in Phillips' constant fetch law	
p	exponent in directional distribution of the wave energy spectrum	
p	pressure	$[N/m^2]$
p_a	atmospheric pressure	$[N/m^2]$
PM	Pierson-Moskowitz	
R_1, R_2	principal radii of curvature of the free surface	$[m]$
s	wave steepness	
S_{diss}	dissipation through whitecapping source term	$[m^2/s]$
S_{in}	wind input source term	$[m^2/s]$
S_{nl}	nonlinear wave- wave interactions source term	$[m^2/s]$
S_i^{*}	nondimensional source term (friction velocity scaling)	
S_{LL}	lower limit for spectral energy growth	$[m^2s]$
S_{UL}	upper limit for spectral energy growth	$[m^2s]$
t	time	$[s]$
T_s	surface tension	$[N/m^2m]$
u_{10}	wind velocity at a height of 10 m	$[m/s]$
$u_{19.5}$	wind velocity at a height of 10 m	$[m/s]$

u_*	wind friction velocity	[m/s]
$u(\lambda/2)$	wind speed at a height equal to half a wave length	[m/s]
U_c	component of the wind in the propagation direction of the waves at the spectral peak	[m/s]
U_λ	wind speed at a height equal to one wave length	[m/s]
$\overline{v}$	velocity field	
$w_{j,i}$	weighting factor	
W	sum of weights	
x	fetch ; distance measured from the shoreline	[m]
x_*	nondimensional fetch (friction velocity scaling)	
$\tilde{x}$	nondimensional fetch (scaling with wind velocity u_{10})	
z	coordinate perpendicular to the mean position of the water surface	[m]
z_0	roughness length in the atmospheric boundary layer	[m]
z_0^*	nondimensional roughness length (friction velocity scaling)	

Greek	Name	Units
α	steplength in the search direction	
$\alpha_{i,cal}^*$	calculated (Donelan; Phillips'; Toba) constant at fetch x_i	
$\alpha_{i,meas}^*$	measured (Donelan; Phillips'; Toba) constant at fetch x_i	
α_{Ch}	Charnock constant	
α_D	Donelan constant	
α_P	Phillips' constant	
α_{PM}	Phillips' constant for a PM spetrum	
α_T	Toba constant	
$\hat{\alpha}$	the integral wave steepness;	
$\hat{\alpha}_{PM}$	integral wave steepness for a Pierson-Moskowitz spectrum	
β	factor in directional distribution of the wave energy spectrum	
β	a parameter in the Janssen wind input term	
γ	peak enhancement factor	
Γ	gamma-function	
Γ	factor in the peak enhancement factor	
δ	Dirac-function	
ϵ	machine precision	
ζ	z-coordinate of the free water surface	[m]

ζ	proportionality factor in dissipation source term	
θ	the angle corresponding to the mean wave direction	
κ	the von Karman constant (≈ 0.4)	
λ	wavelength (= $2\pi/k$)	[m]
λ	coefficient which determines angle between wavenumber vectors in the nonlinear wave-wave interactions	
μ	coupling coefficient between the induced surface stress and the water surface	
ν_a	the kinematic viscosity of air	[m^2/s]
$\Pi(\overline{k},\omega)$	three dimensional wavenumber, frequency spectrum of the random atmospheric pressure fluctuations	[kg^2/s^3]
ρ_a	the density of the air	[kg/m^3]
ρ_w	density of water	[kg/m^3]
σ	the net scattering coefficient in the wave-wave interaction source term	
σ	peak width	
σ_a	left peak width	
σ_b	right peak width	
τ	shear stress or the momentum transfer per unit of time and per unit of area	[N/m^2]
τ_{ad}	momentum advected by the wave field	[N/m^2]
τ_f	form drag	[N/m^2]
τ_{diss}	momentum dissipated in the wave field	[N/m^2]
τ_{in}	momentum supplied by the wind	[N/m^2]
τ_{nl}	momentum exchanged through nonlinear interactions	[N/m^2]
τ_{turb}	turbulent stress	[N/m^2]
τ_{visc}	viscous stress	[N/m^2]
τ_w	wave drag	[N/m^2]
Φ	velocity potential	
Φ	coefficient for numerical scheme	
ω	angular frequency	[rad/s]
$\overline{\omega}$	the mean angular frequency	[rad/s]
Ω	a profile parameter $\equiv$ nondimensional roughness	

1 Introduction

1.1 General

Wave modelling has evolved in the last three decades from a nearly empirical science with hand solution methods, to a science where the use of a supercomputer is absolutely necessary. Wave models have evolved from first generation models where the physics are only partially included to second generation models where the sea state evolution is represented in a parametric way, as to reach third generation models where no 'a priori' restrictions are put on the evolution of the shape of the wind sea spectrum. Earlier emphasis has mainly been on hindcast calculations to obtain proper design parameters for coastal protection works, harbours, and off-shore activities. Now the interest has broadened and has shifted to forecasting for the guidance of ships, planning of works, or moving unusual constructions by sea, as well as to coupling with meteorological models to improve both the weather forecast and wave forecast. Just as for weather forecasts, it is now possible to do wave forecasting and again it is the European Centre for Medium Range Weather Forecast (ECMWF) in Reading that plays a central role. At Reading, a third generation wave model runs on a relatively coarse grid. It provides realistic and fairly accurate wave forecasts on a global scale. On a smaller scale the results are not so good, for a great part due to the fact that the coarse grid resolution cannot resolve the requirements of a detailed coastal geometry or local bathymetry. Regional models are developed to fulfil these needs (HYPAS at the Belgian Coast, since November 1991, NEDWAM in the Netherlands since about June 1991, ...). These models have a much finer resolution since they work on a much smaller grid. Waves generated outside the regional grid but travelling into the regional grid can be provided by the global model and introduced at the boundaries of the regional model.

To generate wind waves, one needs wind. At the European Centre they use the winds they forecast by means of their weather models as an input for their wave model. It does not need much explanation to understand that a good wind forecast is absolutely necessary to obtain a reliable wave forecast. Wave modellers nearly happily blame poor wave forecasts on poor wind forecasts and one has to admit wave modellers are at least partially right. Recently effort has been made to accommodate the influence of the waves on the wind profile. Especially the work of Peter Janssen cannot be overlooked. His theoretical ideas on the interaction of waves and wind have been implemented in the Cycle 4 version of the WAM model. WAM is the name of an international group of researchers with special interest in wave modelling. A subgroup named WAMDI (Wave Model Development and Implementation) is the author of the model currently running at ECMWF in Reading.

The WAM-group was founded nearly 10 years ago, with as most important objectives; the development of a third generation model, both on global and on regional scale; to perform physical studies of wave dynamical processes; to extend the understanding of the wave evolution; and to develop data assimilation techniques as to make full use of satellite observations of the sea state. Today, one can say that the development of a global and of regional third generation models has been carried out successfully and that the interest of many researchers has shifted in the direction of data assimilation techniques. The WAM-group is working out a final report in book form. The book is most likely to appear still in 1992. Next to bringing a historical review, it should contain the state of the art in wave modelling, highlighting the tendencies for future evolution and pinpoint the areas where research can still improve our understanding of not so well understood phenomena.

The area least understood in wave modelling is the area of the individual source terms. As Snyder et al. (1990) put it : '... Assumptions as to the form of the various source terms have been hit or miss, and there has been little or no attempt to optimize the form of these terms ...'. Also the interaction of waves and wind are still not fully understood. Not only are the phenomena

of wind input, wave breaking, bottom dissipation and nonlinear interactions complicated phenomena, it is also nearly impossible to separate these source terms by measurement. Also, the fact that measurements over a wide variety of wave and wind conditions are difficult and costly to carry out, does not need much additional explanation.

1.2   Scope of this study

Two main objectives were set at the beginning of this study. The first objective was to find out why the atmosphere sees the ocean, even with sometimes huge waves, as a much smoother surface, compared to its passage over land where it is slowed down much more, even if obstacles are small compared to the size of ocean waves. The answer to this question might seem obvious to a good observer who notices right away that waves travel with the wind and therefore do not give much resistance. However, the details of how much resistance there actually is and its variation with wind speed and parameters defining the wave conditions has been a hot topic for the last 35 years. Since it is a crucial question in the understanding of the air-sea interface and since it has major implications in wave modelling, in storm surge modelling, and also in modelling of the atmospheric boundary layer above the ocean, some effort has been spent as to extract the important parameters.
A second objective of this work is to get a better view and understanding on the working of the source terms in third generation models for wind input and for dissipation through white capping. The question is how values of measured physical quantities such as wave energy and peak frequency of the waves can be optimally reproduced. The approach should be one of inverse modelling, with the emphasis on building a framework for "tuning" unknown parameters in the formulation of the forces involved in wave generation and wave dissipation. Preferably, standard optimization routines should be used to minimize a particular cost function. Such a framework could prove useful in

increasing our understanding of individual source terms. Standard available routines facilitate usage by other interested researchers.

1.3   Methodology

The first objective has been reached by means of a literature search and some numerical experiments. The results can be found in Chapter 2. In the first part of Chapter 2, the sea surface is described as a superposition of an infinitesimal number of irrotational gravity waves. The result is a spectrum which has been parametrized. A number of formulations are popular and it is sufficient to mention the formulation for the JONSWAP, the Toba and the Donelan spectrum to obtain a good picture of our ability to describe a wind sea spectrum. The wave spectrum can be described in the wavenumber space and in the frequency-direction space. The two formulations are linked through the dispersion relation of the gravity wave. For this work, the preference is given to the frequency-direction space, since it is somewhat easier to interpret the results.

In the second part of Chapter 2, the atmospheric boundary layer is studied. The formulation of the logarithmic profile for the mean horizontal velocity is looked at. Especially the current understanding and formulation of the two parameters, i.e., the friction velocity u_* and the roughness length z_o, are covered in more detail and a literature review is given.

In the third part of this Chapter 2, the fetch limited growth curves for the total energy, the peak frequency, and the parameter describing the tail of the spectrum in casu the Phillips' constant α_p are reviewed in terms of the velocity at 10 m height and in terms of the friction velocity. The JONSWAP growth curves and the Kahma and Calkoen growth curves are withheld for further use (see Chapter 6). In the rest of the work however, the friction velocity will be used as the appropriate variable to obtain nondimensional parameters.

4

In the last part of Chapter 2, it is attempted to relate the different formulations for the spectra (i.e., JONSWAP, Toba and Donelan) in the high frequency range to see in how far they tell the same story and to find out if there is a possible link between the high frequency waves and the roughness of the sea waves.

In working out the second objective, two distinctive aspects can be seen. A first aspect was to find a third generation model and to become familiar with it. This asked for extensive contacts with researchers from other institutions, especially the Max-Planck Institut für Meteorologie in Hamburg (Germany). A second aspect was the formulation of a cost function and the implementation into a framework for minimization. The approach will be as described below.

Chapter 3 looks at the energy and momentum transport of surface gravity waves and at the source terms that play a role in this process. Since the modelling in this work is limited to deep water waves, only the source terms applicable to these deep water waves are covered. For the wind input term, the Phillips' and Miles' mechanisms are briefly described together with a summary of Janssen's quasi-linear theory for the spectrum of wind generated gravity waves. A literature review of wind input terms will be given as to make a selection for a formulation to be used in the numerical wave model. Also the dissipation term and the term describing the nonlinear interactions are given.

Chapter 4 will be used to give a description of the wave program ONEDMOD that will be used in this study. The program is a one-dimensional wave model. One-dimensional here means that only time or fetch will play a role. For the rest, it is identical to a third generation model, including the same physics. It is therefore well suited to look at the behaviour of formulations for the individual source terms. The structure as well as initial conditions to run the program will be discussed. Details concerning the numerical scheme, source term calculations, the limitation of the growth of the energy in a particular frequency-direction bin, the cut-off frequency, and the high frequency tail

are written down. A number of runs will point out the scaling ability or disability of the program when run for different input velocities. Also, the evolution of the energy spectrum, the source terms, and the momentum balance with fetch will be displayed.

In Chapter 5 it is explored how to make use of existing optimization routines to match the growth curves calculated by the wave program and the ones measured in field experiments. In the first place a cost function is defined in the form of a weighted sum of squares, whereby the difference between the calculated and observed wave characteristics will be minimum. To obtain some feeling as to the behaviour of this cost function, a sensitivity test was done for a number of selected parameters. In the sensitivity analysis only one parameter is allowed to vary. To fulfil the criterium of using a standard optimization routine, the search for a suitable routine was done in the widely available NAG-subroutine library. These kinds of libraries usually have a variety of routines available with different levels of complexity and necessity for user interference.

Chapter 6 is solely dedicated to cover the results and the interpretation of computer runs done with the program that was developed in the above proposed framework. First of all, a number of choices were made with regard to the source terms and to the measured wave quantities in the form of growth curves. For the source terms this results in two types of wind input formulation; one which is linear in the friction velocity and which will be indicated as the Snyder type wind input term; and one which is quadratic in the friction velocity, which will be indicated as the Stewart type wind input term. For the dissipation term, the formulation proposed by Komen et al.(1984) is chosen, but a number of parameters are free to vary. For the nonlinear interaction, the discrete interaction approximation is used without the possibility for tuning. For the growth curves, the JONSWAP relations and the ones recently proposed by Kahma and Calkoen were withheld.

Then a distinction was made between trying to fit wave quantities in the growing stage only (i.e., for about two orders of

6

magnitude in the nondimensional fetch), and trying to fit both the growing stage and the fully developed stage. Although the number of tunable parameters will be limited to two in these runs, the proposed framework will in principle be able to handle a much larger number of adjustable parameters.

Chapter 7 should summarize the most important findings of this study and give a number of suggestions for further research in the field of wind waves and its mathematical modelling.

2 Description of the sea surface and the atmospheric boundary layer above the ocean

2.1 Introduction

In this chapter the sea surface and the atmospheric boundary layer are described. In a first part, the water surface is treated as consisting of an infinite number of irrotational gravity waves. Although capillary waves are important for many processes in the ocean, they fall outside the scope of this work. Also viscous effects, although responsible for wave damping, are not covered. After giving the basic principles of an irrotational gravity wave, the main emphasis is put on the spectral description of wind seas. Three formulations from literature are covered in more detail; namely the well known JONSWAP spectrum (Hasselmann et al., 1973), the Toba spectrum (Toba, 1973), and the Donelan spectrum (Donelan et al., 1985). The JONSWAP frequency spectrum has an f^{-5} tail based on the dimensional arguments of Phillips (1958), while both the Toba and the Donelan spectrum have an f^{-4} tail. The main difference in the Toba and the Donelan formulation is the presence of the friction velocity u_* in the Toba spectrum and the peak frequency f_p in the Donelan spectrum.

The velocity profile of the atmospheric boundary layer is thought of as being logarithmic. The roughness length z_0 or equivalently the drag coefficient C_D are not so clearly defined. An overview from values found in literature is given, and although the overview is far from complete, we can conclude that there is evidence that the roughness of the waves depend on the wind speed and also on the age of the waves. Roughness increases with wind speed and younger waves are felt as more rough than older waves.

In a next part the growth curves are discussed. With growth curves one means the change with fetch of important wave parameters such as the total energy in the waves or the peak

frequency of the wave spectrum. The single most important
experiment to establish these relationships is without doubt the
JONSWAP (JOint North Sea WAve Project) experiment described by
Hasselmann et al. (1973). Most recently Kahma and Calkoen (1991)
combined data from different sources (including the JONSWAP
data). Scaling or nondimensionalizing of these growth curves, is
usually done with the velocity at a particular height (most often
taken at 10 m). In this work the friction velocity is chosen as
the correct scaling parameter, since it has a direct physical
meaning.

In a last paragraph an attempt is made to compare the different
spectral formulations in the saturation range. This leads to the
discovery that the Donelan 'constant' in the Donelan spectrum may
be a direct measure of the roughness length in the atmospheric
boundary layer. Comparing the Donelan spectrum and the Toba
spectrum, yields the same relationship for the Donelan constant
(excluding a multiplication factor) as Maat et al. (1991) found
for the nondimensional roughness length (nondimensionalized with
the friction velocity u.). This would mean that the roughness at
sea is mainly caused by high frequency waves. The suggested idea
that the Donelan constant and the nondimensional roughness length
are the same variable is then verified with some field data from
the HEXOS experiment (Katsaros et al., 1987; Smith et al., 1990).

2.2 The sea surface

2.2.1 Mathematical formulation of irrotational gravity waves

The main assumptions commonly used in the treatment of
surface water waves is that water can be treated as incompres-
sible and inviscid and that gravity is the only external force.
The main consequence is that wave motion is irrotational and that
therefore the velocity field $\bar{v}$ is the gradient of a velocity

9

potential Φ. Since water is essentially incompressible, one has introducing the continuity equation :

$$\overline{v} = \nabla\Phi \quad and \quad \nabla\cdot\Phi = 0$$
$$\downarrow$$
$$\nabla^2\Phi = 0$$

(2.1)

The pressure p in the fluid is given by the Bernoulli equation (equation of motion) :

$$\frac{\partial\Phi}{\partial t} + \frac{1}{2}(\nabla\Phi)^2 + \frac{p}{\rho_w} + gz = 0$$

(2.2)

where   g   :   acceleration of gravity = 9.81 [m/s^2]

ρ_w :   density of water [kg/m^3]

The above two equations are supplemented by the boundary conditions. The bottom of a water mass can, for the purpose here, be seen as impermeable, so that one has the condition that the velocity normal to the bottom boundary is zero. A second boundary, namely the surface boundary, has the property that fluid does not cross this boundary and that a water particle once at the surface remains at the surface. Also at the water surface the pressure is equal to the atmospheric pressure. Mathematically this translates into :

- for the bottom (z = -d ; d is the water depth)

$$\frac{\partial\Phi}{\partial n} = 0$$

(2.3)

- for the surface

$$\frac{\partial\zeta}{\partial t} + \frac{\partial\Phi}{\partial x}\frac{\partial\zeta}{\partial x} + \frac{\partial\Phi}{\partial y}\frac{\partial\zeta}{\partial y} - \frac{\partial\Phi}{\partial z} = 0$$

(2.4)

$$at \quad \zeta = \zeta(x,y,t)$$

$\zeta(x,y,t)$ is z-coordinate of the free water surface in a coordinate system xyz ; z = 0 corresponds to the mean position of the water surface

and

$$\frac{\partial \Phi}{\partial t} + \frac{1}{2}(\nabla \Phi)^2 + g\zeta + \frac{T_s}{\rho_w}(\frac{1}{R_1} + \frac{1}{R_2}) = \frac{-p_a}{\rho_w} \qquad (2.5)$$

$$at \quad \zeta = \zeta(x,y,t)$$

T_s is the surface tension of the water and R_1 and R_2 are the principal radii of curvature of the free surface.

For the propagation of waves one can assume the atmospheric pressure p_a to be known and constant, since the density of air is much lower than the density of water. In the generation of waves however, the pressure fluctuations in the air due to wave motion will play an important role and there it should not be neglected. When wave amplitudes are small compared to the wavelengths, the second and third term in equation (2.4) and the second term in equation (2.5) can be neglected. If one then takes the direction of propagation equal to the x-direction and does not take into account the effect of surface tension, one obtains :

$$\frac{\partial \zeta}{\partial t} - \frac{\partial \Phi}{\partial z} = 0$$
$$\frac{\partial \Phi}{\partial t} + g\zeta = 0 \qquad (2.6)$$

The above equations are valid at z equal to zero. The atmospheric pressure was taken as reference or zero pressure. A solution to the differential equations is given by :
-    a wave with amplitude A [m], wavenumber k [1/m], wavelength λ (= $2\pi/k$) and angular frequency ω [rad/s]

$$\zeta = A \cos(kx - \omega t) \qquad (2.7)$$

-    a corresponding velocity potential

$$\Phi = \frac{A \omega \cosh k(z + d)}{k \sinh kd} \sin(kx - \omega t) \qquad (2.8)$$

-    and a dispersion relation

$$\omega^2 = gk \tanh kd \qquad (2.9)$$

The effects of surface tension are only important for the capillary and capillary-gravity waves, i.e., waves with a

11

wavelength λ less than 5 cm, and will be reflected in the dispersion relation (see Donelan and Hui, 1990).

The phase velocity c of a wave is the angular frequency ω divided by the wavenumber k. The propagation velocity of the energy in a wave is also called the group velocity c_g. It is the partial derivative of the angular frequency to the wavenumber k.

In deep water (kd >> 1 or which in practice corresponds to kd > $\pi/2$) one obtains from equation (2.9) :

$$c = \frac{\omega}{k} = \frac{g}{\omega} = \frac{g}{2\pi f}$$
$$c_g = \frac{\partial \omega}{\partial k} = \frac{g}{4\pi f}$$

(2.10)

where $f = \omega/2\pi$ = frequency

The above description is a short summary with a simplification to deep water of the linear wave theory, also called small-amplitude wave theory, sinusoidal wave theory, and Airy wave theory. More details and the expressions for deep water waves can be found in, e.g., LeBlond and Mysak (1978).

Although viscosity as such is not considered in the above derivation of the wave equation, it plays an important role in the damping of wave motion. It has been shown by Lamb (1930), that waves with a short wave length (capillary range) are rapidly damped by viscosity, whereas longer waves (gravity range) need a much longer time to be damped. Since details of this dissipation process are not needed for the rest of this work, we can refer to Donelan and Hui (1990) for further reading. There one can also find some aspects of nonlinear theories for gravity waves.

2.2.2   Spectral description of the sea surface elevation

The sea surface does not contain a single wave component but many different ones. The different wave components can be seen as varying randomly in both space and time. A combined picture of the sea surface is given by either the frequency

spectrum or the wavenumber spectrum. One of the main properties of this spectrum is that the integral over either all frequencies or over all wavenumbers is equal to the mean of the surface displacement ζ squared. It is a measure of the energy in the wave field per unit of area and per unit of weight. In a mathematical formulation this becomes :

$$\overline{\zeta^2} = \int_0^\infty E(\omega)\, d\omega = \int_0^\infty F(\overline{k})\, d\overline{k} \qquad\qquad [m^2] \qquad (2.11)$$

where $E(\omega)$:   (angular) frequency spectrum

$F(\overline{k})$:   the wavenumber spectrum with $\overline{k}$ the wavenumber vector

Note that the frequency spectrum is integrated over all possible directions while the wavenumber spectrum contains in principle directional information.

Most often the frequency spectrum is given in terms of the frequency f and not in terms of the angular frequency ω. Both spectra are simply related by :

$$E(\omega)\, d\omega = E(f)\, df$$

$$or \qquad\qquad\qquad\qquad (2.12)$$

$$E(f) = \frac{d\omega}{df} E(\omega) = 2\pi E(\omega)$$

Also the wavenumber spectrum is often seen in terms of the modulus of the wavenumber and the corresponding angle of the wavenumber vector. These spectra are related by :

$$F(\overline{k})\, d\overline{k} = F(k,\theta)\, k\, dk\, d\theta \qquad\qquad (2.13)$$

where k is   the   modulus   of   the   wavenumber   vector $\overline{k}$ ($\overline{k} = (k\cos\theta,\ k\sin\theta)$).

In what follows only wind seas will be studied, i.e. spectra where the full frequency range or wavenumber range is still under the influence of the current wind field. In real ocean conditions, the wave field will quite often contain waves that are no longer influenced by the wind field and propagate more or less freely through the region of interest. Although these swell waves, as they are called, have important practical applications

13

(to give one example swell waves are the dominant problem for ship routing to the Belgian harbours (Van den Eynde and Monbaliu, 1989; Van den Eynde and De Wolf, 1990)), they are not considered in the rest of this study.

2.2.3 The JONSWAP formulation for the wave spectrum

Hasselmann et al.(1973) found that a windsea spectrum measured under various wind conditions can be described quite well with the JONSWAP spectrum. This one dimensional frequency spectrum is shown in Figure 2.1. Mathematically it is described by the five JONSWAP parameters $f_p, \gamma, \alpha_p, \sigma_a$ and σ_b

$$E_J(f) = \alpha_p g^2 (2\pi)^{-4} f^{-5} \exp\{-\frac{5}{4}(\frac{f}{f_p})^{-4}\} \gamma^\Gamma \qquad (2.14)$$

where

$$\Gamma = \exp(-\frac{(f-f_p)^2}{2\sigma^2 f_p^2}) \qquad (2.15)$$

$g = 9.81$ = acceleration of gravity [m^2/s]
f = frequency

The scale parameters are :
f_p= frequency of the peak of the spectrum
α_p= Phillips' constant

The shape parameters are :
γ = peak enhancement factor ≈ 3.3
σ_a = left peak width $\rightarrow \sigma = \sigma_a = 0.07$ if $f < f_p$
σ_b = right peak width $\rightarrow \sigma = \sigma_b = 0.09$ if $f > f_p$

For a fully developed sea, the JONSWAP spectrum (equation (2.14)) should reduce to the Pierson-Moskowitz spectrum, further noted as PM spectrum (Pierson and Moskowitz, 1964) :

$$E_{PM}(f) = \alpha_P \, g^2 (2\pi)^{-4} f^{-5} \, \exp\{-\frac{5}{4}(\frac{f}{f_p})^{-4}\} \qquad (2.16)$$

Note that equation (2.14) and equation (2.16) are equal for γ equal to one. Also for a PM-spectrum the scale parameters are fixed

$\alpha_P \quad = 0.0081 = \alpha_{PM}$

$f_p = f_{PM} = 0.13 \, g \, / \, u_{10} = 0.14 \, g \, / \, u_{19.5}$

      (Hasselmann et al., 1973)

$f_{PM} = 5.6 \; 10^{-3} \, g \, / \, u.$

      (Komen et al., 1984)
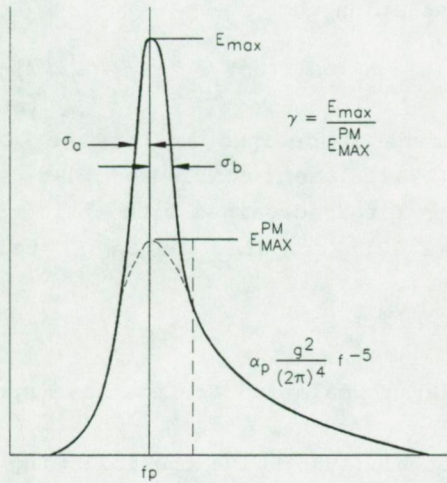
Figure 2.1 : The JONSWAP spectrum (after Hasselmann et al., 1973)

15

2.2.4   The Toba formulation for the wave spectrum

At about the same time as the JONSWAP paper (Hasselmann et al., 1973), Toba (1973) published his formulation for the saturation range of wave spectra. According to Toba (1973) the high frequency tail of the spectrum can be described by

$$E(f) = (2\pi)^{-3} \alpha_T \, g \, u_* \, f^{-4} \qquad (2.17)$$

where α_T is a universal constant and u_* is the friction velocity of the wind. Toba's idea has been supported since by a number of people, including Phillips who changed his original idea based on dimensional analysis of a saturation range proportional to f^{-5} (Phillips, 1958) to an f^{-4} proportionality (Phillips, 1985). Also Battjes et al.(1987) reanalysed the spectral data measured in the JONSWAP experiment (Hasselmann et al., 1973). They therefore extended the formulation to:

$$E_T(f) = \alpha_T \, g \, u_* \, (2\pi)^{-3} f^{-4} \, \exp\{-(\frac{f}{f_p})^{-4}\} \gamma^{\Gamma} \qquad (2.18)$$

The peak enhancement is defined as for the JONSWAP spectrum. Battjes et al.(1987) then concluded that a statistically significant better fit is obtained with an f^{-4} tail according to Toba (equation (2.17)) compared to an f^{-5} tail according to JONSWAP (equation (2.14)).

2.2.5   The Donelan formulation for the wave spectrum

Donelan et al.(1985) give the following formulation for the wave spectrum :

$$E_D(f) = \alpha_D \, g^2 (2\pi)^{-4} f_p^{-1} f^{-4} \, \exp\{-(\frac{f}{f_p})^{-4}\} \gamma^{\Gamma} \qquad (2.19)$$

where

$$\alpha_D = 0.006 \ (U_c/c_p)^{0.55} \quad for \quad 0.83 < U_c/c_p < 5 \qquad \textbf{(2.20)}$$

U_c is the component of the wind in the propagation direction of the waves at the spectral peak and c_p is the phase velocity of the wave at the spectral peak (see equation 2.10). For wind blowing perpendicularly off a straight shore, this corresponds to the wind direction. The peak enhancement factor is now defined as:

$$\begin{array}{ll} \gamma = 1.7 & 0.83 < U_c/c_p < 1 \\ \gamma = 1.7 + 6.0 \ \log \ (U_c/c_p) & 1 \leq U_c/c_p < 5 \end{array} \qquad \textbf{(2.21)}$$

and the peak width parameter in Γ (compare with equation (2.15))

$$\sigma = 0.08 \ [\ 1 + 4 \ / \ (U_c/c_p)^3 \ ] \qquad 0.83 < U_c/c_p < 5 \qquad \textbf{(2.22)}$$

It is interesting to see that Donelan uses a local variable (U_c/c_p) to describe the characteristics of the wave spectrum. The main reason for using a local variable is that in practice the fetch is rarely known, whereas the above data can be readily deduced from measurements or from numerical models.

2.2.6 Comparison of the JONSWAP, Toba and Donelan spectral formulation

The above three formulations are not the only three formulas proposed in literature. For example, the Kruseman spectrum was used in the GONO-model (Janssen et al., 1984). The spectra try to summarize the complex history of actions and interactions on the water surface with just a few parameters. This has been, and still is, the base of the success of the parametric wave models, such as HYPAS (Günther, 1981). Only a limited number of parameters has to be updated on every grid point so that it is in practice possible to do operational wave forecasting for an extended area with a limited amount of computer power. For example waves for the southern bight of the

17

North Sea can be predicted using only two work stations (Van den Eynde en De Wolf, 1990; MUMM-Activity Report No.5).

The JONSWAP, Toba, and Donelan formulations are drawn in the Figures 2.2 to 2.5 all having the same peak frequency of 0.4 Hz for a wave age of 0.25 or equivalently U_c/c_p equal to 4 and for a wave age of 0.83 or U_c/c_p equal to 1.2. Wave age is a measure of the state of the wind waves and is defined as the phase velocity of the waves at the spectral peak divided by a characteristic wind velocity (u_* and u_{10} are used frequently). These numbers were chosen to correspond with Figure 17 of Donelan et al. (1985). Figure 2.2 is representative for a young wind sea and Figure 2.3 is representative for a fully developed sea. The calculation of the friction velocity u_* was done with the formula of Garratt (1977) (see also 2.3) as was suggested by Battjes et al.(1987) in their reanalysis of the JONSWAP data. The relevant data to draw the Figures 2.2 to 2.5 are brought together in Table 2.1.

$f_p = 0.4$ Hz	JONSWAP	Donelan	Toba
$u_{10} = 15.6$ m/s	$\tilde{x} = 175$	$\tilde{x} = 100$	$u_* = 0.66$
	$\alpha_p = 0.0244$	$U_c/c_p = 4$	
$u_{10} = 3.2$	$\tilde{x} = 2.13 \ 10^4$	$\tilde{x} = 1. \ 10^5$	$u_* = 0.099$
	$\alpha_p = 0.0085$	$U_c/c_p = 0.83$	

Table 2.1   Data used to make the figures 2.2 to 2.5

Note that to calculate the Phillips' constant and the non-dimensional fetch for the JONSWAP spectrum, the peak frequency of 0.4 Hz had to be nondimensionalized with the velocity at 10 m and then replaced in the JONSWAP growth curves (see 2.4.1; equation (2.41)). The other data needed can be retrieved from the equations (2.14) to (2.22).

We can see that the spectra for the growing wind-sea (fetch limited condition) are very similar. The spectra for the fully developed sea state however, are quite different. The JONSWAP and

18

the Toba spectrum are much sharper peaked than the Donelan
spectrum although the values of the energy density at the peak
for the Donelan and Toba spectrum are about equal. As remarked
in Donelan et al. (1985), the Donelan spectrum resembles the shape
of the PM-spectrum. The Toba spectrum would also resemble this
broader spectrum if the peak width parameter σ would take the
form as for the Donelan spectrum, see equation (2.22). The Toba
spectrum with Donelan spreading function is shown in Figure 2.5.
It is interesting that the peak enhancement factor γ for the Toba
spectrum does not have to be adjusted for wave age dependency.
The peak enhancement factor γ for the JONSWAP spectrum in Figure
2.3 was still equal to 3.3 . In the JONSWAP report no tendency
towards a reduction of γ with fetch is noticed, although it was
mentioned that for a fully developed sea the peak enhancement
should not be there any more and one should obtain a PM-spectrum.
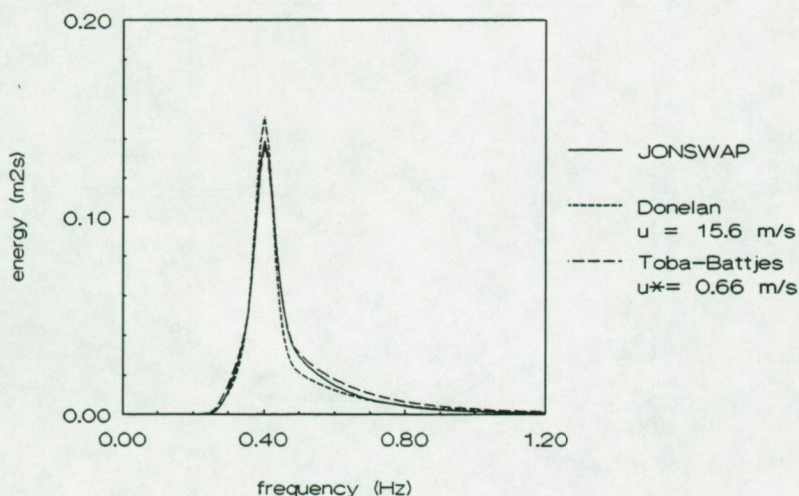
Figure 2.2 : Spectra for fetch limited conditions
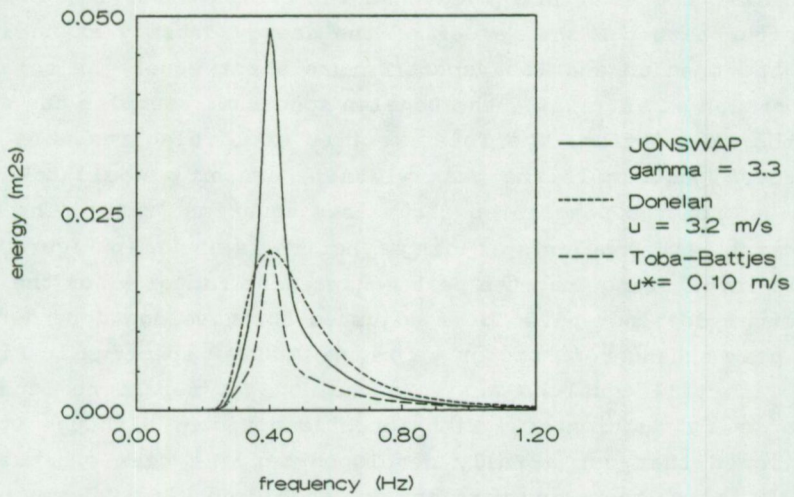
Figure 2.3 : Spectra for fully developed conditions ($\gamma=3.3$)
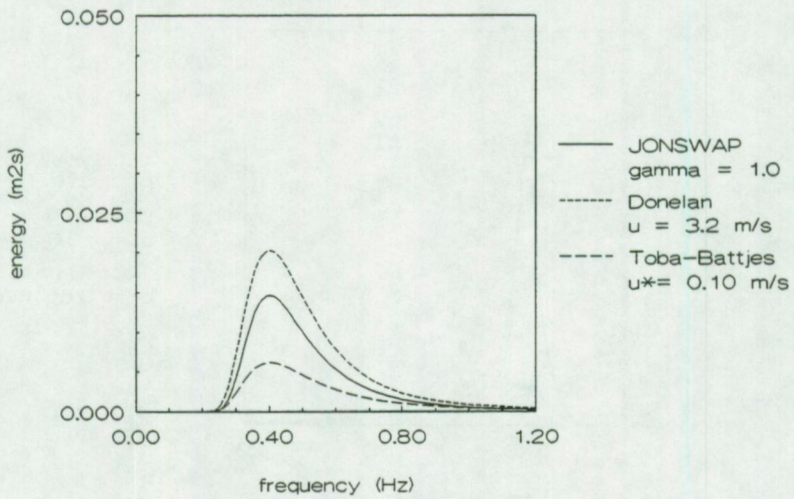
Figure 2.4 : Spectra for fully developed conditions ($\gamma=1.0$)
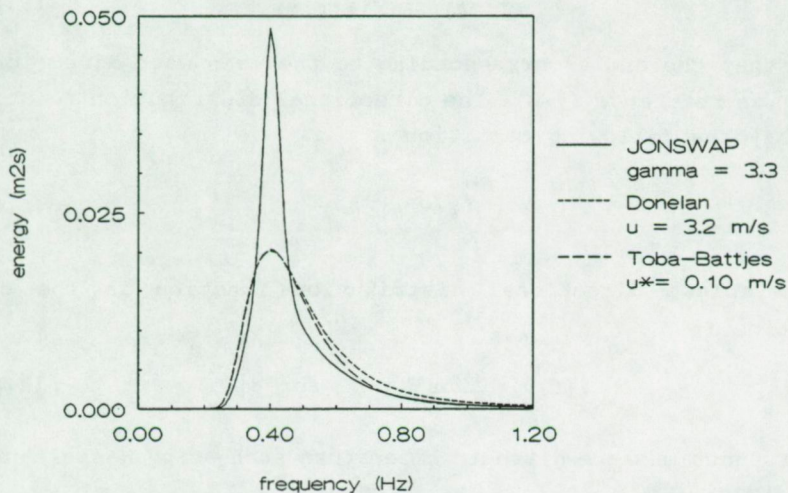
Figure 2.5 : Spectra for fully developed conditions (Γ in Toba spectrum according to Donelan ≡ equations (2.15) and (2.22))

The parametric representation of the wave spectrum is not necessary in the so called third generation models as for example 3G-WAM (WAMDI (1988)). These models incorporate all the known physics on a discrete frequency-direction grid and then extract the information needed (such as low frequency swell energy or significant wave height) by integration of the discrete quantities in the frequency-direction domain at the desired location. It is such a model which will be used in this study (see Chapter 4).

2.2.7   Directional distribution of energy spectra

To obtain a spectrum in the two-dimensional frequency and direction space, the frequency spectrum is multiplied with a directional energy distribution function :

21

$$E(f,\theta) = E(f)\Phi(f,\theta) \qquad\qquad (2.23)$$

Note that the angle corresponding to the mean wave direction is taken as reference ($\theta=0$). The directional distribution functions satisfy the following condition :

$$\int_{-\pi}^{+\pi}\Phi(f,\theta)d\theta = 1 \qquad\qquad (2.24)$$

The simplest directional distribution function is the $\cos^2\theta$ function :

$$\Phi(f,\theta) = \frac{2}{\pi}\cos^2\theta \qquad for\,|\theta| < \frac{\pi}{2} \qquad\qquad (2.25)$$

Other functions are given in literature such as by Hasselmann et al. (1980) :

$$\phi(f,\theta) = N_p^{-1}\cos^{2p}(\frac{\theta}{2})$$

$$p = 9.77(\frac{f}{f_p})^\mu \qquad N_p = 2^{1-2p}\pi\frac{\Gamma(2p+1)}{\Gamma^2(p+1)} \qquad\qquad (2.26)$$

$$\mu = 4.06 \qquad f < f_p$$
$$= -2.34 \qquad f > f_p$$

(note that Γ stands here for the gamma-function and is not the same as used above in the peak enhancement factor)
Donelan et al. (1985) use :

$$\Phi(f,\theta) = \frac{1}{2}\beta\,sech^2\beta\theta$$

$$\beta = 2.61(\frac{\omega}{\omega_p})^{+1.3} \quad for \quad 0.56 < \frac{\omega}{\omega_p} < 0.95$$

$$\beta = 2.28(\frac{\omega}{\omega_p})^{-1.3} \quad for \quad 0.95 < \frac{\omega}{\omega_p} < 1.6 \qquad (2.27)$$

$$\beta = 1.24 \qquad\qquad\qquad otherwise$$

Although in the rest of this work little attention is paid to the directional distribution of the spectrum, the reader should be aware that the directional spreading of the waves plays an important role in the detailed calculations of the nonlinear interactions (see Chapter 3).

2.3   The atmospheric boundary layer above the ocean

If one assumes that the surface boundary layer can be
treated as a layer of constant stress, then the velocity profile
above the ocean is logarithmic (Panofsky and Dutton, 1984) :

$$u(z) = \frac{u_*}{\kappa} \ln\left(\frac{z}{z_o}\right) \qquad (2.28)$$

where   z   =   height above the mean water level [m]
         u_* =   friction velocity [m/s]
         κ =   the von Karman constant (≈ 0.4)
         z_o =   roughness length [m]

A distinction should be made between aerodynamically smooth and
aerodynamically rough flow. In smooth flow the roughness elements
are buried within the viscous sublayer and they do not affect the
flow outside the viscous sublayer. The roughness then only
depends on the imposed stress and on the fluid viscosity. In
fully aerodynamically rough flow, the roughness elements produce
form drag and account for virtually all the stress in the surface
layer. In between there is a transition region. In equation
(2.28) only the outer layer is described since the viscous
sublayer is very small (O(mm)). More details on the profile in
the viscous sublayer and the distinction between smooth and rough
flow can be found in Donelan (1990).

The roughness length z_o is one way of measuring the surface
roughness. An equivalent expression is the drag coefficient C_D.
The drag coefficient is defined as :

$$u_*^2 = C_D(z)\,(u(z))^2 = \frac{\tau}{\rho_a} \qquad (2.29)$$

Note that τ is the shear stress or the momentum transfer per unit
of time and per unit of area and ρ_a the density of the air
[kg/m³]. It is easy to see from equations (2.28) and (2.29) that
z_o and C_D are linked by :

$$C_D(z) = \kappa^2 (\ln(\frac{z}{z_o}))^{-2} \qquad\qquad (2.30)$$

Equation (2.28) is valid for neutrally stable conditions. It becomes more complex in the case of temperature or moisture stratification. Expressions for these conditions can be found in Janssen and Komen (1985). Unstable conditions will not be considered here.

Although equation (2.28) looks simple in the case of neutral stability, its evaluation is far from evident. Over a flat plate with fixed obstacles the roughness length is a constant. Waves propagate over the ocean and the obstacles (waves) are not fixed. Stewart (1974) remarked that there might be some increase in the drag coefficient with increasing wind speed, some dependency upon the stability of the air column, some dependency upon wind duration and fetch and perhaps on other parameters, but anyone who did not wish to believe in these dependencies would be difficult to convince from the data. Since the publication of Stewart's 1974 paper, more experiments have been carried out (see e.g. section 2.5.3) and we see that the roughness length is a function of wind speed and wave age, possibly of other parameters.

The simplest expression for the roughness length is the one proposed in Charnock (1955) and is based on dimensional analysis :

$$z_0 = \alpha_{Ch} \frac{u_*^2}{g} \qquad\qquad (2.31)$$

where α_{Ch} is the Charnock constant.

Note that the expression (2.31) only depends on the friction velocity and not on the sea state. Wu (1969) gave for the Charnock constant a value of 0.0112 determined from laboratory channel measurements and a value of 0.0156 for oceanographic data. For the drag coefficients $C_D(10)$, Wu(1969) then proposed the following formulas :

$$C_D(10) = 0.5 \sqrt{u_{10}} \ 10^{-3} \qquad 1 \ m/s < u_{10} < 15 \ m/s$$

$$C_D(10) = 2.6 \ 10^{-3} \qquad u_{10} > 15 \ m/s$$

(2.32)

Note that u_{10} is the wind speed at a height of 10 m. The discontinuity at 15 m/s Wu(1969) attributed to a 'natural division' between light and strong winds.

Later, Wu(1972) suggested that the discrepancy between laboratory and field data for roughness is due to the fact that for laboratory situations the roughness of the surface is due to the dominant waves, whereas for oceanic conditions the surface roughness consists of superimposed ripples on the dominant waves. Wu (1980;1982) changed the Charnock constant to a value of 0.0185 and claimed that equation (2.31) is indeed valid for all sea states. The drag coefficient can then easily be obtained from equation (2.28) after using equation (2.31). This drag coefficient can also be approximated with a maximum error of about 1% up to a speed of about 50 m/s by the linear relationship (Wu(1982)):

$$C_D(10) = (A + B \ u_{10}) \ 10^{-3}$$

(2.33)

with A = 0.8 and B = 0.065 .

Many researchers have proposed a linear relationship between the drag coefficient and the wind speed at 10 m. A number of these are brought together in Table 2.2.

Note that some authors (e.g. Garratt) use a von Karman constant κ of 0.41 for the definition of the logarithmic velocity profile, while others use a value of 0.40 (e.g. Wu).

A	B	wind speed range	author
0.63 ± 0.23	0.066		Smith and Banke (1975)
0.75	0.067		Garrat (1977)
0.61	0.063		Smith (1980)
1.14	0	$4 < u_{10} < 10$ m/s	Large and Pond (1981)
0.49	0.065	$10 < u_{10} < 25$ m/s	
0.8	0.065		Wu (1982)
0.96	0.041	$4 < u_{10} < 16$ m/s	Donelan (1982)
0.577	0.085	$4 < u_{10} < 24$ m/s	Geernaert et al. (1987)
1.29	0	$u_{10} < 7.5$ m/s	WAMDI (1988)
0.8	0.065	$7.5 < u_{10} < 50$ m/s	

Table 2.2 Linear relationships for the drag coefficient in function of the wind speed u_{10} (see equation (2.33))

Many researchers however have arguments that Charnock's formulation does not tell the whole story. Amorocho and Devries (1980) divided the trends in the relation between the shear velocity u_* and the velocity at 10 m (u_{10}) in three regions. In the development of shear stress there is :
- a lower region in which there is no wave breaking and the drag coefficient remains therefore approximately constant :
  $u_* = 0.0323\ u_{10}$ for $0 < u_{10} < 7$ m/s
- a transitional region where waves start to break ; the drag coefficient varies nonlinearly
- a limiting region where breaking is saturated ; the drag coefficient is again constant
  $u_* = 0.0504\ u_{10}$ for $u_{10} > 20$ m/s

As final expression they retain :

$$C_D(10) = 0.0015 \left[1 + \exp\left(-\frac{u_{10}-12.5}{1.56}\right) \right]^{-1} + 0.00104 \qquad \textbf{(2.34)}$$

Although their ideas included a dependency on the sea state, in casu wave breaking, the formulation depends only on the wind speed and therefore does not differ much from the Charnock formulation.

Donelan (1982) said that the mobility of the waves and wave breaking play an important role. To model the drag coefficient he separated the surface waves in two parts :

- the peak region of the spectrum characterized by wave breaking near the spectral peak ; off-wind travel of the waves is possible for fetch-limited or non-stationary conditions; the characteristic wave speed is the one of the spectral peak and the part of the spectrum up to two times the peak frequency is marked as long waves.
- the equilibrium range characterized by quasi-saturation, non-visible wave breaking and down wind travel; the characteristic wave speed is taken at two times the peak frequency; the part of the spectrum with frequencies larger than twice the peak frequency is marked as short waves and adjusts very rapidly to changing wind conditions.

Attaching an equivalent immobile surface roughness proportional to the root mean square height of the waves in their assigned part of the spectrum, Donelan (1982) then defines the drag as the sum of these two contributions :

$$C_D = f(\text{sea state}) * \{ [C_D]_{long} + [C_D]_{short} \}$$

Long and short refer here to long waves and short waves respectively. The drag coefficient in the above equation is further corrected for the wind speed dependency of the wave breaking (white capping becomes more widespread for increasing wind speed).

Wu (1986), in addition to Wu(1982) showed that only the short waves provide roughness elements and consequent resistance through form drag. Only these short waves should relate to a roughness length and be described by Charnock's relation. The

27

direct momentum flux to the long waves which have a phase velocity comparable to the wind velocity, is not described by Charnock's relation. The net momentum flux to the wave field from the wind is defined by Donelan (1979) as the difference between the wind input to the waves and the local wave dissipation. For fully developed seas there should be no net momentum flux : whatever is put in, should be dissipated. The direct momentum flux or wave drag (τ_w) is only a small portion of the total wind stress and is estimated around 10 to 20 percent. The total wind stress can be written as :

$$\tau = \tau_w + \tau_f \qquad\qquad (2.35)$$

(τ_w : wave drag ; τ_f : form drag)

Donelan (1982) and Wu (1986) put forward the same physical idea that the resistance of the water surface to the air flow is governed by two different processes, namely a process of energy transfer to the waves that is advected away by the wavefield (long waves), and a process of drag resistance, whereby turbulence is created in the atmospheric boundary layer (short waves). The distinction between short and long waves is given on an rather arbitrary basis.

According to Hasse (1986) it should not be possible to relate z_o in a simple way to geometric properties of the sea surface (as for fixed roughness). Hasse (1986) finds the use of a drag coefficient less deceiving since it does not have the dimension of a length and that it is therefore more transparent that one tries to summarize a rather complicated process in a single coefficient.

Some researchers do relate the roughness to geometric properties of the sea, adding the additional factor of the age of the waves. Hsu (1974) chose the 'dominant' wave height H_p, the corresponding wave celerity c_p and the friction velocity as the important

28

parameters to characterize the roughness of the sea and came up
with the following relation:

$$z_o = \frac{1}{2\pi} \frac{H_p}{(c_p / u_*)^2} \qquad (2.36)$$

Although Hsu's averaged data seem to confirm his relationship,
the scatter between the individual data points is enormous.
Another interesting approach to the parametrization of the
surface roughness can be found in Donelan (1990). He tried to
relate the ratio of the roughness length z_o and the root-mean-
square wave height to various measures of the wave age. He hoped
in this way to get rid of the discrepancy between field and
laboratory measurements, but did not succeed in this task.
A similar exercise was done by Blake (1991). Blake gives a
formulation of the wind stress (characterized by the friction
velocity squared) in function of the wave height and the wind
speed at 10 m.

$$C_D(u_{10}, H) = A_0 + (A_1 + B_1 H) u_{10} + (A_2 + B_2 H) u_{10}^2 \qquad (2.37)$$

A_0, A_1, A_2, B_1 and B_2 are coefficients to be determined by a least
square fit to measurements and H is the significant wave height.
This approach has the advantage that smooth flow (low wind
speeds) is modelled in a more consistent way. Also, lower wave
heights for the same wind speed give a larger drag coefficient,
in accordance with the knowledge that young wind seas are felt
as rougher than mature or fully developed wind seas. However, the
drag coefficients Blake (1991) found, seem to be consistently
lower than what other researchers have found (see Table 2.2).
This needs further investigation.
Maat et al.(1991) came to the conclusion that the most important
variables that contribute to the roughness of the sea surface
are: acceleration of gravity g, the roughness length z_o, the
friction velocity u_* and the wave velocity at the peak frequency
c_p. Note that they used the finite depth wave dispersion

29

relationship for determining the wave celerity. They proposed the hypothesis that :

$$z_o^* = \frac{gz_o}{u_*^2} = F(\frac{c_p}{u_*})$$ (2.38)

They found :

$$z_o^* = \mu \ (\frac{c_p}{u_*})^n$$ (2.39)

where $\mu = 0.7$ and $n = -1$
For a logarithmic wind profile this gives the following relation between u_* and u_{10}

$$\frac{u_{10}^2}{gz_{10}} (\frac{c_p}{u_{10}})^n = \mu^{-1} c_{DN}^{n/2-1} \ \exp(\frac{-\kappa}{\sqrt{c_{DN}}})$$ (2.40)

where c_{DN} = neutral drag coefficient.
The relationship of Maat et al.(1991) appears to be able to explain to a large extent the range of roughness coefficients found in literature. When using field data, where usually the velocity at 10 m is measured and also the frequency of the peak of the wave spectrum is determined, one obtains realistic drag coefficients. However when one wants to use the formula for laboratory data it is sometimes not possible to even find a numerical solution for Maat's equation. As an example one can take the laboratory measurements of Donelan et al.(1985), given in Table 2.3. Only the runs 2, 3, and 29 will give a solution to the logarithmic boundary layer profile and the Maat roughness length z_o. It looks as if for greater wind speeds the waves cannot resist the shear force and therefore probably break. Donelan et al. (1985) mention that ' at high values of u/c_p visual observation suggests that the waves near the peak of the spectrum are being dissipated by wave breaking'. Therefore the roughness length obtained through form drag will be reduced, and a smaller roughness length than the one predicted by Maat et al. (1991) will be in effect at the water surface. Janssen (personal communication, 1991) suggests that for laboratory data the

30

run	u(0.26) [#] [m/s]	c_p [m/s]
2	3.29	0.611
3	4.80	0.809
5	7.79	1.01
6	9.46	1.10
7	10.87	1.18
29	3.24	0.624
30	12.00	1.33

[#] : the wind speed was measured at 0.26 m ; the reference
level of 10 m in equation (2.40) should be replaced by a
reference level of 0.26 m

Table 2.4   Laboratory measurements (from Donelan et al., 1985)

relationship of Maat (equation (2.39) with $\mu = 0.7$ and $n = -1$)
is not appropriate, as field and lab data are completely
different things. The strong presence of bound harmonics in the
runs 3,5,6 and 7 (see Donelan et al., 1985), is an indication of
this difference. This may also be seen from a plot of the
Phillips' constant α_p versus fetch $\tilde{x}$ (see 2.4.1, Figure 2.9); the
best fit to laboratory data differs from a best fit to field
data.
That the air flow over the water surface is the result of a
complex interaction process, can also be found in Oost (1991),
where he indicated that the presence of irregular waves in a wave
flume experiment led to large discrepancies between measured and
calculated boundary layer parameters whereas regular waves showed
good agreement.

Equation (2.39) is quite general. One can write Charnock's
relation in that form and find : z_o^* = constant.
Equation (2.36) (Hsu, 1974) corresponds to an exponent -0.5 in
equation (2.39) if one takes the significant wave height

31

H_s ($\sim \sqrt{E}$) as a measure for the dominant wave height. Hsu's relationship can also be written as : $z_o^* \sim (gH_s/c_p^2)$;
H_s is the significant wave height and c_p the wave celerity at the peak frequency. For deep water this translates into : $z_o^* \sim s$;
s is the wave steepness, defined as H_s divided by L_p when L_p is the length and H_s the height of the dominant wave. Assuming the above relationship to be valid and also accepting u_* scaling, then one recovers Charnock's relation for a fully developed sea. Indeed for a fully developed sea the Pierson-Moskowitz frequency is given by : $f_{PM} \sim g/u_*$. Since L_p is proportional to the inverse of the peak frequency squared and therefore proportional to the friction velocity squared, the wave steepness becomes independent of wind speed and one recovers Charnock's relation.

The relationship of Maat et al. (1991) does not differentiate between form drag and wave induced drag. Although form drag and therefore also the roughness length is supposed to be determined by the high frequency waves, the peak frequency and the corresponding wave speed is used as characteristic variable in the dimensional analysis. It would be more consistent to use a characteristic value such as the Phillips' constant α_P, the Donelan constant α_D or the Toba constant α_T, which are determined by the high frequency tail of the spectrum, as the important parameter in determining the roughness length at the sea surface. This would give a direct relationship between the high frequency tail of the spectrum and the roughness length. The importance of the peak frequency in determining z_o would then be greatly reduced. Not the waves at the dominant frequency make up for the roughness of the water surface, however, their influence is felt due to the fact that the spectral shape for wind waves is self-similar (see also section 2.5).

Janssen (1991) mentions that in his experiments with a coupled ocean-atmosphere model the wave age dependency of the drag coefficient does not show any clear stratification. He gives as reason that in mixed cases of wind sea and swell no definite relation between wave age and the high frequency part of the

spectrum exists and that the wave stress is indeed determined by
the high frequency part of the spectrum.

In Figure 2.6 a number of the formulations of the variation of
the drag coefficient with the variation of the wind velocity at
10 m are brought together. The formulations of Maat et al.(1991)
and Hsu(1974) allow for a variation of the drag coefficient
depending on the wave age of the sea. Young wind sea corresponds
to a wave age (c_p/u_*) value of 10, while fully developed
corresponds to a wave age value of 40. It is hereby interesting
to note that Janssen's (Janssen, 1991) coupled atmospheric-wave
model, displays a similar spread of the drag coefficient for
varying wave age. The measured drag coefficients from a small
subset of the HEXOS data (see section 2.5) are also drawn. The
measured drag coefficients from the HEXOS experiment, display for
the same wind speed a variability which can only be explained by
a wave age dependent behaviour of the sea surface roughness.
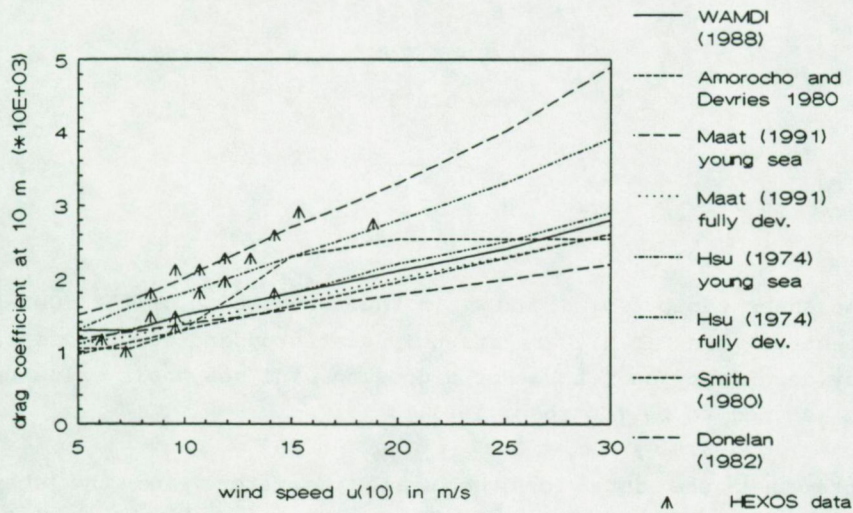
Figure 2.6 : Drag coefficient $C_D(10)$ versus wind speed u_{10}

2.4   The growth curves

2.4.1   The JONSWAP growth curves

In the late sixties a cooperative venture by an international group of scientists led to the Joint North Sea Wave Project (JONSWAP). Along a 160 km long stretch from the coast of the island of Sylt (Germany) into the North Sea, wave spectral data were collected with a number of wave and weather stations, as to be able to determine the source terms in the energy transport equation (see Chapter 3) empirically. Since the velocity at 10 m height (u_{10}) is easier to measure routinely than the friction velocity, the JONSWAP researchers scaled their measured data with this velocity u_{10}.

For the special case of a stationary, homogeneous wind blowing perpendicularly off shore, the evolution of the JONSWAP parameters is described by the following growth curves (Hasselmann et al.,1973) :

$$\tilde{E} = 1.6 \ 10^{-7}\tilde{x}$$

$$\tilde{f}_p = 3.5 \ \tilde{x}^{-.33}$$

$$\alpha_p = 0.076 \ \tilde{x}^{-.22}$$

(2.41)

$$\tilde{E}=\frac{Eg^2}{u_{10}^4} \qquad \tilde{f}_p=\frac{f_p u_{10}}{g} \qquad \tilde{x}=\frac{xg}{u_{10}^2}$$

$$E=\int E(f)\,df$$

The shape factors γ, σ_a and σ_b in the formulation of the JONSWAP spectrum (see 2.2.3), are strongly scattered and do not display any dependency on fetch. For a growing wind sea their value can be assumed to be (Günther, 1981) :

$$\gamma = 3.3 \ ; \quad \sigma_a = 0.07 \ ; \quad \sigma_b = 0.09$$

Note that the data for the scale parameters and the shape parameters were obtained by simultaneously trying to optimize these five parameters. Other fitting techniques may lead to different answers. The large variability of the shape parameters and also of the Phillips' constant α_p is attributed to the gustiness of the wind.

34

Hasselmann et al.(1973) suggest a drag coefficient $C_D(10)$ of 10^{-3} to convert the velocity at 10 m to the friction velocity u_*, so that the growth curves can also be nondimensionalized with respect to u_*. :

$$E_* = 1.6 \ 10^{-4} \ x_*$$
$$f_p^* = 1.082 \ x_*^{-.33}$$
$$\alpha_p = 0.35 \ x_*^{-.22} \qquad\qquad (2.42)$$

$$E_* = \frac{Eg^2}{u_*^4} \qquad f_p^* = \frac{f_p u_*}{g} \qquad x_* = \frac{xg}{u_*^2}$$

(x is the distance in m measured from the shoreline)
According to Janssen et al. (1987) the ratio between the power law exponents of the nondimensional peak frequency seems to be well supported by

$$E_* = 2.23 \ 10^{-4} \ (f_p^*)^{-3} \qquad\qquad (2.43)$$

For the JONSWAP growth curves nondimensionalized with the friction velocity and given above in equation (2.42), the proportionality coefficient is $2.027 \ 10^{-4}$ and differs from equation (2.43) given by Janssen et al. (1987), not only because they extended the JONSWAP data set with data from other sources, but also because the authors took the JONSWAP data set and used Wu's drag coefficient relationship (equation (2.33)) for each individual spectrum analyzed.

For the power law relationship of the Phillips' constant α_p, an exponent value of -0.4 is a better approximation for the JONSWAP data alone (Hasselmann et al.(1973)). The value -0.22 for the exponent is a result of including data from other experiments (mainly laboratory data). Janssen (1989) referring to Janssen (1984) says that a -0.5 fits both the JONSWAP data set and a data set from KNMI (Royal Dutch Meteorological Institute) quite well. It should however be emphasized that in order to have a self-similar spectrum the power law exponents n_f for f_p^*, n_α for

α_P and n_E for E. should satisfy the following relationship (Hasselmann et al., 1973) :

$$4n_f - n_\alpha + n_E = 0 \qquad (2.44)$$

The values given in the JONSWAP report yield a result of -0.11, which means that if one determines a spectrum at a particular nondimensional fetch for a given friction velocity u., then the spectrum determined by the peak frequency and the Phillips' constant α_P from the fetch laws does not yield the same amount of energy as one would expect from the energy growth curve. A power law exponent of -0.33 for the Phillips' constant α_P with a proportionality factor of 1.25 however, would give a more consistent set of growth curves (see also Chapter 6, section 6.2.3 on the initial spectrum).

2.4.2   The Phillips growth curves

Phillips (1977) assumes friction velocity scaling and gives for the energy growth curves the same relationship as given for the JONSWAP experiments (see above):

$$E_* = 1.6 \ 10^{-4} \ x_* \qquad (2.45)$$

For the peak frequency, Phillips (1977) gives the following relationship

$$f_p^* = 0.35 \ x_*^{-0.25} \qquad (2.46)$$

The growth curve for the peak frequency is similar to the findings of Donelan (see 2.4.3).
Phillips (1977) mentions that the balance of dynamical processes in laboratory measurements (the fetch x. varies between 10^2 and 10^4) appears to be quite different from those in the field. Therefore arguments to include laboratory data with field data for fitting empirical relations are rather weak. If it is done, the exponent for relating peak frequency to fetch would be -0.33 (as was the case in the JONSWAP study). Using the equations (2.45) and (2.46), the spectrum would be self similar if

36

according to equation (2.44), n_α would be equal to zero or in other words if the Phillips' constant would be really constant.

2.4.3   The Donelan growth curves

Donelan et al. (1985) did their measurements on a research tower in Lake Ontario during the years 1976-1977. Their main interest was to find out more details about the directional distribution of the wave spectrum; to establish a small number of parameters to describe the fetch limited spectrum; and to determine the dispersion relation appropriate to natural wind waves. They also used laboratory data to extend the range of observations. The efforts of Donelan et al.(1985) resulted in the following growth curves for the energy and peak frequency :

$$\tilde{E} = 8.4 \ 10^{-7} \tilde{x}^{0.76}$$
$$\tilde{f}_p = 1.85 \ \tilde{x}^{-.23} \qquad (2.47)$$
$$\alpha_D = 0.023 \ \tilde{x}^{-.13}$$

or in terms of u. with a realistic drag coefficient value of 1.5 10^{-3} (a value suggested by Battjes et al., 1987) :

$$f_p^* = 0.320 \ x_*^{-0.23}$$
$$E_* = 2.67 \ 10^{-3} \ x_*^{0.76} \qquad (2.48)$$

Note that the peak enhancement factor and the spectral width parameter are also fetch dependent (see 2.2.4 on the Donelan formulation of the wave spectrum). The growth curves (2.47) yield a nearly self similar spectrum according to condition (2.44).

2.4.4   The Kahma and Calkoen growth curves

Kahma and Calkoen (1991) tried to reconcile discrepancies in the measured growth of wind generated waves. The principal reason for doing this, was the striking difference between the growth relations deduced from the JONSWAP data (Hasselmann et

37

al., 1973) and the Bothnian Sea data (Kahma, 1981). The Bothnian Sea data showed double the amount of energy compared to the JONSWAP data for the same nondimensional fetch.

One of the main problems remains the wind speed that should be used for nondimensionalizing. Kitaigorodskii (1962) proposes u_∞, the wind speed at the upper boundary of the surface boundary layer, although he originally proposed the friction velocity u_*. Hasselmann et al. (1973) say that the velocity at 10 m is the closest to u_∞ and the easiest to measure. Others (e.g. Donelan and Pierson, 1987) have used the wind speed at half the wave height. The main problem in using u_* is that almost no direct measurements are available and researchers usually use Wu's formula to convert the measured velocity to the friction velocity. Kahma and Calkoen (1991) also use Wu's relationship. As discussed in section 2.3 this may be an oversimplification of the physics since wave age effects should not be ignored. Kahma and Calkoen (1991) went through great trouble to obtain the wind field, and after they obtained it, they further calculated the wind speed in a coordinate system moving with the group velocity of the waves at the peak of the spectrum. They say that this is the wind field felt by the waves. In such a coordinate system, fetch can equally well be interpreted as time. The scaling to obtain dimensionless parameters was then done using the average wind speed in the moving coordinate system. Looking at the wind in this way, Kahma and Calkoen (1991) remark that originally as steady wind accepted cases are in fact cases of decreasing or unsteady wind. If one looks at the steady or the steadily increasing wind cases only, the scatter in the data is reduced considerably compared to data where also unsteady or fluctuating wind cases are included. One should realize that a steady wind speed at 10 m height in a moving coordinate system, would be similar to a steady friction velocity u_* when one accepts a wave age dependent roughness length (as in Maat et al., 1991) for the logarithmic velocity profile. To obtain in a fixed coordinate system a particular value for the wind speed at 10 m height for short fetches and corresponding slow group velocity, a larger friction velocity is needed since the roughness length felt by

38

the air is greater for young wind seas than to obtain this same
wind speed at 10 m for a fully developed sea. A constant wind
speed at 10 m in a moving coordinate system, corresponds to an
increasing wind speed at 10 m in a fixed coordinate system since
the group velocity increases with fetch. The increase in wind
speed needed at 10 m in a fixed coordinate system, can be
obtained by decreasing the roughness length and thereby keeping
the friction velocity more or less constant. Therefore, for the
numerical experiments in Chapter 6 where it is tried to obtain
an optimal fit to measured growth curves by means of standard
optimization routines, u.-scaling is used. A constant shear
stress ($\equiv$ constant friction velocity) is taken as being
representative for looking at fetch limited growth of waves.
Another important factor to explain the differences between
measured growth curves that surfaced during the analysis by Kahma
and Calkoen (1991) of the WAM data base, was the effect of
atmospheric stability. Clearly, unstable stratification leads to
enhanced wave growth, especially when scaled with u_{10}. Scaling
with u. seems to bring stable and unstable groups together, but
according to Kahma and Calkoen (1991) does not remove all the
difference. Visually there seems to be no difference between the
stable and unstable case although the regression line is
different. Another possible reason for discrepancies, is the fact
that the fetch range for the stable and the unstable data are
different. One also has to realize that the stability parameters
in the JONSWAP experiment were not measured. They are guessed 20
years after the facts.
Here, only the results for the stable stratification will be
used. They are given by :

$$
\begin{aligned}
E_* &= 2.4 \ 10^{-3} \ x_*^{0.78} \\
f_p^* &= 0.358 \ x_*^{-0.244}
\end{aligned}
\tag{2.49}
$$

The above results are quite similar to the Donelan growth curves
(see 2.4.3). Note that no fetch relations for the Phillips'
constant or for the shape parameters are given in Kahma and
Calkoen (1991).

2.4.5 Fully developed sea

There is no real evidence that for a constant wind field a stationary sea state exists since in nature infinite fetch and infinite duration do not occur. However, Komen(1984) states that it is plausible that the growth rates for well developed seas are strongly reduced, and that most wave models take the Pierson-Moskowitz spectrum as a stationary limiting spectrum. Accepting u.-scaling as the correct scaling, Komen et al.(1984) convert the measurements of Pierson and Moskowitz(1964) to

$$f_{PM}^* = f_{PM}\frac{u_*}{g} = 5.6\ 10^{-3}$$

$$E_*^{PM} = \frac{E^{PM}g^2}{u_*^4} = 1.1\ 10^3 \tag{2.50}$$

$$\alpha_{PM} = 0.0081$$

A fully developed sea should be reached at a nondimensional fetch x. of $8.46*10^6$ according to the JONSWAP growth curve for the peak frequency, and at $6.875*10^6$ according to the JONSWAP growth curve for the total energy. For the Donelan growth curves this becomes $4.35*10^7$ for the peak frequency and $2.44*10^7$ for the total energy respectively. Again other values will be obtained for the other sets of growth curves (e.g. $1.811\ 10^7$ for the Kahma and Calkoen energy growth curve). This illustrates that the transition to an asymptotic state is not clear-cut. For practical application in wave models the uncertainty of when or where a fully asymptotic stage is reached, is not so important since the growth rates in that area should already be reduced considerably and for high wind speeds they correspond to such large fetches that these do not occur in nature anyway.
In the optimization exercise (see Chapter 5 and Chapter 6), one will have to attach little weight to calculated values in the transition zone and only try to match the growing part and the fully developed part. The growing part extends for about two orders of magnitude in x., i.e. from $5*10^4$ to $5*10^6$, while the fully developed part can be seen as starting from about $5*10^7$. Komen et al.(1984) showed that principal features of the

40

Pierson-Moskowitz spectrum such as the total energy, the peak frequency and the Phillips' constant α_p can be obtained for large nondimensional fetches(they take a value of $1.2*10^8$ for x. as being representative). However, the detailed directional distribution of the energy differs from a simple $\cos^2\theta$ or from the more sophisticated distribution as given by Hasselmann et al.(1980).

The growth curves as suggested from the JONSWAP experiments (section 2.4.1), by Phillips (section 2.4.2), by Donelan (section 2.4.3) and by Kahma and Calkoen (2.4.4), are drawn in Figures 2.7 to 2.9. Also the asymptotic level (fully developed sea) is indicated.
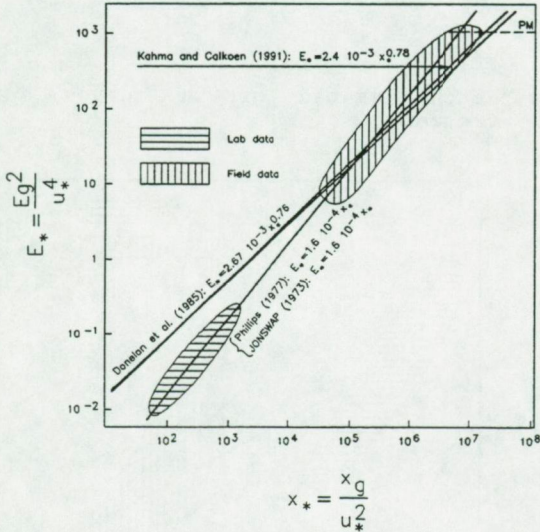
Figure 2.7 : Fetch limited growth curves for the energy
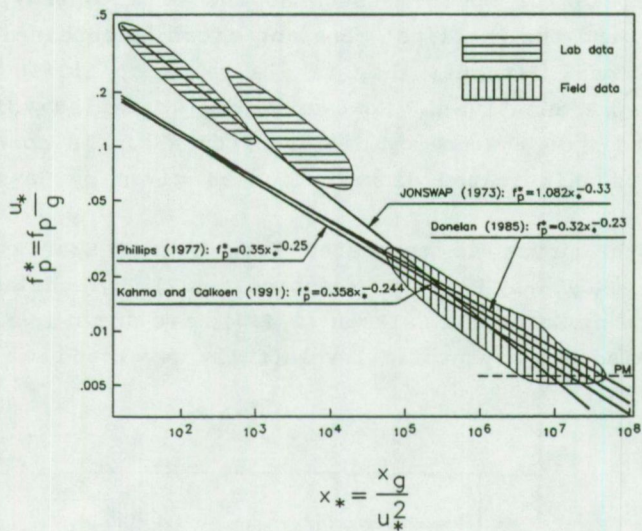
Figure 2.8 : Fetch limited growth curves for the peak frequency
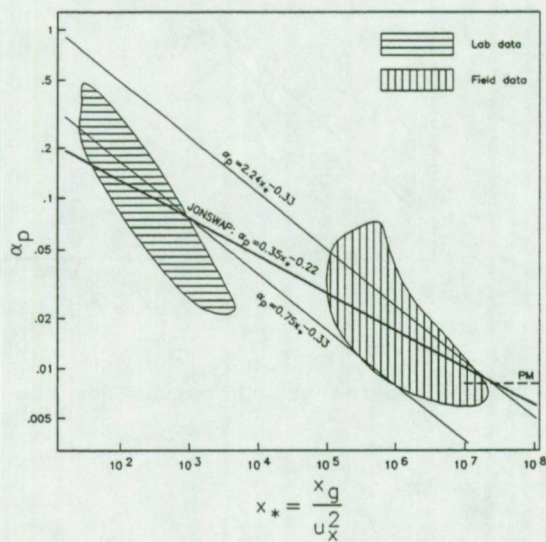
Figure 2.9 : Fetch limited growth curves for the Phillips' constant α_p

2.5   Making a link between the wave spectrum and the atmospheric boundary layer

2.5.1   Introduction

From the preceding discussions we feel that there is a connection between the parameters describing the atmospheric boundary layer and the parameters describing the wave spectrum. For the atmospheric boundary layer, the relevant parameters are the friction velocity u. and the roughness length z_0. For the wave spectrum the relevant parameters in the saturation range are the Phillips' constant α_P for the JONSWAP spectrum, the Toba constant α_T for the Toba formulation of the spectrum, and the Donelan constant α_D for the Donelan spectrum. Together with the characteristic velocity (u. or u_{10}) and also the peak frequency f_p, which determines the wave age, they determine the main characteristics of the wave spectrum. In section 2.4 the growth curves obtained during different measuring campaigns were given. In what follows the JONSWAP, Donelan, and Toba formulations for the energy spectrum are compared to see under which conditions they tell the same story. Finally it is attempted to make a link between the sea surface elevation spectra and the logarithmic formulation of the atmospheric boundary layer.

2.5.2   Relating the JONSWAP, PM, Donelan and Toba formulations in the saturation range

The saturation range is the frequency range of the spectrum where the different processes are in equilibrium. It should no longer be affected by the wind speed. This translates into a stable shape of the spectrum for frequencies substantially larger than the peak frequency. Comparing the JONSWAP (equation 2.14), the PM (equation 2.16), the Toba (equation 2.17), and the Donelan (equation 2.19) expressions for the wave energy in the

equilibrium range, one sees that they are equal under the following conditions :

$$E_J = E_D = E_T$$

$$\alpha_p g^2 (2\pi)^{-4} f^{-5} = \alpha_D \, g^2 (2\pi)^{-4} f_p^{-1} f^{-4} = \alpha_T \, g \, u_* \, (2\pi)^{-3} f^{-4}$$

(2.51)

The JONSWAP and PM formulations contain an f^{-5} tail. This tail has to be replaced by an f^{-4} to make it compatible with the Donelan and Toba expression. To do this one could take a particular frequency, f_r, representative for the tail and change f^{-5} dependency into $f_r^{-1} f^{-4}$ dependency. Note that

$$f_p \leq \quad f_r \leq 3 \, f_p$$

Setting the JONSWAP or PM spectrum equal to the Toba spectrum, the following u_* nondimensionalized growth curve for α_p is obtained for a value of 0.11 for α_T (Battjes et al. (1987) and Kahma (1981)):

$$\alpha_p = 0.75 \, x_*^{0.33} \text{ for } f_r = f_p$$

(2.52)

$$\alpha_p = 2.24 \, x_*^{-0.33} \text{ for } f_r = 3 \, f_p$$

(2.53)

Note that the $x_*^{-0.33}$ dependency for the Phillips' constant α_p was also found by Kahma (1981). He calculated the α_p values the same way as was done by Hasselmann et al. (1973), i.e., an average value in the frequency range between 1.35 f_p and 2 f_p. Plotting this onto Figure 2.9 one sees that these curves do not conflict with the JONSWAP measurements. The curves form more or less a lower and an upper limit for the α_p values.
Equalling the Donelan expression with the Toba expression, one obtains :

44

$$\alpha_D = \alpha_T\, u_* \, f\, 2\pi \, / \, g$$
$$2\pi\alpha_D = 2\pi\alpha_T\, (u_*/C_p)$$
$$or \tag{2.54}$$
$$2\pi\alpha_D = 0.7\, (u_*/C_p)$$

This is exactly the same expression as equation (2.39) of Maat et al. (1991) for the nondimensional roughness height of the atmospheric boundary layer. We could state that :

$$2\pi\alpha_D = z_o^* \tag{2.55}$$

2.5.3 Experimental data

A small subset of the preliminary HEXMAX (the HEXOS Main Experiment) data set was made available to the author by the HEXOS team. HEXOS was a comprehensive experiment including field experiments on and around the Dutch research platform, Meetpost Noordwijk, as well as wind and wind-wave tunnel experiments concerning flow distortion due to the platform and concerning investigation of processes near the air-sea interface (Katsaros et al.,1987 ; Smith et al.,1990). The small subset of preliminary data used here, consisted of the neutral drag coefficient, the wind speed at 10 m, the friction velocity, the peak frequency f_p, the phase speed c_p at the peak frequency, the significant wave height and the one-dimensional frequency spectrum. Only the one-dimensional frequency spectrum was available. The frequencies were spaced equidistantly with the first frequency at 0.01021 Hz, the distance between two frequencies Δf equal to 0.01021 and the maximum frequency at 1.021 Hz. The data set is the same as the one used by Maat et al. (1991). As far as it was possible all cases where swell was present, were removed. The HEXMAX friction velocity data were obtained with a sonic anemometer (eddy correlation method); the wave data with a waverider buoy. The flow distortion error of the vertical momentum flux was estimated around 10%, while the calibration error of the sonic anemometer

45

was better than 1% on average (Maat et al.,1991). The data used were not corrected yet for flow distortion. Methods for correction have recently been developed (Oost, 1991). The newly corrected data do not differ much from the preliminary data (Oost, personal communication (1992)).

It was suggested above that the nondimensional roughness length could be set equal to the Donelan constant taking into account a factor 2π. To do this, the data, originally measured on a linear frequency grid, were interpolated onto a logarithmic frequency grid with an initial frequency of 0.0418 Hz and $f_{i+1} = f_i(1 + CO)$, where CO is equal to 0.1. This logarithmic frequency grid corresponds to the WAM frequency grid (WAMDI, 1988), see also Chapter 4. By doing this, the data are smoothed, reducing the inherent spread on spectral estimates and making it easier to fit a spectral formulation to the data. The Donelan constant was obtained by fitting an f^{-4}-tail in the frequency range between 1.5 and 2.5 times the peak frequency. The result is displayed in Figure 2.10.
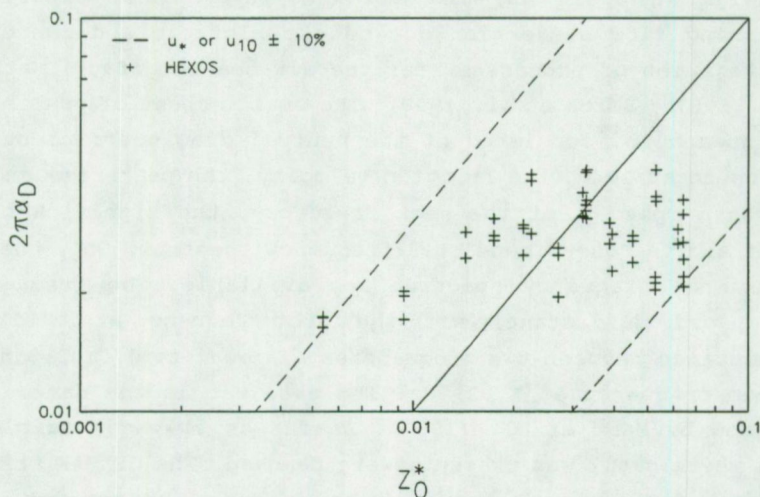
Figure 2.10 :   The Donelan constant α_D in function of the nondimensional roughness z_o^*.

The full line represents the suggested relationship. On first view the suggested relationship gives a good representation of the data. On the other hand the range of values for the Donelan constant α_D corresponding to a particular value of nondimensional roughness is large. However, when we think how the roughness length is obtained from the measurement of u_{10} and u_*, we should not be totally surprised. We used the following formula :

$$z_0 = \frac{10}{e^{\frac{\kappa u_{10}}{u_*}}} \qquad (2.56)$$

Considering a 10 % error for the wind speed at 10 m or for the friction velocity as acceptable, a factor 2 to 3 difference is introduced in the calculated roughness length because of the exponential function. This is also the typical order of the maximum difference between the proposed curve and the measured values, indicated by the dashed lines for a factor 3. We cannot make definite conclusions as to the correctness of the proposed curve. A more extensive data set will be necessary to decide one way or the other. Note also that measured wind speed values such as the velocity at 10 m and the friction velocity u_* are average values over a period of 1 hour while the wave data were averaged over a period of 20 minutes.

In Figure 2.11 the surface roughness is set out against wave age (c_p/u_*). A number of previously proposed parametrizations are also displayed. Taking a drag coefficient of $1.5*10^{-3}$ (Battjes et al., 1987), we can rewrite equation (2.20) as follows:

$$2\pi\alpha_D = 0.225(u_*/c_p)^{0.55} \qquad (2.57)$$

We see in Figure 2.11 that this gives an overestimate of the data used. The drag coefficient suggested by Battjes et al. (1987), was on the basis of the Charnock relation with the Garratt (1977) constant (Table 2.2, equation (2.33)). No friction velocity measurements were available. In Figure 2.11 the relationship of the nondimensional roughness length obtained by Hsu(1974), is also plotted.

47
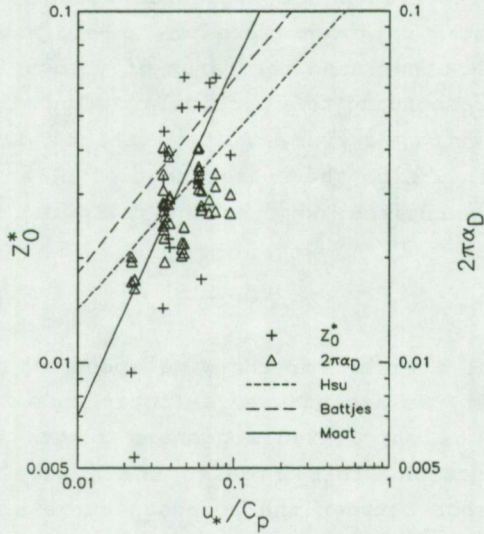
Figure 2.11 :   The surface roughness in function of wave age

Hsu's relationship (2.36) has been rewritten assuming that :

-   $H = 4 \sqrt{E}$
-   E given by the JONSWAP growth curve (u. scaling)
-   f_p also given by the JONSWAP growth curve (u. scaling)

so that

$$z_o^* = 0.14 \ (u_*/c_p)^{0.5} \qquad\qquad (2.58)$$

Under the different assumptions made, equation (2.58) is still within the scatter of the data of Maat et al.(1991). It also fits the calculated Donelan constants quite well.

It is of interest to look at the data in terms of the drag coefficient since we can get rid of the exponential function.

$$C_D(z) = (\frac{u_*}{u(10)})^2 = \left[\frac{\kappa}{\ln(\frac{z}{z_o})}\right]^2 \qquad (2.59)$$

If we replace z_o in equation (2.59) by the relationship suggested in equation (2.55) or the one suggested by Maat et al.(1991) in equation (2.39), we obtain the results as displayed in Figure 2.12.
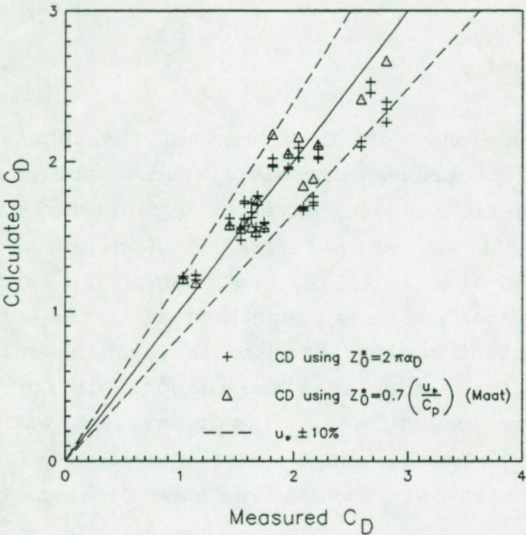
Figure 2.12 : Calculated versus measured drag coefficient

It is not surprising that the results for the Maat et al. (1991) substitution of z_o are very good, because the data set used here, is a part of the data set they used to establish their relation. The question is whether the apparent deviation of the one to one line for the substitution of z_o by the relationship suggested here, can be explained. If we look at the influence of the measurement error, particularly the error in measuring the fluctuating component of the horizontal and vertical velocity, we introduce large errors in the measured drag coefficients. If

indeed the measured friction velocity is overestimated, it would hardly affect the calculated drag coefficient. It would however, seriously overestimate the measured drag coefficient, thereby producing a biased picture as can be seen in Figure 2.12. In Figure 2.12, it is indicated what happens to drag coefficients which are correctly calculated (the full line) and which are displayed against a measured but by 10 % over- or underestimated drag coefficient. The value of 10% can be accounted for on flow distortion effects alone (see above). Nearly all calculated values fall within this assumed error band.

2.5.4   Discussion

From the above it is clear that the saturation range of the frequency spectrum is closely linked to the roughness length of the atmospheric boundary layer. The published data by Maat et al.(1991), Battjes et al.(1987), Donelan et al.(1985), Kahma(1981) and also Hsu(1974) are strongly in favour of setting the nondimensional roughness length equal to the Donelan constant (taking a constant factor into account). This would indeed mean that the high frequency waves are responsible for the roughness of the sea surface. This is also consistent with the idea of Wu(1986) that only the short waves provide resistance through form drag and that only those waves should relate to a roughness length.

The findings of Maat et al.(1991) cannot be applied to very young wind seas or to very short fetches as in laboratory tanks. Possibly for these very young wind seas or for the very short laboratory fetches the obtained waves are not gravity dominated. One has to realize that obtaining a realistic turbulent wind spectrum in a wind-wave tank is quite difficult since there is usually no fetch available to create it, whereas in field experiments the wind is inherently turbulent since the friction over land or over the sea has already created a turbulent wind spectrum. It remains to be investigated if the suggested relation

50

between the Donelan constant characterizing the high frequency range of the wave spectrum and the nondimensional roughness length remains valid for very young wind seas and for laboratory situations. The suggested relationship does have the advantage that it limits the roughness length and corresponding C_D to realistic values even for these situations. Laboratory waves may be of a different nature and no longer have a spectral shape similar to field waves. Another integral parameter of the wave field may then be necessary to represent the roughness length, an integral parameter of the boundary layer in the air.

The merits of the JONSWAP formulation cannot be overlooked. It has been successfully used for many years in many applications and the familiarity of many researchers and engineers with the JONSWAP expressions, guarantee that it will be used for quite a bit longer. One feels intuitively, that the Phillips' constant α_P, being similar to the Donelan constant, could also be considered as a measure for the roughness at sea. However, the data published recently are in favour of an f^{-4} tail and the use of the Donelan spectrum or equivalently the Toba spectrum should be encouraged. The simple link, if confirmed, between the saturation range of the sea surface elevation spectrum and the roughness length of the atmospheric boundary layer, make it also quite elegant.

2.6   Conclusions

The JONSWAP spectrum, the Donelan spectrum, and the Toba spectrum (as interpreted by Battjes et al. (1987)), are very similar for fetch limited conditions. For a fully developed sea, they look quite different. Only the Donelan spectrum is close to a Pierson-Moskowitz spectrum under fully developed conditions.

The Toba spectrum in combination with a peak width parameter σ as defined for the Donelan spectrum, combines the merits of a strongly peaked spectrum for young wind seas and a broader spectrum for a fully developed sea without the need to define a

51

wave age dependent peak enhancement factor γ. The use of this spectrum should be encouraged.

The variability of the drag coefficient for the same wind speed can be explained by a wave age dependent behaviour of the roughness at sea. At the same wind speed, young waves are felt as rougher compared to fully developed waves.

To obtain wave parameters which are nondimensionalized with the friction velocity, the currently available wave data should be reanalysed using a wave age dependent drag coefficient.

The nondimensional roughness length z_o^* is closely related to the Donelan constant α_D. When equalling the Donelan spectrum to the Toba spectrum in the high frequency range, i.e., the tail or the saturated frequency range, α_D and z_o^* show the same wave age dependency. This confirms the notion that the high frequency waves are mainly responsible for the form drag.

The wave age dependency of the roughness length, and therefore also of the drag coefficient C_D, for young wind seas or for short fetches cannot be given by the formulation of Maat et al.(1991). This may be an indication that the shear stress exerted onto the waves cannot exceed a certain limit. When exceeding this limit, the waves may break thereby reducing the form drag and therefore also reducing the exerted shear stress.

It appears that the friction velocity u. is the important scaling factor. The above conclusions are possible only because the friction velocity has been used as the scaling velocity.

3 The gravity wave energy transport equation

3.1 Introduction

The energy to be found in ocean waves is the result of the different forces involved. In this work only wind waves are studied. The action of the wind is considered as the only source of energy input. The total energy accumulated over time or the total momentum gained by the wind can therefore not be larger than what has been put in by the wind. Wave breaking (whitecapping) and bottom friction are dissipative processes. They can only extract energy from the wave field. The wave field can be looked at as consisting of an infinite number of individual linear waves. It is possible that a number of these waves form combinations in which energy is exchanged through nonlinear interactions. The above processes, i.e. wind input, dissipation through wave breaking and bottom friction, and the exchange of energy between different wave components through nonlinear interactions form the basis of the current understanding of the energy balance of wind generated waves. Other processes (such as viscous dissipation) are not considered important, at least not for appreciable wind speeds and in the region of our interest which is the gravity wave region. In this chapter one will find the expressions for the energy and the momentum transport equation together with physical background on the different source terms for deep water waves.

3.2 The energy transport equation

The energy transport equation in deep water can be written as (Sobey, 1986) :

$$\frac{dF}{dt} = S_{tot}$$
$$\Downarrow$$
$$\frac{\partial F}{\partial t} + \frac{\partial F}{\partial x}\frac{dx}{dt} + \frac{\partial F}{\partial y}\frac{dy}{dt} + \frac{\partial F}{\partial k_x}\frac{dk_x}{dt} + \frac{\partial F}{\partial k_y}\frac{dk_y}{dt} = S_{tot}$$

(3.1)

where

  x,y : position coordinates

  $F = F(\overline{k},t;x,y)$: wavenumber-direction energy spectrum at position (x,y)

  t :   time

  $\overline{k} \equiv (k_x,k_y)$: wavenumber vector

  S_{tot} : total source term, a function of wavenumber, position and time

The first term on the left hand side represents the temporal gain of energy. The second and third term indicate that there is propagation of energy, and the last two terms take care of the shoaling and refraction of waves. The source terms should include all physical processes that contribute to the spectral evolution. Note that shoaling and refraction as such are already taken care of on the left hand side in the equation. Dissipation due to bottom friction as a result of moving into shallow water should on the other hand, be explicitly modelled.

In one dimension and in deep water where there is no shoaling effect, i.e., the wavenumber does not change with water depth and only depends on the frequency, one obtains the simple equation (Komen et al., 1984) :

$$\frac{\partial E}{\partial t} + c_{gx}\frac{\partial E}{\partial x} = S_{tot} = S_{nl} + S_{in} + S_{diss}$$

(3.2)

where

c_{gx} : group velocity in the x-direction $\equiv dx/dt$

$E = E(f, \theta; x)$

θ :   angle with respect to the main wave direction x

f :   frequency

$S_{nl} = S_{nl}(f, \theta)$:   nonlinear wave-wave interactions source term

$S_{diss} = S_{diss}(f, \theta)$:   dissipation through whitecapping source term

$S_{in} = S_{in}(f, \theta)$:   wind input source term

$2\pi f = \sqrt{gk}$:   the dispersion relation in deep water

The energy transport equation (3.2) in deep water is written in the frequency-direction space since it makes interpretation of results easier. One has to bear in mind however that energy is not necessarily conserved for wind waves. This is only so in absence of currents. In cases where there are nonuniform currents, the wave energy is not conserved since the horizontal momentum transport of the wind waves can exchange energy with the mean current (Phillips, 1977; Tolman, 1990).

3.3   The energy and momentum balance

The wave field receives its energy from the air flow above the waves. It is not so difficult to see that the shear stress supplied by the air and which is defined as

$$\tau = \rho u_*^2 \qquad\qquad (3.3)$$

has to be found back at the water surface (ρ_a is the air density and u. is the friction velocity). Note that the momentum transfer is given here per unit of time and per unit of area. The energy available in the wind will be either transferred to the wave field or lost through the generation of turbulence in the air. The momentum transferred from the wind field will be either advected away by the wave field or lost through whitecapping

55

dissipation and additionally through bottom friction in shallow water.

The part of the momentum transferred to the water surface advected away by the wave field has been estimated by Hasselmann et al. (1973):

$$\tau_{ad} = \rho_w g \int_0^{\infty} \frac{k_x C_{gx}}{2\pi f} \frac{dE(f,\theta)}{dx} df d\theta = \frac{3}{8} \rho_w g \frac{dE}{dx} \tag{3.4}$$

where τ_{ad} =   the advection term in the energy transport equation

   k_x =   wavenumber in the x-direction

   c_{gx} =   group velocity in the x-direction

   f =   frequency

The factor 3/8 comes from the fact that a $\cos^2\theta$ directional distribution was assumed to evaluate the above integral.

Taking the JONSWAP growth curves (equation (2.42)), one obtains :

$$\frac{dE}{dx} = \frac{1.6 \ 10^{-4}}{g} u_*^2$$

$$\downarrow$$

$$\tau_{ad} = \frac{3}{8} \times 1000 \times 1.6 \ 10^{-4} \ u_*^2$$

In percentage of τ and with a value of 1.23 kg/m³ for the air density ρ_a, this results in :

$$\frac{\tau_{ad}}{\tau} = \frac{0.06 \ u_*^2}{1.23 \ u_*^2} = 0.049$$

This means that the momentum advected away by the wave field is only about 5% of the total momentum supplied by the shear stress in the surface layer. This is equal to the net momentum advected away by the wave field and also equal to what is really put into

the wave field and not dissipated. The net momentum transfer can be written as :

$$\tau_{ad} = \rho_w g \int_0^\infty \int_0^{2\pi} \frac{\overline{k}}{2\pi f} S_{tot} \, df d\theta \qquad (3.5)$$

Remark that for a fully developed sea equation (3.4) states that no momentum is advected away by the wave field since the energy then does not change any more with fetch.

Donelan (1979) suggests that up to maybe 25% of the locally transferred momentum may be retained and advected away by the wave field. Donelan tries to prove this by field and laboratory measurements. The field measurements confirm greatly the 5% order of magnitude proposed by Hasselmann et al. (1973). The laboratory measurements give values up to 30%. The scatter is so great that it seems unjustified to attach too much value to these measurements.

For the individual source terms we write, following the above expression :

- momentum supplied by the wind

$$\tau_{in} = \rho_w g \int_0^\infty \int_0^{2\pi} \frac{\overline{k}}{2\pi f} S_{in} df d\theta \qquad (3.6)$$

- momentum dissipated in the wave field

$$\tau_{diss} = \rho_w g \int_0^\infty \int_0^{2\pi} \frac{\overline{k}}{2\pi f} S_{diss} df d\theta \qquad (3.7)$$

- momentum exchanged through nonlinear interactions :

$$\tau_{nl} = \rho_w g \int_0^\infty \int_0^{2\pi} \frac{\overline{k}}{2\pi f} S_{nl} df d\theta \qquad (3.8)$$

The nonlinear interactions should conserve energy and momentum. Whatever is obtained after integrating is due to shortcomings in the numerical formulation as the frequency integration interval and the simplification in the formulation (see discrete interaction approximation in Chapter 4).

57

3.4   The wind input term

3.4.1   The physics

3.4.1.1   *The Phillips' and Miles' mechanisms*

That waves can be generated by wind is clear to everyone. The detailed mechanical processes and the verification of these processes by measurement however are not so evident.

Jeffreys(1924,1925) attributed the growth of waves to a 'sheltering' effect in the lee of the waves. The induced pressure difference across the waves was responsible for the energy input into the waves. Although Jeffreys assumption is straightforward, his theory did not match subsequent measurements (Phillips(1977)).

The more elaborate theory from Phillips (1977) investigates the stress distribution on the moving water surface under the influence of wind. Both surface pressure and shear stress influence wave growth. One can picture the stress fluctuations on the water surface as caused by a combination of turbulent eddies in the wind and of the shear stress at the water surface due to the air flow over the irregular waves.
The initial generation of waves is quite often attributed to the so called Phillips' mechanism. Phillips (1957) sees the wind as composed of atmospheric eddies ('puffs' and 'lulls') which travel along the initially undisturbed water surface with a certain 'convection' velocity. Although the mathematical definition of this convection velocity is complicated, for the physical understanding of the process it is sufficient to know that the convection velocity of eddies with wavenumber k is of the same order of magnitude as the mean velocity at a height k^{-1} above the water surface. This means that small eddies are carried close to the surface at a lower speed than larger eddies which extend higher and which will travel at a faster speed (see also Figure 1). The eddies and the consequent pressure distribution will

carry components (next to many other components) with a wavenumber and a frequency which coincide with that of the free surface water waves. There is a 'resonance' effect between the eddies at a particular wave number and frequency, and the waves which have the same wavenumber k and travel in the same direction (i.e. the wind direction). If the pressure pattern were rigidly travelling, the phase difference between the waves and the eddies would remain the same and there would continuously be an input from the wind. However the pressure pattern is randomly evolving in amplitude and phase with respect to the waves. This random effect makes the waves grow less fast than if the phase would remain constant. The final result is that the energy of the waves grows proportionally to the energy in the pressure fluctuations or linearly in time.

A second mechanism of wave generation is associated with the existence of a pressure difference between the windward and the leeward face of the wave. It is quoted under the name Miles' mechanism and differs from the pressure difference as described by Jeffreys(1924,1925 /see above). The theoretical principles on which the mechanism is based are explained by Stewart (1974) in an easy to understand way. The main ideas are briefly highlighted below. For more details the reader is referred to the original papers of Miles (1957, 1959 and 1962) and to the book by Phillips (1977). First Stewart (1974) assumes that in the case of a simple sinusoidal wave, it does not seem unreasonable to accept a pressure field which has the same length characteristics (i.e. wavelength) as the underlying wave. Applying Bernoulli's law for the case that there is no shear stress in the system, Stewart shows that a Reynolds stress transporting momentum downwards exists when streamlines are not in phase nor in opposite phase with the pressure fluctuations. This corresponds to a slower flow on the windward face of the flow, i.e. increased pressure and a faster flow on the leeward face of the wave, i.e. reduced pressure (see Figure 1.b). In the case of a shear flow above the waves, one can look at the flow in a coordinate system fixed relative to the waves. The mean velocity profile then looks like in Figure 1.b. There is a 'critical height' where the mean motion

Phillips :

Miles :

streamlines above a wave (no shear flow)

wind

critical height

c

view when moving in a reference axis
system fixed to the waves (shear flow)
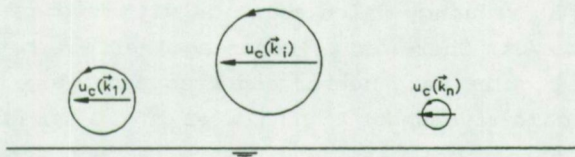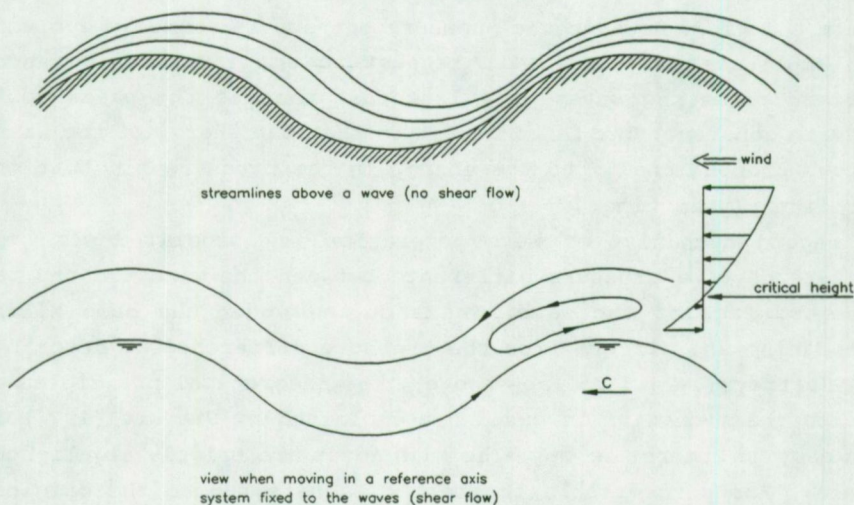
Figure 3.1 : The Phillips' and Miles' mechanism

of the air is stationary. Below the critical height the mean
airflow is in the opposite direction of the mean air flow above
the critical layer. Due to the shear stress an asymmetrical flow
pattern is created. This gives a gradient in the vorticity as one
moves upwards. It is this vorticity change that creates a phase
difference between the different streamlines in the air, a phase
difference necessary for the development of a pressure difference
between the windward and the leeward face of the wave. The
effectiveness of the wave generating mechanism then depends upon
the rate of change of mean vorticity as one moves through the
critical layer or in other words on the curvature of the mean
profile.

The shear stress at the water surface is due to the air flow over the waves and from the turbulent eddies near the surface. The total surface stress is then the sum of directly induced variations (pressure + shear) and the random variations due to atmospheric turbulence. The turbulent stresses are an energy input over a large spectral range and are in fact not considered in the theory of Phillips and Miles. The directly induced stresses however provide a selective 'feedback', augmenting the growth of certain components.

The final result of the thoughts of Phillips and Miles is that the linearized gravity equations solve to (Phillips(1977) :

$$F(\overline{k},t) = \frac{\pi \Pi(\overline{k},\omega)}{\rho_\omega^2 c^2} \left[\frac{\sinh \mu \omega t}{\mu \omega} \right] \qquad (3.9)$$

where $F(\overline{k},t)$:   displacement spectrum of the water surface

$\Pi(\overline{k},\omega)$:   three dimensional wavenumber, frequency spectrum of the random atmospheric pressure fluctuations

μ :   coupling coefficient between the induced surface stress and the water surface

c   :   phase speed of the wave

Equation (3.9) can be separated in two parts :
-   $\mu \omega t \ll 1$:   linear growth ; there is no coupling between wind and waves ; this is the case when t is small,
-   $\mu \omega t \gg 1$:   exponential growth ; coupling between wind and waves ; this is the case when t is large.

Equation (3.9) can be written in terms of the frequency spectrum $E(f,\theta)$ of the waves.

Since in deep water

$$F(\overline{k},t) = \frac{cc_g}{2\pi\omega}E(f,\theta)$$ (3.10)

we can write that

$$E(f,\theta) = \frac{2\pi^2\omega\,\Pi(\overline{k},\omega)}{\rho_w^2 c^3 c_g}t + \frac{\pi^2\omega\,\Pi(\overline{k},\omega)}{\rho_w^2 c^3 c_g \mu\omega}e^{\mu\omega t}$$ (3.11)

and therefore

$$S_{in} = \frac{\partial E(f,\theta)}{\partial t} = a + b\,E(f,\theta)$$

$$a = \frac{2\pi^2\omega\,\Pi(\overline{k},\omega)}{\rho_w^2 c^3 c_g}$$ (3.12)

$$b = \mu\omega$$

The linear term a in equation (3.12) is responsible for the
initial excitation of the sea and is the so called Phillips'
mechanism as it was described first by Phillips in 1957. It only
includes the effects caused by pressure fluctuations due to
turbulent eddies. Or as Snyder et al. (1990) put it : '... a is
a known linear function of the generally unknown energy spectral
density of turbulent air pressure fluctuations; it is thought to
be generally small but may be incorporated close to an upwind
land boundary ....'. In wave models the linear term in the source
function for the wind input is usually dropped since it is
quickly overruled by the exponential term (Hasselmann, S.(1987);
Tolman(1989)). Barnett (1969) gives an expression for the linear
term but remarks that it leads to too high energy prediction at
low frequencies.
The exponential term b in equation (3.12) represents the so
called Miles' mechanism where there is 'feedback' or coupling
between the wind and the waves. The normal stress in phase with
the wave slope increases with increasing wave slope, and
therefore supplies more and more energy to the waves. The rate
of growth of the waves shows the characteristics of an
instability.

Riley et al. (1982) extend Miles' inviscid theory of surface wave generation in two ways. First of all they include viscous effects so that the logarithmic profile can be extended down to the water surface. Secondly they include the effects of air turbulence. The surface pressure is shown to depend very much on the flow condition being aerodynamically smooth or rough. The authors consider the results of their theory at the same time discouraging and encouraging ; discouraging because the distance between theoretical and observational results seems to be increased, encouraging because the effect of turbulence accounts for observed wave damping in adverse wind.

3.4.1.2   The Janssen quasi-linear theory for the spectrum of wind-generated waves

The term quasi-linear reflects the approximation that is made by assuming that waves exist independently from one another and interaction between waves can be neglected. The energy density of these waves then changes in time only due to linear effects. This is in accordance with Miles' resonance mechanism (Janssen, 1982). Janssen's theory predicts a limitation of the amplitude of an initially unstable water wave for large times ($t \rightarrow \infty$). In the process he neglects air turbulence and nonlinear wave-wave interactions and although experimental evidence for his theory is hard to find, he concludes that the effect of waves on the wind profile may be important in the evolution of the wave spectrum.

The application of Janssen's theory to wave forecasting needs some more explanation. Although the coupling of an atmospheric model and an ocean wave model is outside the scope of this research work, it does need some attention first of all because the Janssen's physics are implemented in the Cycle 4 version of the 3G-WAM at the ECMWF in Reading (Janssen (1992), personal communication) and secondly because results presented in Monbaliu (1991), also indicate a possible dependency of the wind input term on the sea state.

63

Although Janssen (1991) points out that his quasi-linear theory has restricted validity since for high frequency waves the effects of viscosity and of air turbulence are not taken into account, he finds realistic results when he models the energy loss to the short gravity-capillary waves by means of a roughness length z_0 (Charnock's relation in Janssen (1991)). The momentum equation in air becomes :

$$\frac{1}{\rho_a}\frac{\partial U}{\partial t} = \frac{D_w}{\rho_a}\frac{\partial^2 U}{\partial z^2} + \frac{\partial}{\partial z}\frac{\tau_{turb}}{\rho_a} + \frac{\partial}{\partial z}\frac{\tau_{visc}}{\rho_a} \tag{3.13}$$

$\tau_{turb} = \rho_a l^2 \left|\frac{\partial U}{\partial z}\right| \frac{\partial U}{\partial z}$:   turbulent stress

with $l = \kappa z$ (l is a mixing length, κ is the von Karman constant and z the height above the mean water surface)

$\tau_{visc} = \rho_a \nu_a \frac{\partial U}{\partial z}$:   viscous stress (ν_a is the kinematic viscosity of air)

D_w :   wave diffusion coefficient (a rather complex function of the wave spectrum)

The wave diffusion coefficient is based on the quasi-linear theory and it represents the effect waves have on the wind. As a term in the momentum balance it is similar to the viscous stress and one can look at it as if the waves experience an additional stress compared to the air flow over a flat plate (= the wave induced stress τ_w). In steady state the momentum balance can be integrated over z to give :

$$\tau_w + \tau_{turb} + \tau_{visc} = \tau = \rho_a u_*^2 \tag{3.14}$$

The wave induced stress reflects the momentum lost from the air and should be found back in the momentum gained by the water waves. According to Janssen (1991) the growth rate of waves can be written as a function of the wave age ($\equiv c_p/u_*$), the local wave steepness ($\equiv k^4E$) and the nondimensional roughness (gz_0/u_*^2). In case the local wave steepness and the nondimensional roughness can be written as a function of the wave age, the growth rate or

the coupling between wind and waves can be considered as depending on the wave age only. Numerical experiments in Janssen (1989) showed a strong dependency of the aerodynamic drag on the wave age. With a wind input term according to Snyder et al. (1981) and adapted by Komen et al. (1984) (see equation (3.15) and (3.16)), and for a simple spectral shape, Janssen (1989) obtained for a strong dependency of the Phillips' constant α_P on the wave age ($\alpha_P \sim (c_p/u_*)^{-3/2}$), a wave induced stress which is larger than the total stress (Figure 1 in Janssen (1989)). This cannot be correct. However, Janssen's coupled theory reduces the wave induced stress to realistic values (Figure 5 in Janssen (1989)). It can also partly be attributed to the fact that the chosen dependency of the Phillips' constant α_P on the wave age may be too strong. A dependency of the Phillips' constant α_P on the wave age which is not so strong (e.g. $\alpha_P \sim (c_p/u_*)^{-1}$) is probably more appropriate. An exponent -1 was also suggested in Chapter 2 when the saturation range of the different spectral formulations (JONSWAP, Donelan and Toba) were compared to one another.

The growth of the low frequency waves depends on the presence of high frequency waves. The high frequency waves make the air flow rougher and therefore influence the position of the critical height, i.e. the height where the wind speed equals the wave speed (an important parameter in the Miles' resonance mechanism theory). According to Janssen (1989), the growth rate is reduced for young wind sea compared to old wind sea. Janssen says that this can be understood by realizing that for rougher air flow (young wind sea) and fixed nondimensional phase speed, Miles' resonance mechanism between wave and air flow occurs at a larger height than for smoother air flow (old wind sea). A similar conclusion regarding the wind input term dependency on the wave age was found in the quantitative approach of calculating a best fit to the JONSWAP growth curves (Monbaliu, 1991). The reduction in growth rate for young wind sea compared to the one for old wind sea is about a factor 2 (Janssen (1989); Monbaliu (1991)). This will also have an influence on the air flow velocity profile

over the waves. A young wind sea will be characterized by a larger roughness length than an old wind sea.

3.4.2 Expressions for the wind input term

In what follows, the discussion is limited to the coupling coefficients μ as given in equation (3.12) for the Miles' mechanism. Note that also Janssen's quasi-linear theory can be summarized in a single non-constant coupling coefficient. Two distinct formulations can be found in the literature for this coupling coefficient. There is a category which is linear and a category which is quadratic in the wind velocity.

3.4.2.1 Formulations with a linear wind velocity dependency

a. Snyder

One of the most widely used formulations is the one by Snyder et al. (1981). Their experiments resulted in the following expression for the coupling coefficient :

$$\mu = [0.2 \text{ to } 0.3] \frac{\rho_a}{\rho_w} (\frac{u_s \cos\theta}{c} - 1) \tag{3.15}$$

a_s :   wind speed at 5 m
θ :   angle between wind vector and wave propagation
$c = \omega/k$:   wave speed

The wind speeds in the experiment of Snyder et al. (1981) were around 5 m/s (at 5 m height). The range of wind speeds was limited and a linear fit to this data should be looked at sceptically when extrapolating to other (higher) wind velocities.

Other interpretations of the Snyder et al. (1981) experimental data have been cited in literature :

- Komen

$$\mu = [0.2 \ to \ 0.3] \frac{\rho_a}{\rho_w} (\frac{28u.\cos\theta}{c} - 1)$$ (3.16)

In Komen et al. (1984) friction velocity scaling is assumed to
be governing the coupling processes between the atmosphere and
the water body. Using Wu's relationship (equation 2.33) a value
of 28 is obtained for the inverse of the square root of the
drag coefficient at a wind speed of 5 m/s, i.e. the wind speed
of the measurements of Snyder et al.(1981).
- Young

$$\mu = [0.2 \ to \ 0.3] \frac{\rho_a}{\rho_w} (\frac{u_{10}\cos\theta}{c} - 1)$$ (3.17)

The velocity at 5 m height has been replaced by the more common
velocity at 10 m height by Young (1988).

b. Kahma

$$\mu = 0.19 \frac{\rho_a}{\rho_w} \frac{u_{10}}{c_K}$$ (3.18)

The definition of Kahma for c_K differs from the phase velocity
used in the other formulas. Therefore subscript K is added
(Kahma, 1981). It is an integral quantity of the forward face of
the spectrum and therefore constant for all the frequencies in
that spectrum at a particular sea state. Note that in this way
the wind input becomes sea state (or wave age) dependent. The
value 0.19 follows after numerical substitution of some terms in
Kahma's original formulation.

3.4.2.2   *Formulations with a quadratic wind velocity dependency*

A number of people are in favour of a quadratic
dependency of the wind input term on the wind velocity.

a. Stewart

$$\mu = 0.04 \ (\frac{\rho_a}{\rho_w}) \ [\ \frac{u^2}{c^2} - \frac{u}{c}\ ] \tag{3.19}$$

Notice that Stewart (1974) did not specify a height for the wind speed. His work however is more conceptual and clarifying than meant for direct application. The expression does vanish when the wave speed equals the wind speed but does not have any directional dependency.

b. Plant

$$\mu = [0.04 \pm 0.02] \frac{u_*^2}{c^2} \cos\theta \qquad for \qquad 0.08 < \frac{u_*}{c} < 3 \tag{3.20}$$

Compared to the previous expression, Plant's formula does not set the momentum transfer to zero when waves travel with a speed close to the wind velocity. Therefore this relationship should not hold for that situation. Plant (1982) claims that his relationship is valid for frequencies between $g/2\pi u_{10}$ and 20 Hz.

c. Janssen

$$\mu = \frac{\rho_a}{\rho_w} \beta \ (\frac{u_*}{c})^2 \cos^2\theta \tag{3.21}$$

β ($\equiv \beta(u_* \cos\theta/c, \Omega)$ is a parameter which depends on the wave age (c_p/u_*) and on a profile parameter Ω ($\equiv$ nondimensional roughness $z_0 g/u_*^2$). The roughness length z_0 is a combination of the roughness of gravity-capillary waves, which Janssen (1991) models with the Charnock relation, and the roughness length of the gravity waves, which Janssen models by means of a roughness length). Janssen's formulation is very similar to Plant's expression (equation (3.20)) but is wave age dependent.

68

d. Donelan and Hui

In their contribution Donelan and Hui (in Geernaert and Plant, eds., 1990) use as the variable for the driving force in wind generated waves, the wind speed at the height (or at a fraction of the height) equal to the wave length of the wave considered. Their first expression comes from Al-Zanaidi and Hui (1984) :

$$\mu = \delta_i \frac{\rho_a}{\rho_w} (\frac{U_\lambda}{c} - 1)^2 \qquad (3.22)$$

The coefficient δ_i is positive for waves that travel in the wind direction (0.04 for transitional and smooth flow and 0.06 for rough flow) and negative for waves that travel against the wind (-0.024 for transitional or smooth flow and -0.04 for rough flow). U_λ is the wind speed at a height equal to one wave length. One notices that the above equation is one of the very few which attaches damping effects to opposing winds. Quite a few people have observed this phenomenon (for an overview, see Donelan and Hui in Geernaert and Plant, eds., 1990).
Note that the coefficient δ_i in equation (3.22) is in fact the same as a pressure coefficient since the above expression contains a velocity squared. In this way it can be seen as a value for the sheltering coefficient as proposed by Jeffreys (1924,1925).
A second expression apparently shows good agreement with measured growth rates both in the field (Hsiao and Shemdin, 1983) and in the laboratory (Larson and Wright, 1975) and is given by :

$$\mu = (0.1 \ to \ 0.2) \frac{\rho_a}{\rho_w} (\frac{u(\lambda/2) \ \cos\theta}{c(\lambda)} - 1)^2 \qquad (3.23)$$

where λ again corresponds to the wavelength or a height equal to the wavelength, and θ is the angle between the wind and the waves.

For the work that follows, we retain two expressions for the wind input term and hope to determine some free parameters as to give an optimal fit to measured growth curves (see Chapter 6). The

69

wind input is limited to the exponential term in equation (3.12) or in other words is in the form

$$S_{in} = b \, E(f, \theta) = \mu \, \omega \, E(f, \theta)$$

Since u. scaling is physically more sound than scaling with a velocity at an arbitrary height as 10 m, it has been silently accepted as the right choice although there is no hard evidence for it (Janssen et al., 1987).
The expressions retained are :

expression 1

$$S_{in}(f, \theta) = 0.25 \, a_1 \frac{\rho_a}{\rho_w} (a_2 \frac{28u_*}{c} \cos\theta - 1) \, \omega \, E(f, \theta) \qquad (3.24)$$

where   c   :   phase velocity of the wave (c = ω/k)
        u. :   friction velocity (in the atmospheric boundary layer)
        ρ_a :   density of air
        ρ_w :   density of water

expression 2

$$S_{in}(f, \theta) = 0.04 \, \frac{\rho_a}{\rho_w} \, a_3 [\, (a_4 \frac{28u_*}{c})^2 - a_5 (a_4 \frac{28u_*}{c})] \cos\theta \, \omega \, E(f, \theta) \quad (3.25)$$

Expression 1 is for a value of a_1 of 1, and a_2 of 1 the formulation obtained by Snyder (Snyder et al. 1981) and adjusted for u.-scaling (Komen et al. 1984). For a_3 equal to 1 and a_4 and a_5 equal to 1, expression 2 becomes the wind input term as proposed in (Stewart, 1974) and interpreted by (Plant, 1982). Expression 2 has also been converted to u.-scaling and an angular dependency is added. There are no convincing arguments to bring in this angular dependency. It is only believed that it will make a comparison between expression 1 and expression 2 easier. Plant's own formulation (Plant, 1982) is recovered by taking 1 for a_3, 1 for a_4 and 0 for a_5. The formulation of Plant can be considered as a special case of the formulation of Stewart. Since

70

Plant's formulation does not go to zero for waves travelling at nearly the wind speed, it is not dealt with in this analysis. The parameter a_5 will therefore always be set equal to 1.

3.5 The dissipation term

According to Hasselmann (1974) whitecapping or wave breaking is generally believed to be the dominant dissipative mechanism in a wave field since other mechanisms such as molecular viscosity or turbulence appear inadequate to dissipate the energy imparted to the waves by the wind. Only at low wind speed (<~4 m/s) viscous dissipation could account for all of the momentum transfer across the air-sea interface. Before Hasselmann's 1974 paper on whitecapping, wave breaking was not looked at in terms of a source function but on the basis of a high frequency equilibrium range. It is on the basis of an equilibrium range controlled by wave breaking that Phillips (1958) obtained through dimensional analysis an f^{-5}-tail for the frequency spectrum. However, the JONSWAP measurements showed a fetch dependency of the proportionality factor, i.e. the Phillips' constant α_p (see Hasselmann et al. (1973) and Chapter 2). Recently, Phillips (1985) has abandoned the concept of an f^{-5}-tail. Indeed the equilibrium range is not governed entirely by wave breaking. Also the wind input and the nonlinear interactions which transfer energy from the peak region of the spectrum to lower and higher frequencies, play an important role.
Hasselmann (1974) shows that an interior force field can drive an irrotational wave field in just the same way as a surface pressure field. For a surface pressure field, the equation of motion of the fluid can be written as the harmonic-oscillator equation. Only the component of the interior force field which can contribute to the generation of surface waves is considered. The component of the interior force field which generates currents, is neglected. Remark that this is the component which results in storm surge and could therefore be quite useful for accurate storm surge prediction. However, the wave breaking process is strong locally and weak in the mean. With weak in the

71

mean, a small change in the wave spectrum per unit wave length is understood. Hasselmann's theory leads to a dissipation source term proportional to the spectrum and the square of the frequency.

$$S_{diss}(k) = -\eta \, \omega^2 \, F(k) \tag{3.26}$$

The proportionality factor depends only on the wavenumber and integral spectral parameters such as the average wave steepness. Komen et al. (1984) tried to obtain the proportionality factor η from the energy balance of a Pierson-Moskowitz spectrum with $\cos^2\theta$ angular spreading. This gave however some negative values for the dissipation function. Since friction always should be an energy loss irrespective of frequency or wavenumber, this result seemed unreasonable. Therefore a parameter approach was taken with a dissipation function of the form

$$S_{diss}(f,\theta) = -c_1 \, \bar{\omega} \, \left(\frac{\omega}{\bar{\omega}}\right)^n \left(\frac{\hat{\alpha}}{\hat{\alpha}_{PM}}\right)^m \, E(f,\theta) \tag{3.27}$$

where

$\bar{\omega} = E^{-1} \int E(f,\theta) \, \omega \, df d\theta$:   the mean frequency;

$E = \int E(f,\theta) \, df d\theta$:   the total energy in the spectrum

$\hat{\alpha} = E\bar{\omega}^4/g^2$:   the integral wave steepness;

$\hat{\alpha}_{PM} = 4.57 \; 10^{-3}$:   integral wave steepness for a Pierson-Moskowitz spectrum

The dissipation constant c_1 influences the overall level of dissipation. The coefficient n can shift the maximum dissipation level relative to the frequency of the spectral peak. The coefficient m adjusts the dependency of the dissipation level on the wave steepness. Suggested values used for the above coefficients are $3.33 \; 10^{-5}$ for c_1, 2 for n and 2 for m respectively (Komen et al. 1984). In what follows the dissipation parameters c_1, m and n will be considered adjustable.

It should be noted that about all wave models contain some implicit form of damping. In earlier models (Barnett, 1968), the dissipation term as such did not exist. In stead a multiplication factor (<1) for the wind input was introduced so that the spectrum beyond the peak had an f^{-5} dependency as suggested by the dimensional arguments of Phillips (1958). In parameter models such as the HYPA model (Günther, 1981), damping is included in the parametrization scheme and therefore does not appear explicitly. Even in the third generation models (such as the WAM-model (WAMDI, 1988)) some implicit damping is present next to the source term as given above. Namely, the high frequency cut-off level with the prescribed tail is an implicit form of damping (see also Chapter 4).

Cavaleri et al.(1989) discuss the possibility of adjusting the coefficient m according to wave age to allow for a direct coupling with the wind. They argue that observational evidence shows that wave breaking is highly frequent in the early stage of development and this should be reflected in higher dissipation for young wind seas.

Janssen (1991), in his exercise to couple the atmospheric boundary layer with the water surface, increases the value of m to 3 in stead of 2 as suggested in Komen et al.(1984). It gives him a much better behaviour of the Phillips' constant α_P.

Rosenthal (1989) discusses turbulent diffusion as a mechanism for energy dissipation. According to Rosenthal it is then possible to calculate an order of magnitude for the Phillips' constant α_P and thereby possible to define the energy content in the saturation range.

In this study we will only work with the dissipation term as formulated in Komen et al. (1984) and given in equation (3.27). We will consider the parameters c, n and m as adjustable.

However, these parameters will be independent of wave age. Their value will be obtained as to give a best fit to the measured growth curves (see Chapter 5 and Chapter 6).

3.6   The non-linear interactions

The nonlinear interactions arise from the fact that the sea surface is described by means of an energy spectrum which is composed of the summation of sinusoidal waves. Each sinusoidal component of the spectrum makes a contribution to the fulfilment of the linearized boundary condition at the free surface. This is the essence of the linear small amplitude wave theory. Due to the linear approximation a number of higher order terms are neglected. Hasselmann (1962, 1963a and 1963b) showed that a set of four waves could exchange energy if they fulfil the following resonant conditions :

$$\overline{k}_1 + \overline{k}_2 = \overline{k}_3 + \overline{k}_4$$
$$\omega_1 + \omega_2 = \omega_3 + \omega_4$$

(3.28)

The nonlinear resonant third order wave-wave interactions are described by the Boltzmann-integral (Hasselmann & Hasselmann, 1985):

$$S_{nl}(\overline{k}_4) = \omega_4 \int \sigma \, \delta(\overline{k}_1 + \overline{k}_2 - \overline{k}_3 - \overline{k}_4) \times \delta(\omega_1 + \omega_2 - \omega_3 - \omega_4)$$
$$[n_1 n_2 (n_3 + n_4) - n_3 n_4 (n_1 + n_2)] \, d\overline{k}_1 \, d\overline{k}_2 \, d\overline{k}_3$$

(3.29)

where

n_j	:	the action density $(n(\overline{k}_j) = F(\overline{k}_j)/\omega_j)$
$F(\overline{k}_j)$	:	wavenumber energy spectrum
k_j	:	wavenumber (magnitude of the vector $\overline{k}_j$)
$\omega_j = 2\pi f_j$	:	angular frequency
$\omega_j = (gk_j)^{1/2}$	:	the dispersion relation in deep water
σ	:	the net scattering coefficient, an expression for the probability of the wave-wave interaction
δ	:	Dirac-function

74

The interaction contributions here given in the wavenumber space have to be stored in the corresponding frequency-direction bin. Wavenumber and frequency are related through the dispersion relation. The calculation of the nonlinear interaction is very time consuming since there are many possible combinations of four wavenumbers which fulfil the resonance condition (3.28). Therefore the discrete interaction approximation (Hasselmann et al., 1985) will be used to limit the calculational effort (see also Chapter 4).

3.7 Summary and conclusions

In this chapter the wave energy transport equation was described. The emphasis was on the application of wind generated waves travelling in deep water. Different processes are involved. These processes are translated mathematically into source terms for the energy transport equation. In deep water these source terms are limited to wind input, dissipation through whitecapping and nonlinear interactions between the different wave components.

The physics of the wind input term have been explained in terms of Phillips' and the Miles' mechanisms. The Phillips' mechanism describes the response of the water surface to pressure fluctuations in the air flow. In time, it gives a linear growth to the waves. It is believed to be responsible for initial wave growth.
The Miles' mechanism describes the consequences of shear flow over the waves. Due to a shear flow, streamlines in the air above the waves will not be in phase. This creates a pressure difference between the windward and the leeward side of a wave. This process is enhanced as the waves grow and has therefore the characteristics of an instability giving rise to an exponential growth rate of the waves. This mechanism quickly overrules the Phillips' mechanism and most often is the only term in mathematical expressions for the wind input term.
The quasi-linear theory of Janssen has been briefly highlighted because of its importance in coupled wind wave models.

A number of expressions for the wind input term were given from literature. Two expressions were kept for further use in this work. One is called the Snyder type wind input term, and is an expression which is linear in the characteristic wind velocity. The other one is called the Stewart type wind input term, and this expression is quadratic in the characteristic wind velocity.

For the dissipation term, the expression as proposed by Komen et al. (1984) is chosen. It is based on the whitecapping theory of Hasselmann (1974). For further use in this study, three parameters in the dissipation source term are considered adjustable. These parameters will however not depend on wave age.

The nonlinear interaction source term is based on first principles and is therefore considered exact and known. It explains how energy is exchanged between different wave components which fulfil the resonant conditions. However, to limit the computational effort, this source term will be approximated in the numerical model.

4   The wave program

4.1   Introduction

The wave program used for this work is the program ONEDMOD developed by S. Hasselmann at the Max-Planck Institut für Meteorologie in Hamburg (Germany). The program ONEDMOD solves the energy transport equation (3.2) for two special conditions :

$$\frac{\partial E}{\partial x} = 0 \qquad : \text{ fetch limited} \qquad\qquad (4.1)$$

$$\frac{\partial E}{\partial x} = 0 \qquad : \text{ duration limited} \qquad\qquad (4.2)$$

Only the Miles' mechanism is considered important for the wind input. Some initial energy level is therefore necessary to have wind input. The initial energy is provided by means of an initial energy spectrum.

The energy transport equation is integrated with respect to time or to fetch. The one-dimensional (i.e. along the fetch axis in space or along the time axis) wave program ONEDMOD is used. The model contains all the physics that are implemented in the full two-dimensional WAM-model (Hasselmann, 1987) but only works in one dimension to limit the computer time. It is also well suited to explore the behaviour of the different source terms and the response to changes in the parameter values.

The program has been extended to look at the momentum balance in growing wind seas. This additional tool will make a further interpretation of selected source terms possible, since for example the momentum input due to the wind input term should not exceed the shear stress.

In a next section it is explained how the source terms are treated numerically. The program ONEDMOD does not deal with all frequencies on the chosen frequency grid. It restricts its working area to a cut-off frequency taken as 2.5 times the peak frequency. Beyond that point a prescribed high frequency tail is added. Also the growth in a particular frequency-direction bin

is restricted in each integration step. If the growth limit is exceeded, the integration step size is reduced.

In a last section some example runs are given for fetch limited conditions. They illustrate how spectra, source terms and momentum balance evolve with increasing fetch. Also the effect of running the program with a different friction velocity is highlighted.

4.2   Initial spectrum

Since in most wave models only the Miles' mechanism is considered for the wind input (exponential term in equation (3.11)), an initial energy level is needed. This initial energy is necessary to have wind input, when the linear term in equation (3.12) is neglected. This is also the case for the program ONEDMOD. The program FRSPEC, developed by S. Hasselmann and described by Van Vledder and Weber (1988), is used for this purpose. FRSPEC can generate different types of spectra such as the Pierson-Moskowitz spectrum for a given wind velocity or a JONSWAP spectrum with given $\alpha_P, f_p, \gamma, \sigma_a$ and σ_b. Usually a JONSWAP spectrum is used. This can be done in combination with a choice of different directional distributions. The choice of frequencies in the spectrum can be arbitrary or logarithmic, see Figure 4.1.
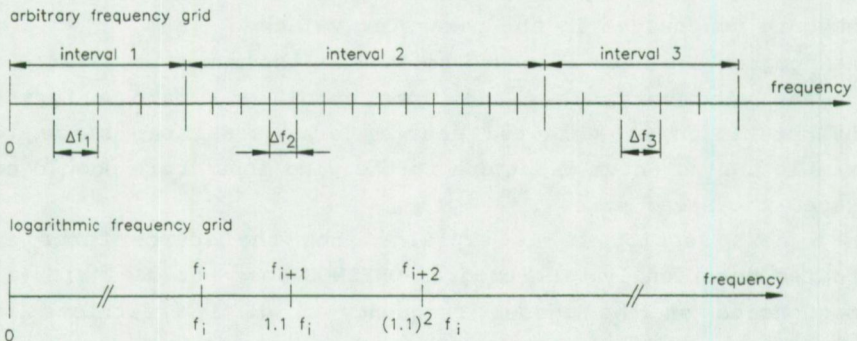
Figure 4.1 : An arbitrary and a logarithmic frequency spacing

The arbitrary frequency distribution is determined by a coarse frequency grid. Each coarse frequency interval can then be subdivided in a number of frequency grid points.

The logarithmic scaling is done as follows :

$$f_{i+1} = f_i(1 + CO) \tag{4.3}$$

where CO is a constant coefficient (usually 0.1) and i varies between 1 and the total number of frequencies considered. The output from FRSPEC is to be used as input for the wave program ONEDMOD. It consists of the number of frequency grid points, the number of directional grid points, the angular increment, the JONSWAP parameters and the two dimensional spectrum in the frequency-direction (f,θ) space. An example spectrum is given in Figure 4.2. It is the initial spectrum which will be used for all of the computer runs in Chapter 6. It is a JONSWAP spectrum with the following characteristics :

- scale parameters : $f_p^* = 0.0193$ and $\alpha_P = 0.0223$
- shape parameters : $\sigma_a = 0.07$; $\sigma_b = 0.09$ and $\gamma = 3.3$

In Figure 4.2 the energy-frequency plot and also a polar plot with contour lines is given. For the energy contour plots, the software package CERES developed by G. van Vledder (1991) was used. The frequency grid is logarithmic with CO in equation (4.3) equal to 0.1. The smallest frequency is 0.04177 Hz. The angular distribution is a $\cos^2\theta$ (equation(2.25)) and the angular resolution is 30°.

79

ENERGY [M^^2/S]

.20

.15

.10

.05

.00

.0   .5   1.0   1.5

FREQUENCY [HZ]

WIND DIRECTION

2-D SPEC CONTOUR
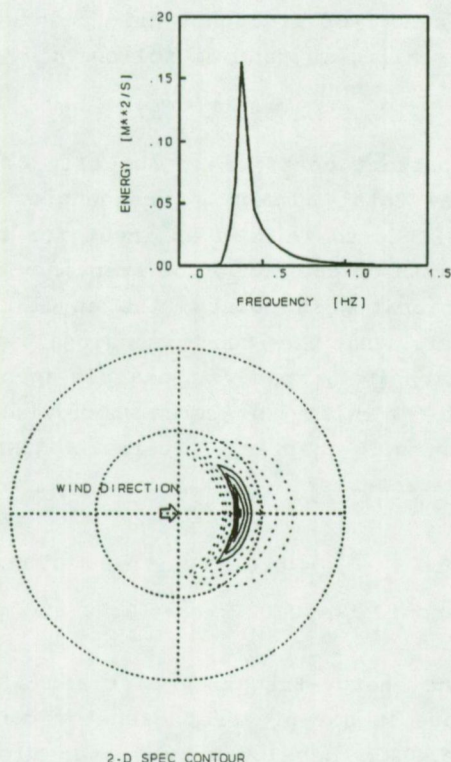
Figure 4.2 : Frequency and frequency-direction spectrum of the wave energy E

4.3   The structure of the wave program ONEDMOD

The structure of the different data blocks is given in Figure 4.3. The ovals in the figure indicate that intermediate results can be stored for future use, such as plotting or continuation of a suspended run. The dashed line means that the program FRSPEC (described in section 4.2), only needs to be run once, as to create the desired initial spectrum.

80
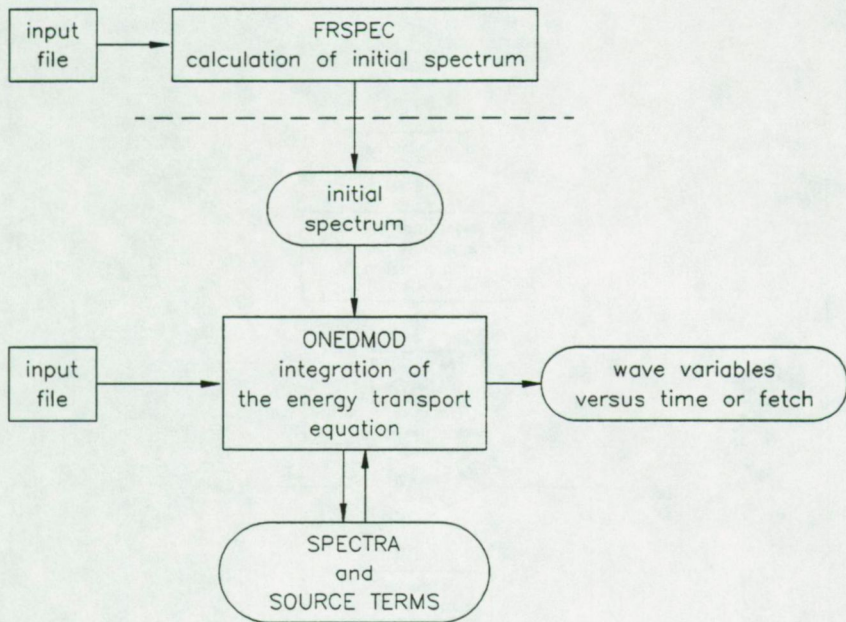
Figure 4.3 : Structure of the wave program

A flow chart of the calculational part of the program is given in Figure 4.4. The program ONEDMOD has been extended to look at the momentum balance of the growing wave field. The momentum supplied by the wind as calculated from the wind input term (equation (3.6)), momentum lost due to whitecapping (equation (3.7)), or exchanged by nonlinear interactions (equation (3.8)) can then be seen with respect to the maximum possible momentum input from the wind. This maximum possible momentum input is equal to the shear stress τ ($\equiv \rho u_*^2$). Note that the momentum transport is taken per unit of time and per unit of area (see also section 3.3).

```
                    ( BEGIN )
                        |
                  ┌───────────┐
                  │ input data│
                  └───────────┘
                        |
            ┌──────────────────────────┐
            │  calculate  coefficients │
            │ for the discrete interaction│
            │       approximation       │
            │      (see 4.4.1.3)        │
            └──────────────────────────┘
                        |
                  ┌───────────┐
                  │ T=T+ Δ T* │
                  │  ΔT=T/2   │
                  └───────────┘
                        |
                      ◇ enough ◇ ──yes──► ( end )
                      ◇ steps ? ◇
                        |
                       no
                        |
                  ┌───────────────┐
                  │   calculate   │
                  │ source functions│
                  │ ─ ─ ─ ─ ─ ─ ─ │
                  │   momentum    │
                  │ in source terms│
                  └───────────────┘
                        |
                      ◇ growth  ◇ ──yes──► ┌─────────┐
                      ◇ of energy◇         │ ΔT=ΔT/2 │
                      ◇ too large◇         └─────────┘
                        |
                       no
                        |
                  ┌───────────────┐
                  │   calculate   │
                  │ new spectrum  │
                  └───────────────┘
```
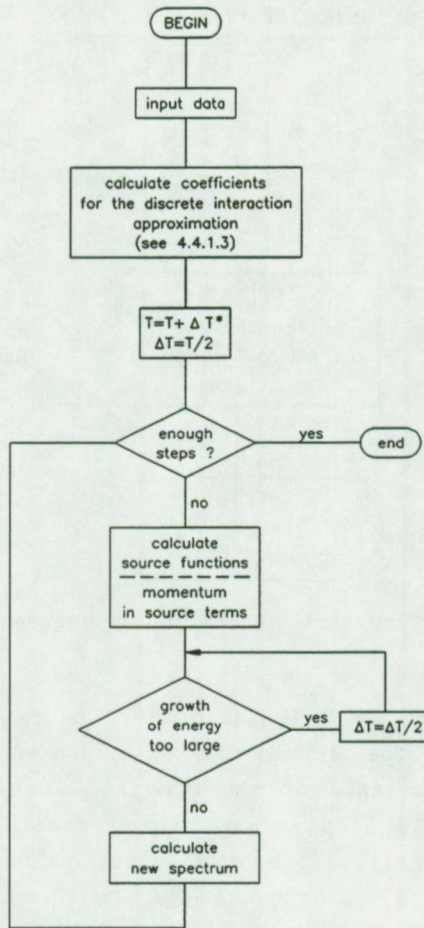
* T : fetch x or time t; note that T+Δt is calculated first before checking on limitation of wave growth

Figure 4.4 : Flowchart of the program ONEDMOD

4.4   The numerical solution

4.4.1   Source term calculation

4.4.1.1   General

The numerical solution has the following features :

$$E(f,\theta)_i = E(f,\theta)_{i-1} + \Delta E(f,\theta)$$ **(4.4)**

where $\Delta E(f,\theta)$ is the increment in spectral energy in a particular frequency-direction bin. By combining equations (4.1) and (4.2) together with equation (3.2), $\Delta E(f,\theta)$ is computed for duration limited wind seas as

$$\Delta E(f,\theta) = S_{tot}(f,\theta) * \Delta t$$ **(4.5)**

and for fetch limited wind seas as

$$\Delta E(f,\theta) = S_{tot}(f,\theta) * \Delta x / c_g \cos\theta$$ **(4.6)**

where Δt is the time step
S_{tot} is the total source function
c_g is the group velocity at frequency f
θ is the angle with respect to the x-axis ($\equiv$ wind direction)

The source term calculation can then generally be written as :

$$S_{tot} = (\Phi S_{tot}^{i-1} + (1-\Phi) S_{tot}^{i})$$ **(4.7)**

where $0.5 \leq \Phi \leq 1.0$
For Φ equal to 1.0, the numerical scheme is explicit; for other values of Φ, the numerical scheme is implicit. The program ONEDIMP, also developed by S. Hasselmann, uses such an implicit scheme with Φ equal to 0.5. Luo (1991) did some numerical experiments with this numerical code. If the source term would depend linearly on the energy level, then equation (4.7) could be solved directly. However the dissipation term depends only quasi-linearly on the energy content and the nonlinear interactions depend highly nonlinearly on the energy content at step i. Although there might be a saving in computer time by

83

using an implicit scheme since a larger step can be taken, it was not done here mainly because the energy and peak frequency growth curves showed some discontinuities (Luo, 1991). Although the discontinuities are small enough not to affect the overall trend of the growth curve, it might lead to severe problems when calculating the Jacobian and Hessian matrices in the optimization procedure (see also Chapter 5). Note that the full two-dimensional WAM model uses the implicit form (equation 4.7 with Φ equal to 0.5) for the calculation of the source terms and an explicit scheme with adjustable step size (see 4.4.3) for the calculation of the advection term.

For a fetch limited wind sea calculation, the program sets all the energy contents of the frequency-direction bins which do not have an energy component in the direction of the wind to zero. This is done by two directional indices (IA1 and IA2 in the program; see also Figure 4.5). It is clear that waves which do not travel in the wind direction will not grow under the influence of the wind and therefore one should not waste time doing calculations in that region of the spectrum.
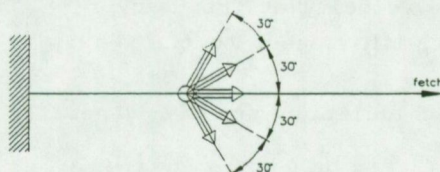
Figure 4.5 : Waves with a component in the wind direction

4.4.1.2   The wind input and the dissipation term

The dissipation term and the wind input term were discussed in Chapter 3. Both of them are proportional to the energy level. In the program ONEDMOD the wind input and the dissipation through whitecapping are based on the current energy content of the frequency-direction bin. In the equations (4.5) and (4.6), the total source term is therefore calculated with the energy content at step i-1 . In the dissipation term the mean

84

frequency is used and calculated in the straightforward way. The mean frequency could also be calculated as the inverse of the mean period as was done for the implicit version of the wave program. To obtain approximately the same growth curves, one will have to adjust the overall dissipation level c_i in equation (3.27), depending if one uses the mean frequency or the inverse of the mean period in the dissipation term formulation (see Luo, 1991).

4.4.1.3 The discrete interaction approximation

In the discrete interaction approximation, only a limited number of all possible interaction combinations in the integral for the nonlinear interactions (equation (3.29)) are calculated. According to Hasselmann et al. (1985) good agreement with the exact computations is obtained by using the superposition of only a small number of discrete interaction configurations. Hasselmann et al. (1985) actually found that one mirror-image pair of intermediate range interaction configurations could do the job. In the first configuration, two wave numbers are identical and the other two wavenumbers are such that they fulfil the resonance condition. The second configuration is then a mirror image of the first around the two identical wave numbers (see Figure 4.6). The resonance conditions then become :

$$\omega_1 = \omega_2 = \omega$$
$$\omega_3 = \omega(1+\lambda) = \omega_+ \qquad (4.8)$$
$$\omega_4 = \omega(1-\lambda) = \omega_-$$

The value 0.25 for λ gives good agreement.

In wavenumber space this comes down to a vector diagram where the wavenumber vectors $\overline{k}_1$ and $\overline{k}_2$ are equal and, $\overline{k}_3$ and $\overline{k}_4$ make an angle of 11.5 and -33.6 with the vector $\overline{k}_1$ and $\overline{k}_2$ (see figure 4.6). The expression for the nonlinear interactions given in Chapter 3 is written in terms of the action density

85

$(n(k) \equiv g\ F(k)\ /\ \omega)$. In practice this needs to be translated into
the frequency direction space. An expression for this is given
in Hasselmann et al. (1985). Note that in their expression there
is a difference between the interpretation of the discretization
in the numerator and the denominator. In the numerator one refers
to the amount of energy involved in the nonlinear interaction,
in the denominator one refers to the bin size into which the
energy is put or from which the energy was extracted. When the
program ONEDMOD is run with a logarithmic frequency scaling,
these bin sizes will not be identical. The WAMDI report (1988)
remarks that with the discrete interaction approximation there
still is an overshoot effect but that it is less pronounced than
in a model with the exact computations of the nonlinear transfer
integral. The peak frequency growth curve and the energy growth
curve correspond to the exact calculations but the Phillips'
constant α_p is somewhat overestimated (Hasselmann et al. 1985).
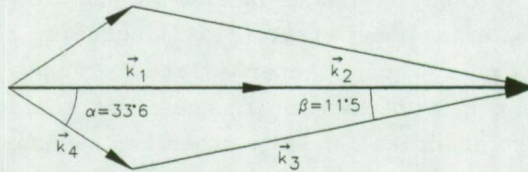
Figure 4.6 : The interaction configuration used in the discrete
interaction approximation

4.4.2   The high frequency tail

The numerical scheme used in this study is an explicit
forward difference scheme applied in the frequency range
$0 - 2.5f_p$. An f^{-5}-tail is attached beyond this highest prognostic
frequency. This corresponds with the dimensional arguments from
Phillips (1958). In view of the discussion on the different
spectral formulations given in Chapter 2, this may not be the
'correct' choice. The level of the tail is adjusted separately
for each direction as to continuously match the spectrum. In the

full two-dimensional WAM model, not an f^{-5} but an f^{-4} tail is attached, corresponding to what was suggested by Toba(1973) and verified experimentally by Battjes et al.(1987). The effect of changing the details of the tail was not investigated but it should not have a great influence on the evolution of the total energy or the peak frequency. It may be important however for coupling an atmospheric model to a wave model (see also Chapter 2).

4.4.3   Limitation of spectral growth in a bin

The growth in a spectral bin is limited by two cut-off levels, a lower limit and an upper limit :

- the lower limit : $S_{LL} = (0.018*0.05*g^2)/(2\pi)^4 f^5)$ **(4.9)**

- the upper limit : $S_{UL} = (0.05g^2\alpha_p)/((2\pi)^4 f^5)$ **(4.10)**

The step size Δx or Δt is reduced by half if the absolute value of the energy increment $\Delta E(f,\theta)$ in equation (4.4) is larger than one third of the initial spectral content and also larger than the upper limit S_{UL} in equation (4.10) or if the calculated energy $E(f,\theta)_i$ in equation (4.4) becomes smaller than zero. The energy does not change when the initial energy in the frequency-direction bin $E(f,\theta)$ of the spectrum is smaller than the lower limit S_{LL} given in equation (3.5) and when also the source function is negative.

In the report on the program EXACT-NL (van Vledder and Weber, 1988), two other values are given for the lower and upper limit :

$S_{LL}{}' = (0.1*0.0054*g^2)/((2\pi)^4 f^5)$

$S_{UL} = (0.3g^2\alpha_p)/((2\pi)^4 f^5)$

Van Vledder and Weber (1988) say that their values are based on experience. No other justification is given. The values used for the numerical experiments in this research work are the first values given and should put a more severe limit on the step size than the other values and should be numerically on the safe side.

---

[1]the value 0.0054 is the value used in their program, in the report 0.054 is printed

No further investigation into the effects created by changing these two limits has been done however.

4.5 Example runs

4.5.1 Introduction

The results in the example runs will be displayed in a form nondimensionalized with the friction velocity u_*. This gives the following relationships between dimensional and nondimensionial variables :

$$E_* = \frac{Eg^2}{u_*^4} \quad ; \quad E_*(f) = E(f)\frac{g^3}{u_*^5}$$

$$S_i^* = S_i\frac{g^3}{u_*^5} \quad ; \quad S_i^*(f) = S_i(f)\frac{g^2}{u_*^4}$$

(4.11)

E stands for energy, f for frequency, g for acceleration of gravity and S for source term. The subscript i refers to wind input, dissipation or nonlinear interactions.

4.5.2 Growth curves for different friction velocities

The program was run for three different friction velocities and the results for the energy growth curves are displayed in Figure 4.7. The friction velocities chosen are 0.5 m/s, 0.25 m/s and 1.0 m/s respectively. The value 0.5 m/s is the value that will be used for all the numerical experiments in Chapter 6. As initial spectrum, the JONSWAP spectrum described in section 4.2 was chosen. Note that this means that the program FRSPEC had to be run before each run, since the velocities differ and the dimensional peak frequency therefore differs for each run.

The wind input was chosen according to Snyder (equation (3.24)) with a_1 and a_2 equal to 1. The dissipation term was according to equation (3.27) with numerical values for the parameters as

suggested by Komen et al. (1984), i.e. a value of 2 for the parameters m and n, and a value of $3.33 \ 10^{-5}$ for the parameter c_1. The growth curves do not scale perfectly (see Figure 4.7), i.e. for different friction velocities the calculated growth curves differ from each other. Especially in the fully developed stage, the difference is appreciable (see details in Figures 4.8 and 4.9). This is probably mainly due to the fact that the frequency grid has a logarithmic scaling. The resolution differs depending on where one is working on the grid. Since there is a coupling of the different frequency-directions bins through the exchanges of energy by the nonlinear interactions, it is possible to spread these energies over different bin sizes. Also the cut-off frequency for attaching the high frequency tail and the limitation of the growth in a particular frequency-direction bin will contribute to the difference in the result.
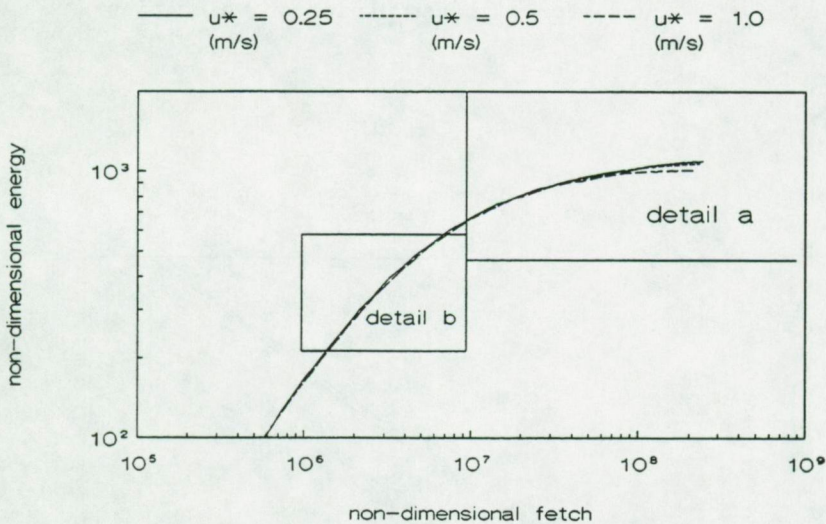
Figure 4.7 : Energy growth curves for different friction velocities u.
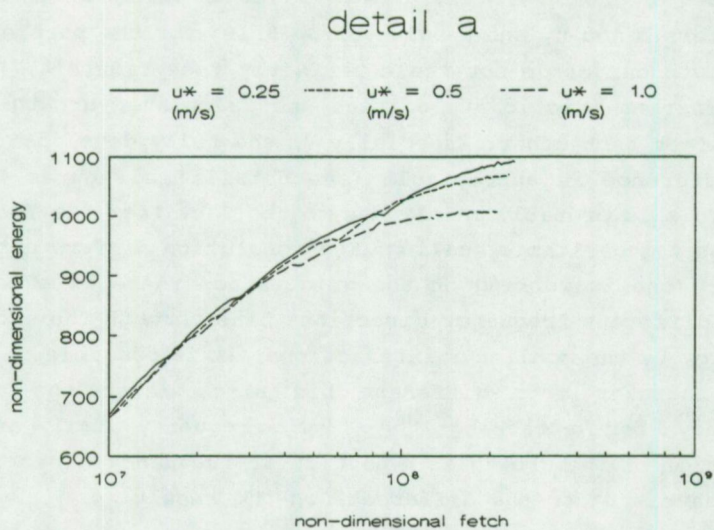
detail a

Figure 4.8 : Detail near full development of the energy growth curve for different friction velocities
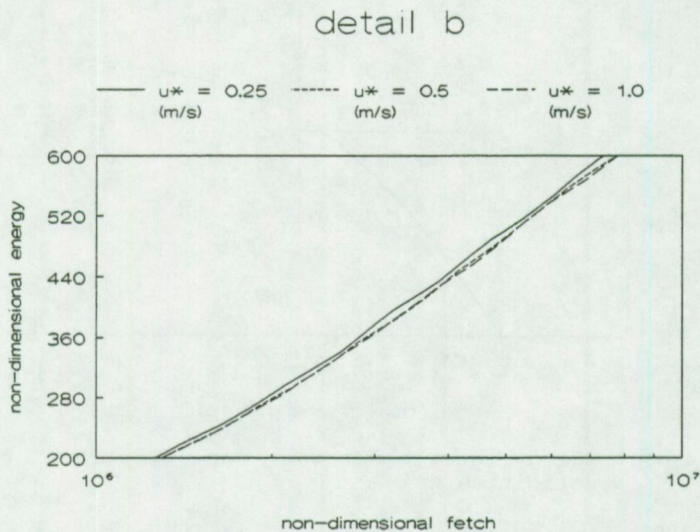
detail b

Figure 4.9 : Detail of the growing part of the energy growth curve for different friction velocities

For low values of the wind speed (e.g. a friction velocity of 0.1 m/s) or for high values of the wind speed (e.g. a friction velocity of 2.5 m/s), the program ONEDMOD produces erroneous results or no results at all. However, it must be mentioned here that for all these runs the frequency grid was identical, i.e. logarithmic frequency grid with CO in equation (4.3) equal to 0.1 and the initial (lowest) frequency equal to 0.04177 Hz. For the run with the low friction velocity (0.1 m/s), the initial spectrum has a high initial peak frequency and loses part of the spectrum because there are not enough high frequency bins left to store the energy. For the run with the high friction velocity, the peak frequency moves under the influence of the source terms towards such a low frequency that the resolution there is inadequate. With an adapted frequency grid, it should be possible to obtain good results even for very low or for very high wind speeds.

In current practice, the problems of obtaining results that do not scale properly remain since the frequency grid is fixed. Increasing the resolution of the frequency grid is not really possible because of computational costs. Ideally, a self adapting frequency grid should be used to resolve this problem. To the author's knowledge this has not been implemented yet in a wave model.

4.5.3   Evolution of wave spectra with fetch

In Figure 4.10 the evolution of the wave spectrum for fetch limited conditions is shown. The initial spectrum is again the one described in section 4.2. The source terms were the same as in section 4.5.2. The overshoot effect, i.e. the temporarily higher energy level during growth compared to the final equilibrium level, is clearly visible. Also visible is that for the given choice of source terms, the energy spectrum virtually does not change any more at high fetch values, compare the energy spectrum at nondimensional fetch x. values of 1. 10^8 and 2.5 10^8 in Figure 4.10.
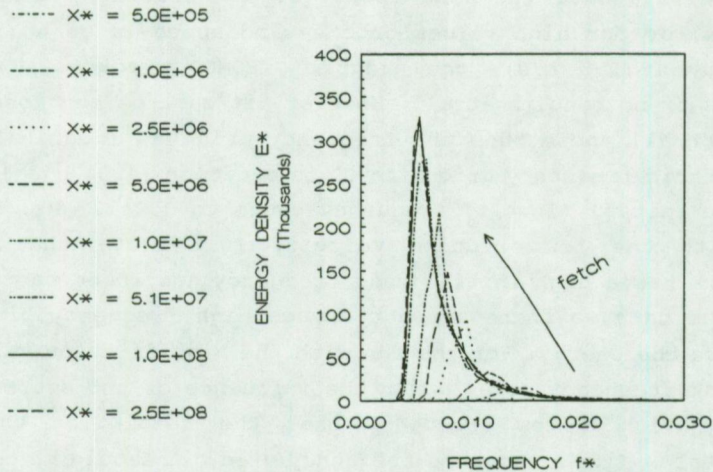
Figure 4.10 : Evolution of the one-dimensional frequency spectrum for a growing wind sea (fetch limited conditions)

4.5.4   Evolution of source terms with fetch

In the Figures 4.11 to 4.14 the evolution of the different source terms with fetch is shown for four different fetches, one fetch in the beginning of growth (young wind sea), one fetch at an intermediate position and two fetches around full development (old wind sea). For young wind seas one notices the wind input (S_{in}) and the nonlinear interactions (S_{nl}) provide extra energy on the forward face of the spectrum (Figure 4.11). At intermediate fetches the wind input has shifted mainly beyond the peak frequency and the nonlinear interactions provide most of the energy input on the forward face of the spectrum, thereby still shifting the peak frequency of the spectrum towards lower frequencies (Figure 4.12). At or near full development, the different source terms approximately cancel (S_{tot} ; see Figures 4.13 and 4.14). The source terms are only drawn up to 2.5 times the peak frequency. Beyond that frequency the spectrum does not longer get calculated explicitly but an f^{-5}-tail is added (see 4.4.2).
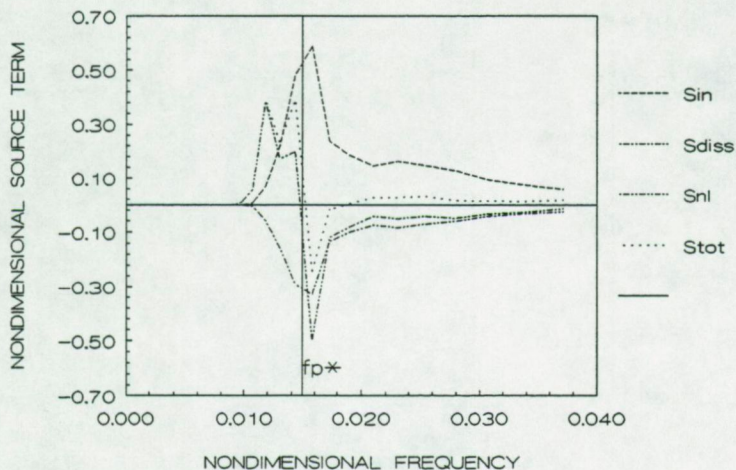
Figure 4.11 : Source terms for young wind sea ($x_*=5 \ 10^5$; $f_p^*=0.0149$)
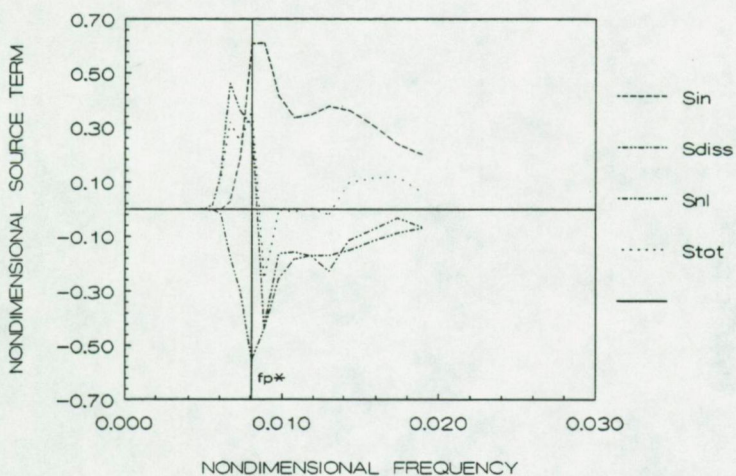
Figure 4.12 : Source terms for growing wind sea ($x_*=5 \ 10^6$; $f_p^*=0.0081$)
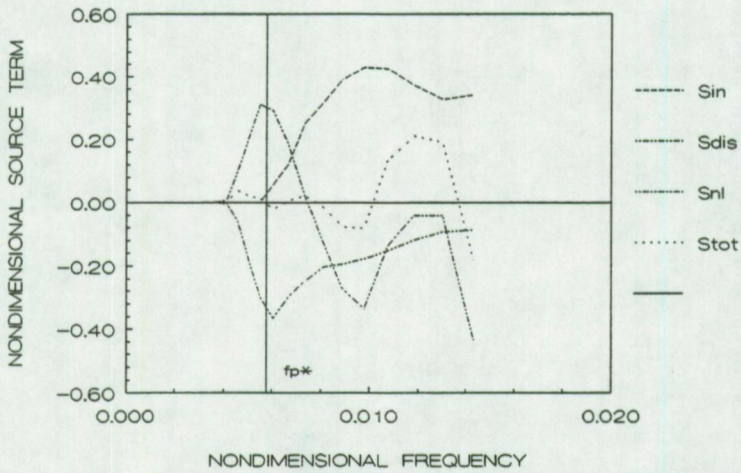
Figure 4.13 : Source terms for nearly developed sea ($x_*=5 \ 10^7$; $f_p^*=0.0058$)
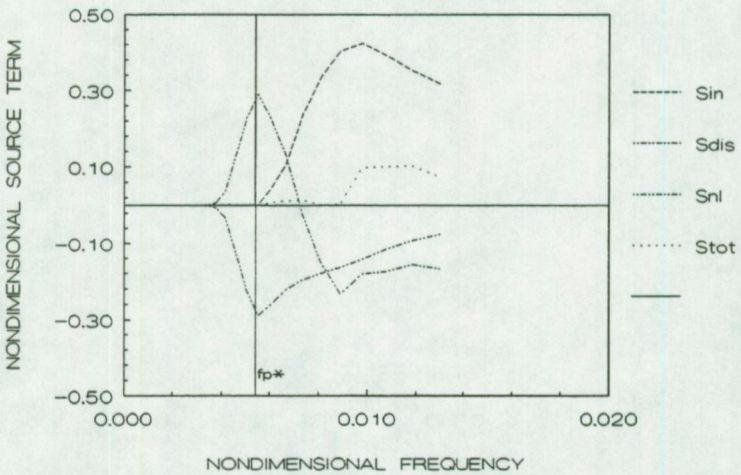
Figure 4.14 : Source terms for fully developed sea ($x_*=2.5 \ 10^8$; $f_p^*=0.0054$)

4.5.5   Evolution of the momentum balance with fetch

In Figure 4.15 the momentum balance in function of fetch is displayed. For the chosen wind input term (Snyder), one sees that a considerable amount of the total stress is transferred into the wave field. For young wind seas this is approximately 60-70 % but still remains approximately 45 % for old wind seas. On the other hand, the momentum loss due to wave breaking decreases from about 30 % for young wind seas to about 15 % for old wind seas. And although nonlinear interactions should in principal have no net gain or no net loss of momentum, we see that the calculations using the discrete interaction approximation produce a small net momentum loss over the full fetch range, thereby producing some kind of damping.
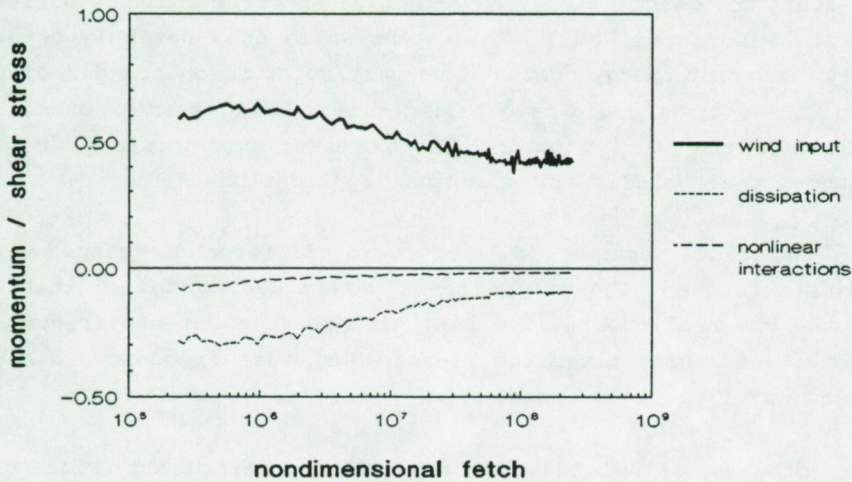
Figure 4.15 :   Ratio of momentum input and shear stress in function of fetch (wind according to Snyder)

Remark that the total effect yields a momentum input which is approximately 20 % higher than what one would expect from physical experiments (see section 3.3). Dijkhuis (1990) indicated that a forward-upwind scheme is strongly damping. Therefore, the

chosen numerical scheme is probably the main cause of the apparent difference between the momentum from the calculations and from the physical experiments. This is then compensated with an artificially decreased damping due to whitecapping or an increased wind input. The added high frequency tail may also artificially contribute to the damping (Janssen, 1992 ; personal communication).

4.6 Summary and conclusions

The program described above will be used for the integration of the one-dimensional energy equation (3.2). It will serve as a subroutine for the optimization program (to be discussed in Chapter 5). The program needs an initial spectrum to start the calculations. This initial spectrum could be omitted if the wind input would have a term which does not only depend on the current energy content in a particular frequency-direction bin, i.e., if it could have a linear term besides an exponential term for the wind input. This increases computational cost, without real benefit for practical applications.

The numerical scheme is a forward difference scheme with adjustable step. The step size is determined by the limitation of the spectral growth in a bin. Also above a cut-off frequency of two and a half times the Pierson-Moskowitz frequency, a high frequency f^{-5} tail is added.

The program calculates the nonlinear interactions with the discrete interaction approximation and not by the exact calculations. Exact calculations for the nonlinear interactions would increase computational cost substantially.

It was shown that when the wave program is run with different friction velocities, the resulting growth curves do not scale perfectly. It was argued that only a finer resolution at a high

computational cost or an adjustable frequency grid might resolve this problem.

The evolution of the wave spectra for a Snyder type wind input term and for a dissipation term as suggested by Komen, shows a pronounced overshoot effect. Also at large fetches, the energy spectrum does not have any tendency to change with increasing fetch, thereby obeying the notions of a fully developed sea.

Using the WAM model source terms (WAMDI, 1988), the calculated net momentum input is higher than what is to be expected from measurements. The numerics of the advection scheme and possibly the added high frequency tail produce some extra damping.

5 The optimization approach

5.1 Introduction

Optimization is the general term for minimizing (or maximizing) an 'objective' function in one or more variables. The variables for which optimal values have to be determined can be restricted to a certain range of values or be subjected to constraint functions. The first job in an optimization problem therefore is to define the objective or cost function and to construct the set of constraint functions. Since an efficient all purpose routine does not exist, it is necessary to tailor a more specialized routine for a particular category of problems. For example if the problem to be optimized is a linear problem and the constraints can also be expressed as linear functions, then one deals with a linear programming problem and one will use a linear programming algorithm. The problem we are facing here deals with obtaining 'optimal' results from a set of coupled nonlinear partial differential equations. The set of partial differential equations, are the wave energy transport equations given in Chapter 3. They are a set because the partial differential equation (3.2) has to be solved for each combination of frequency and direction. They are coupled because the nonlinear interactions can exchange energy between sets of four frequency-direction bins.

The objective in this part of the study is to reproduce the measured growth curves for, e.g. the total energy, the peak frequency, or the Phillips' constant α_p as good as possible. It is hoped to obtain a minimum for the cost function by changing certain parameters in the wind input term and in the dissipation term of the energy transport equation. One will have to take care in the interpretation of the results. Although the optimization routine may not find any further reduction of the cost function, one is never sure that an absolute minimum is obtained. Since the source functions and the energy build-up and propagation are

highly non linear, several local minima may exist. Several starting values for the parameters in the source terms will be used to gain some insight in the possibility of multiple local minima.

The optimization routine will also only minimize the cost function for the given parametrization of the source terms. Although a 'best' fit to the growth curve has been achieved, this still does not give any certainty about the correctness of the source term formulation. It is still important to try to improve our understanding of the underlying physical concepts of each source term. On the other hand the optimization routine will give an excellent tool to evaluate new and different concepts or formulations of the source terms.

Apart from the source terms themselves, there is still the uncertainty concerning the growth curves. There remains the question of nondimensionalizing with respect to the friction velocity u. or to the velocity at an arbitrary fixed height such as u_{10}. Although there is a favourable feeling about u.-scaling, there is no real evidence that it is the correct scaling (Komen et al. 1984, Janssen et al. 1987). The velocity at 10 m height has been used to scale the JONSWAP measurements. A height of 10 m is a convenient height to do wind measurements, but it does not contain any physical elements to justify its use for scaling. The friction velocity u. is a measure for the wind stress in the surface layer of the atmospheric boundary layer and is made to believe to be the only external parameter responsible for the coupling between atmosphere and ocean (Komen et al. 1984). The translation from u_{10} to u. is far from obvious (see chapter 2) and therefore the proposed growth curves that will be used for fitting do not pretend to be the correct ones. There is still some doubt as to whether the growth curves are really represented by power laws and how the transition to a fully developed sea should happen. The work of Kahma and Calkoen (1991) did not really clarify this matter although friction velocity scaling does seem to reduce the scatter.

Ultimately however, one should take an available wave data set, e.g. the combined JONSWAP, Lake Ontario and Bothnian Sea set

described in Kahma and Calkoen (1991), and obtain a best fit model to the scattered data instead of assuming that one has the right, one line growth curve. That way one uses all available information and one is able to make a statistical estimate on how well our model is capable of reproducing the measurements. This approach will not be taken here for several reasons. A first reason is that none of the above data sets is currently available to the author; a second reason is that the added complexity is feared to be such that it would obscure the possibility of gaining more physical insight in the source term formulations by using a more simple approach.

The cost function is formulated in terms of nonlinear least squares. Chavent (1991) states that the reason for the success of the practice of nonlinear least squares is the power of the approach: the only fundamental requirement is to possess a numerical simulator to calculate the output of the model once a set of values has been assigned to the parameters. The admissible set of parameters should be chosen as small as possible by taking into account the largest possible amount of 'a priori' information, i.e. upper and lower bounds, trends,... Still according to Chavent (1991) many people have complained about the lack of uniqueness of the estimated optimal set of parameters, on instability problems of the algorithm or on being stuck in local optima.

5.2 The cost function

A crucial question in any optimization problem is exactly : what does one want to optimize ? In the case of wave models one hopes to be able to calculate wave defining quantities or characteristics, as the significant wave height or mean wave period, with a certain degree of accuracy. To obtain this goal here, we want to minimize the weighted sum of squares of the difference between the measured and calculated total energy, peak

frequency and the Phillips' constant α_p. The following cost function is defined :

$$SUMSQ = \frac{1}{W} \sum_{i=1}^{N} [w_{1,i} (\frac{E_{i,cal}^{*} - E_{i,meas}^{*}}{E_{i,meas}^{*}})^2$$

$$+ w_{2,i} (\frac{f_{p\,i,cal}^{*} - f_{p\,i,meas}^{*}}{f_{p\,i,meas}^{*}})^2 + w_{3,i} (\frac{\alpha_{i,cal} - \alpha_{i,meas}}{\alpha_{i,meas}})^2]$$

(5.1)

where $\quad W = \sum_{i=1}^{N} (w_{1,i} + w_{2,i} + w_{3,i})$

$w_{j,i}$ is a weighting factor and N the total number of sampled values.

The subscripts used stand for :
  j : energy (j=1), peak frequency (j=2), Phillips' constant α_p (j=3)
  i : corresponds to fetch x_i
  cal : calculated values (wave program)
  meas : measured values (growth curve)

The quantity $E_{i,cal}^{*}$ is thus the nondimensionalized energy at fetch x_i obtained by integrating the energy transport equation (3.2) from the initial fetch x_0 up to the fetch under consideration x_i. Similar expressions can be given for the peak frequency and the Phillips' constant α_p (see also 5.4.3). The objective is then to minimize the cost function (5.1) as to obtain an automatic procedure to tune a wave model.
The normalization in equation (5.1) should not lead to numerical problems. The measured wave characteristics used, are all larger than 10^{-3}.

101

5.3 Sensitivity of the cost function to the variation in one parameter

To obtain a better feeling for the variation of the cost function due to possible changes in the free parameters of the source functions, several runs were done with the program ONEDMOD (see Chapter 4). As source terms, the ones proposed by Komen et al. (1984) were used, i.e. the Snyder wind input term and the Komen dissipation term. Only one parameter at the time is varying. The other parameters have the usual values ($a_1=1$; $a_2=1$; $c_1=3.33$ 10^{-5} ; $m=2$; $n=2$). As growth curves the JONSWAP growth curves scaled with u. were taken (equation (2.42)). The program was run with a friction velocity of 0.5 m/s. Only the growing stage was considered here and the fetch choices used in evaluating the cost function can be found in Table 6.1. More details about the initial spectrum and about the choice of fetch values can be found in Chapter 6. The results can be directly compared to the ones found in Chapter 6.

In the Figures 5.1 to 5.5, the value of the cost function versus a particular varying parameter is plotted. In the legend energy stands for the case where only the energy values had a weight of 1 attached and the other weights were zero. Similarly, peak frequency and Phillips stand for the cases where only the peak frequency or the Phillips' constant α_p is considered in the cost function. The other two labels give then combinations of the above.

In the Figures 5.6 to 5.10, the corresponding energy growth curves are given. The growth curves for the peak frequency and the Phillips' constant are given in the Figures 5.11 to 5.15, and Figures 5.16 to 5.20 respectively.
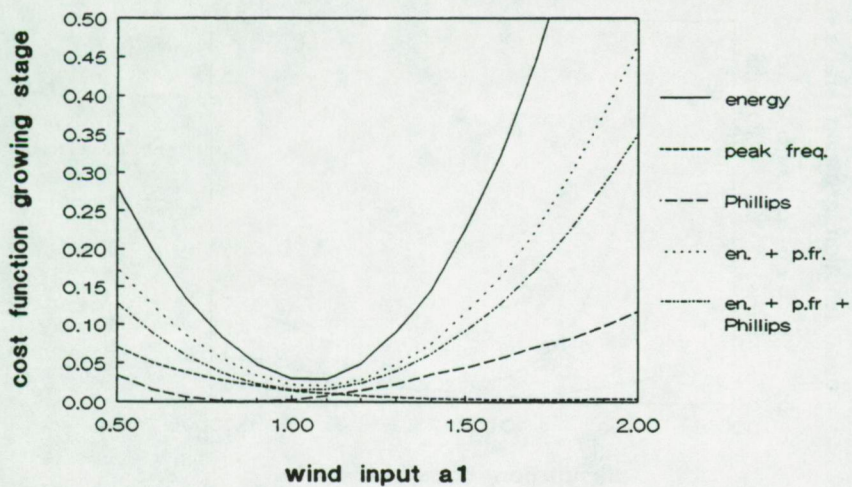
Figure 5.1 : Variation of the cost function with wind input parameter a_1
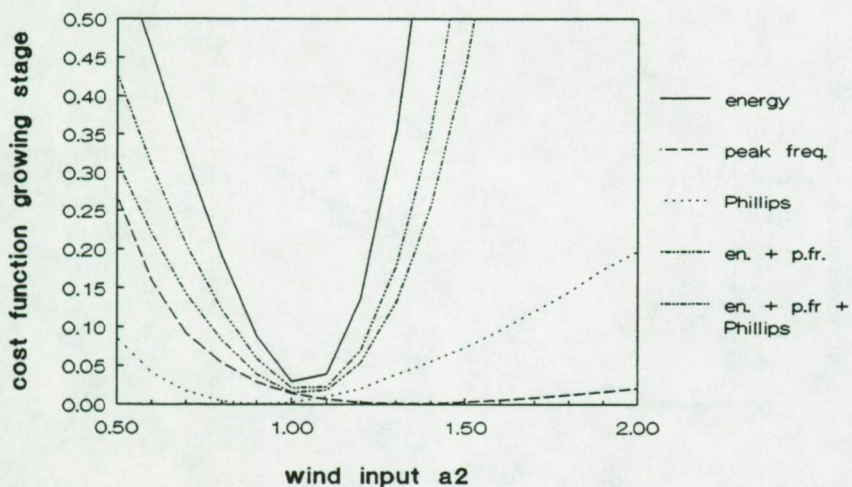
Figure 5.2 : Variation of the cost function with wind input parameter a_2
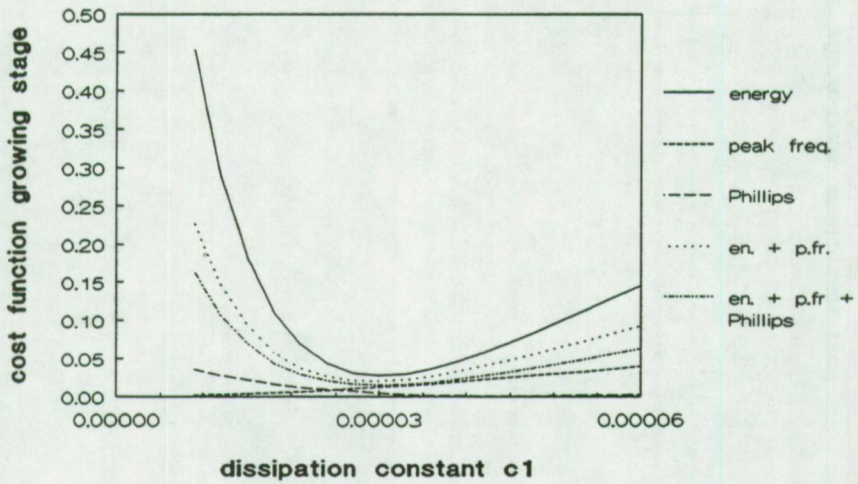
Figure 5.3 : Variation of the cost function with dissipation parameter c_1
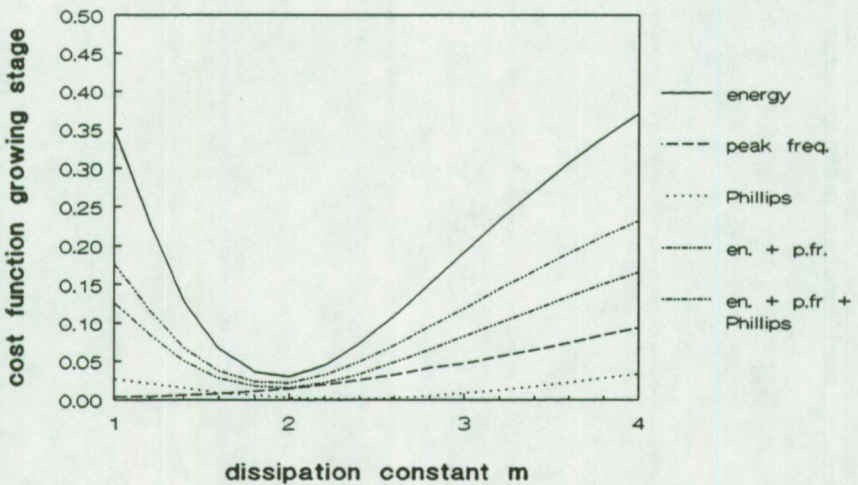
Figure 5.4 : Variation of the cost function with dissipation parameter m
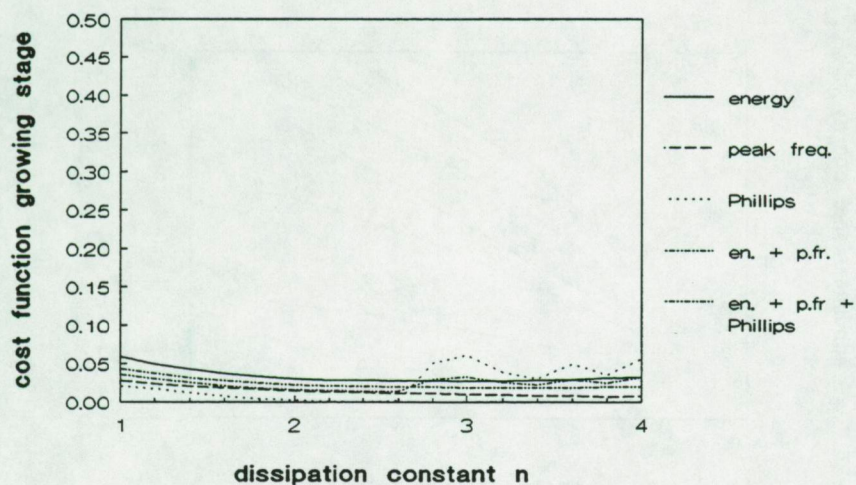
Figure 5.5 : Variation of the cost function with dissipation parameter n
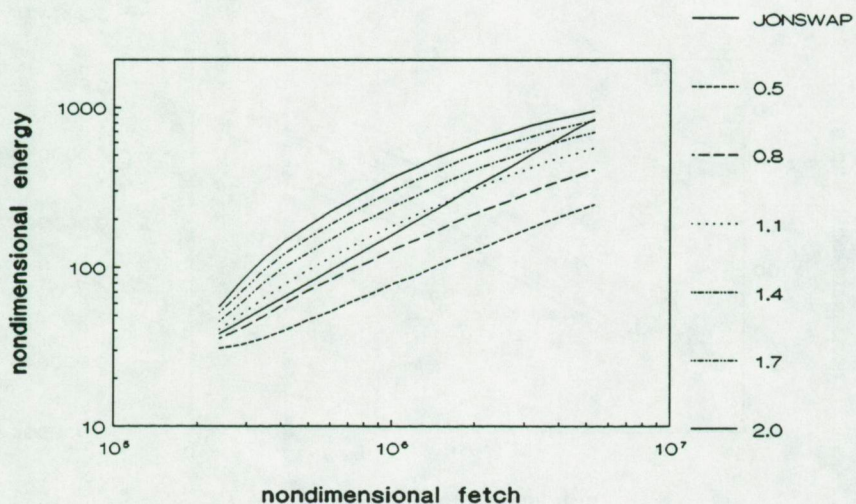
Figure 5.6 : Variation of the energy growth curve with wind input parameter a_l
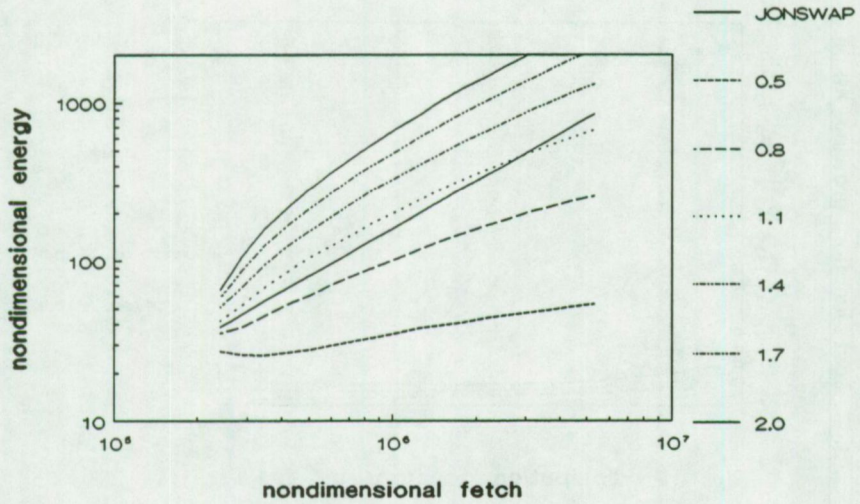
Figure 5.7 : Variation of the energy growth curve with wind input parameter a_2
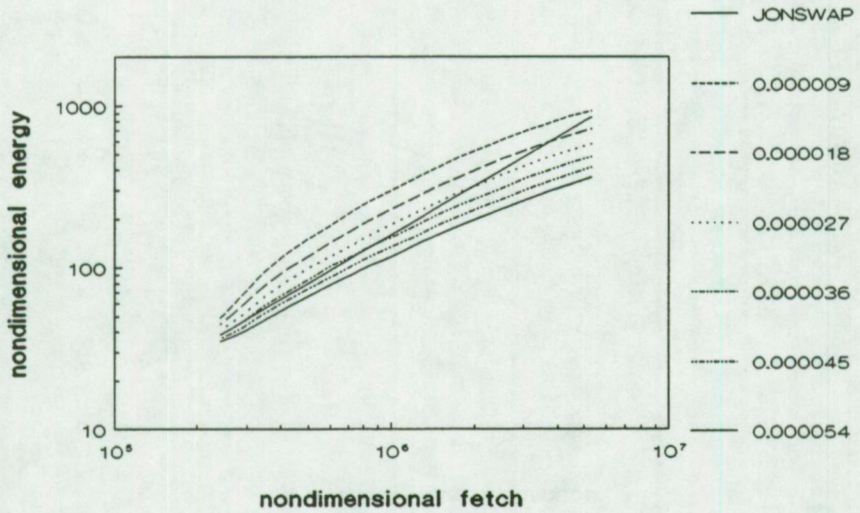
Figure 5.8 : Variation of the energy growth curve with dissipation parameter c_1
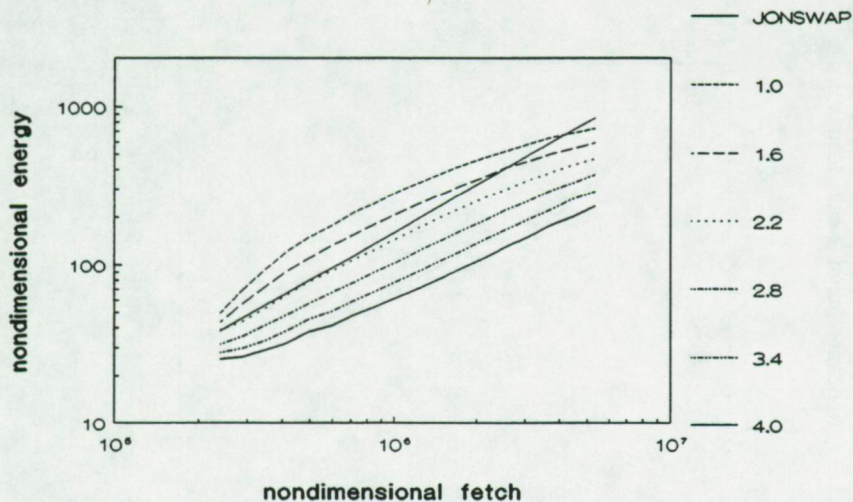
Figure 5.9 : Variation of the energy growth curve with dissipation parameter m
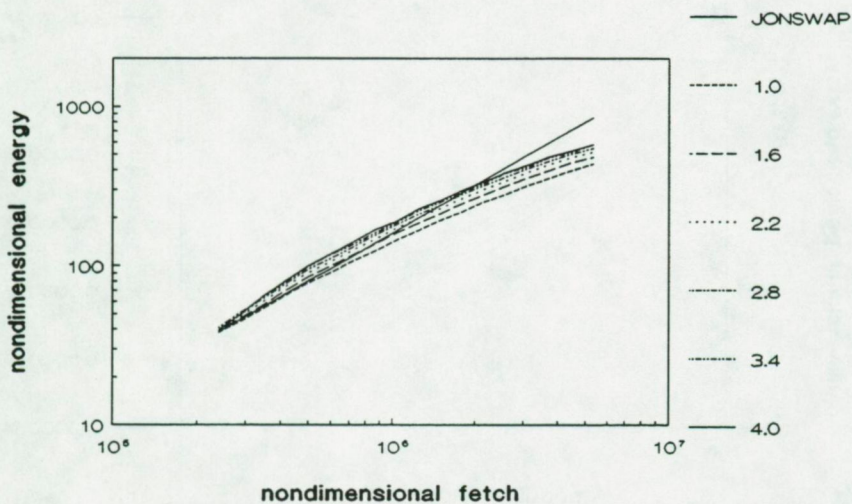
Figure 5.10 : Variation of the energy growth curve with dissipation parameter n

107
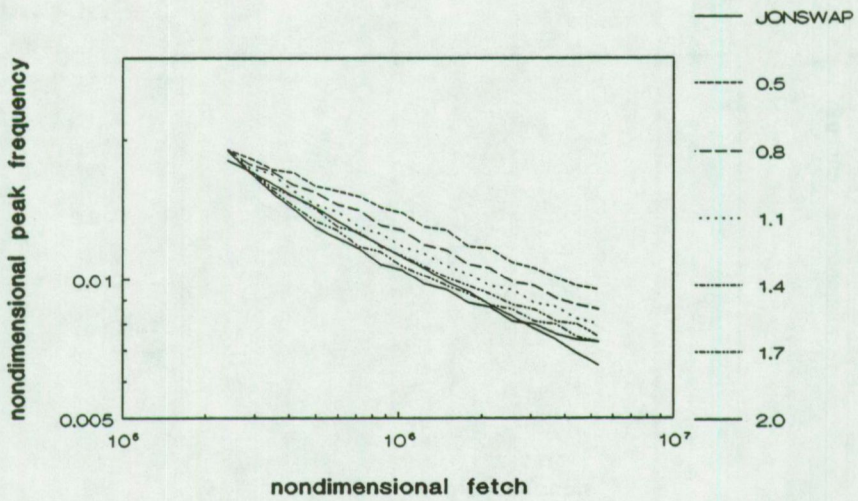
Figure 5.11 :   Variation of the peak frequency growth curve with wind input parameter a_1
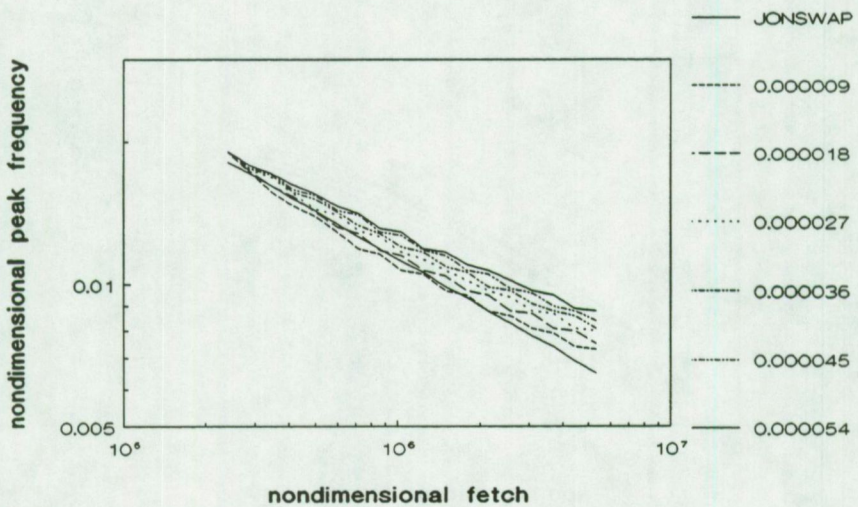
Figure 5.12 :   Variation of the peak frequency growth curve with wind input parameter a_2
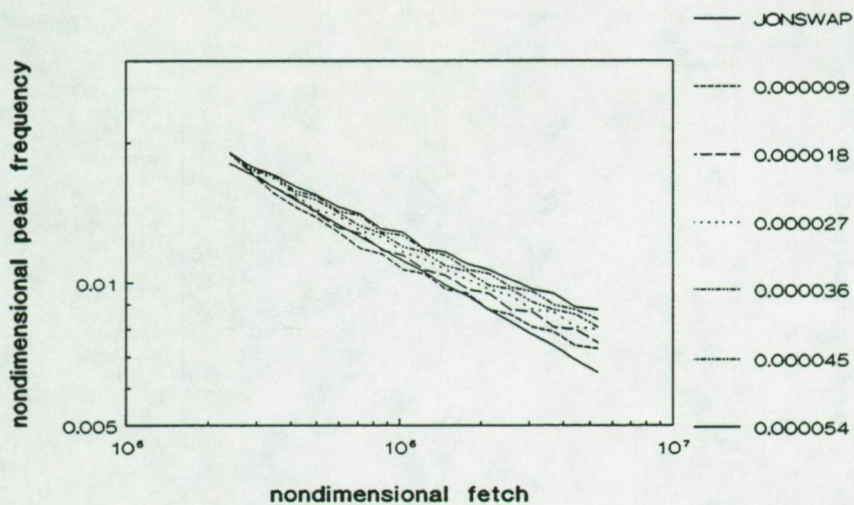
Figure 5.13 : Variation of the peak frequency growth curve with dissipation parameter c_i
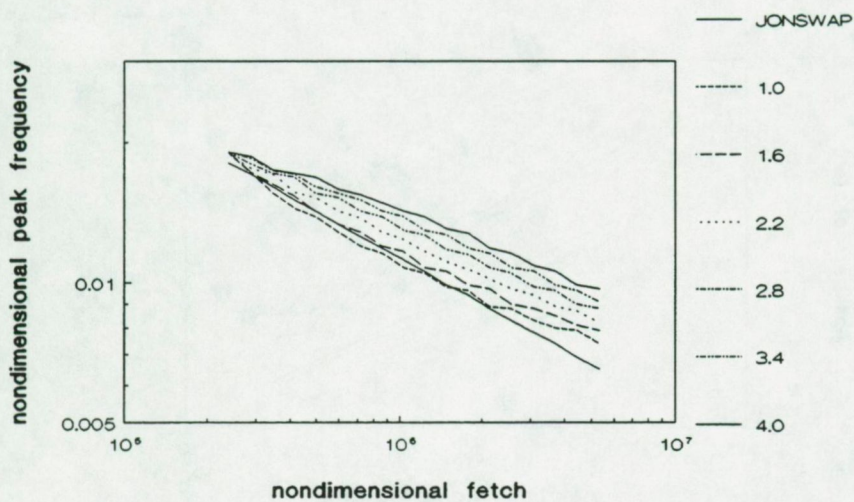
Figure 5.14 : Variation of the peak frequency growth curve with dissipation parameter m

109
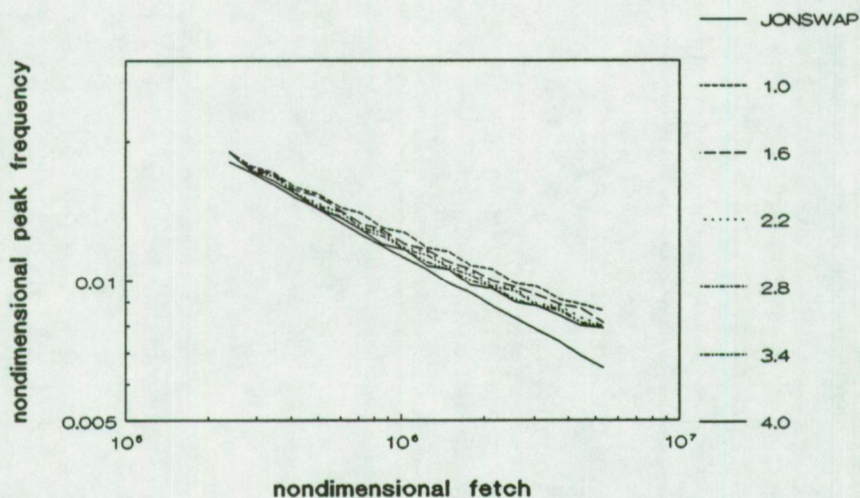
Figure 5.15 : Variation of the peak frequency growth curve with dissipation parameter n
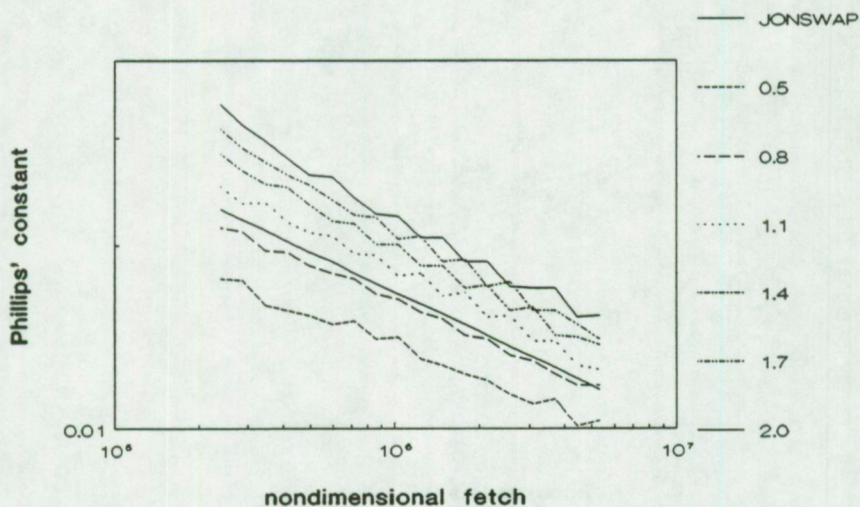
Figure 5.16 : Variation of the Phillips' constant α_P growth curve with wind input parameter a_1

110
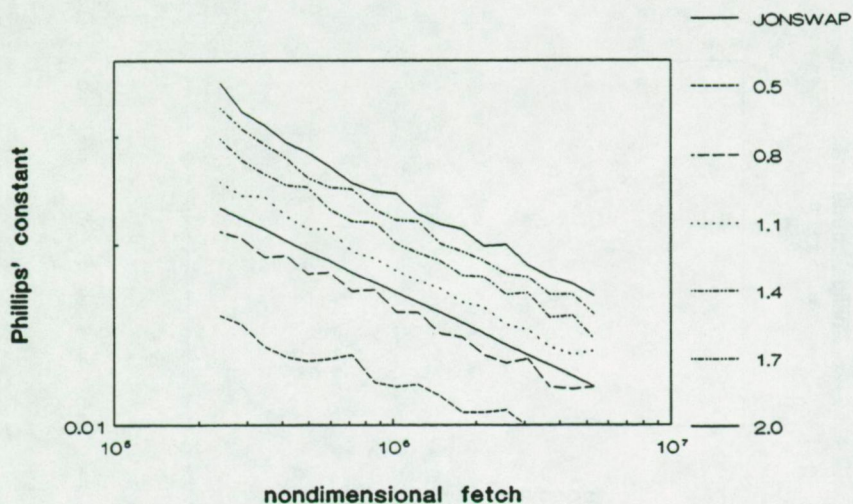
Figure 5.17 : Variation of the Phillips' constant α_P growth curve with wind input parameter a_2
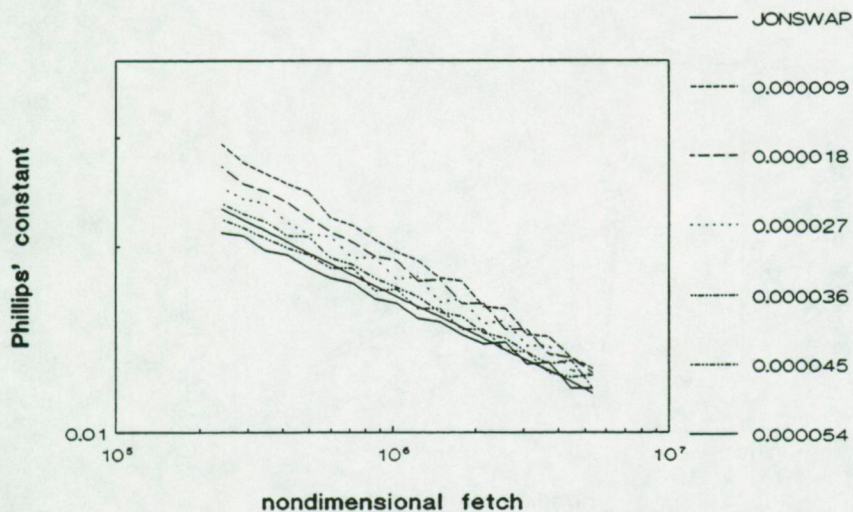
Figure 5.18 : Variation of the Phillips' constant α_P growth curve with dissipation parameter c_1

111
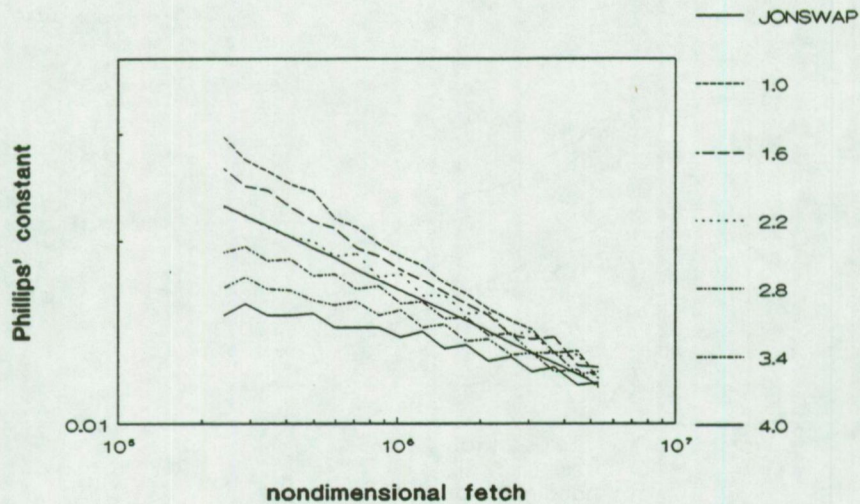
Figure 5.19 : Variation of the Phillips' constant α_P growth curve with dissipation parameter m
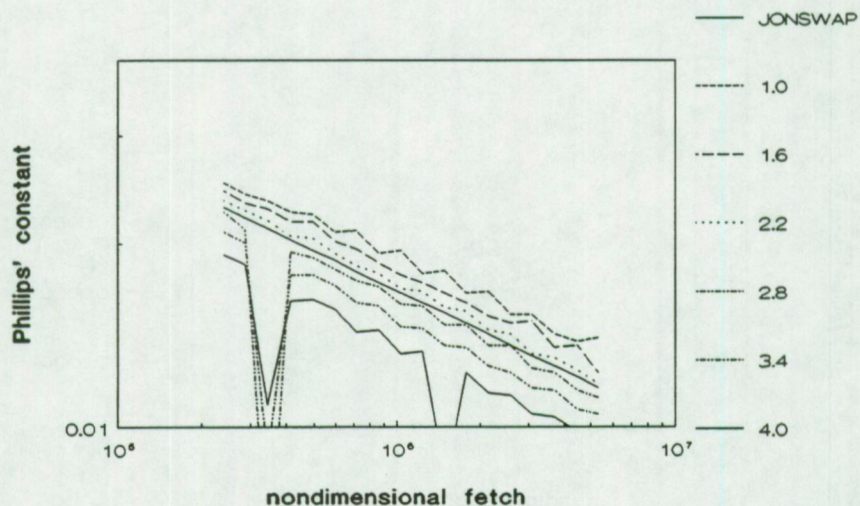
Figure 5.20 : Variation of the Phillips' constant α_P growth curve with dissipation parameter n

A number of conclusions can be drawn from these figures. First of all, the values suggested by Komen et al. (1984) seem to give a solution which is about optimal if you were allowed to change only one parameter in the source term expressions. This is not so surprising since the full 2D-WAM model is capable of producing quite reasonable results in operational circumstances (WAMDI, 1988). Secondly, the magnitude of the cost function is nearly insensitive to variations in the dissipation parameter n (Figure 5.5). Higher values of n (> 2.5) display problems in the estimation of the Phillips' constant α_p. Although total energy and peak frequency remain well represented, the high frequency tail does not show a smooth trend with fetch. Also, variations in the overall dissipation level (parameter c_1, Figure 5.3), do not influence the cost function much in the neighbourhood of its minimum value.

The minima for the cost function when fitting for the energy, peak frequency and Phillips' constant are not located at the same parameter value. It will not be possible to do a good fitting job without compromise. If we want to fit for the energy or the corresponding significant wave height, we may have to be happy with a less accurate prediction of the peak frequency or the Phillips' constant.

More surprising, but nevertheless important is the fact that variations in the different parameters lead to similar growth curves. For example, reducing the dissipation level c_1 has a similar effect on the energy growth curve as increasing the wind input or reducing the wave steepness dependency of the dissipation.

We also notice, in particular for the growth curves of the peak frequency and the Phillips' constant, that these growth curves are not very smooth. They show an undulating behaviour. This is mainly due to the fact that one has to work in a discrete frequency-direction domain and to the way of calculating the nonlinear interactions.

Another problem is the non-smoothness of the cost function (and of its first derivative) for a small variation in the parameter values. A detail of this is given in Figure 5.21. A difference

in cost function value of the order of 10^{-3} can be due to non-smoothness and is therefore about the best resolution one can expect. Problems with local minima will certainly appear and different starting positions in the search for minima will be needed.

One feels already that all of the above remarks, have some consequences on the automatic optimization in one way or another.
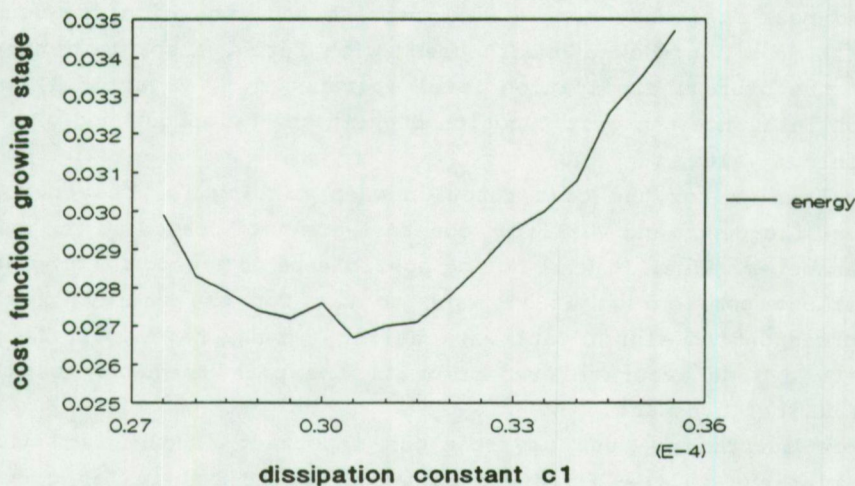
Figure 5.21 : The problem of erratic behaviour in the cost function for small variations in a parameter (e.g. dissipation parameter c_i)

5.4   Solution procedure

5.4.1   General procedure

Quite generally, a minimization problem can be stated mathematically as:

   minimize { F(A) } where A = $(a_1, a_2, \ldots, a_n)$

The parameters a_1 to a_n are the free parameters in the source term formulations considered in this study for the integration of the energy transport equation. The problem we are dealing with here can then be summarized as follows :

parameters A = $(a_1, a_2, \ldots, a_i, \ldots, a_n)$	=>	evaluation of a partial differential equation using A as an input	=>	obtain minimum for the cost function F(A)
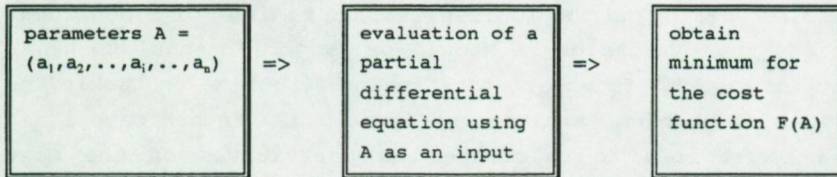
Different methods are available to solve minimization problems. The most efficient of these methods for unconstrained problems are Newton type and quasi-Newton type methods. Newton type methods use the Hessian matrix $G(A^{(k)})$ or a finite difference approximation to the Hessian matrix, quasi-Newton type methods use an approximation of the Hessian matrix to find the search direction (NAG, 1990). The algorithms then generate an iterative sequence $\{A^{(k)}\}$ that is hoped to converge to the solution. The superscript k refers to the kth iteration. The constructed sequence satisfies :

$$A^{(k+1)} = A^{(k)} + \alpha^{(k)} p^{(k)} \tag{5.2}$$

   where $p^{(k)}$:   the search direction
   $\alpha^{(k)}$:   steplength

The direction of search $p^{(k)}$ satisfies the equation
$G(A^{(k)}) p^{(k)} = -g(A^{(k)})$
where $g(A^{(k)})$ is the gradient vector and $G(A^{(k)})$ is the Hessian matrix. The steplength $\alpha^{(k)}$ (a scalar) is chosen so that the next set of parameters yields a smaller cost function value. Note that for finding a good steplength $\alpha^{(k)}$, several evaluations of the

115

partial differential equation may be necessary. Finding this steplength corresponds in these kind of problems to finding the minimum of a function in one variable (i.e. $\alpha^{(k)}$).

5.4.2 Available NAG-routines

Since we are not interested in developing an optimization code as such, use will be made of readily available standard software. The NAG-library (NAG, 1990) supported by the Computing Centre of the KULeuven, provides the possibility of finding a routine for searching the (un)constrained minimum of M nonlinear functions in N variables (M should be larger or equal to N). A summary of the NAG flowchart for finding a routine to tackle the optimization problem is given in Figure 5.22. In our case it is also not feasible to calculate the derivatives of the cost function F(A) analytically, so we have to do it numerically.
It quickly became clear that the use of the most general optimization routine for nonlinear functions subject to bounds, i.e the routine E04JAF, required excessive computer time since both the gradient (i.e. the first partial derivatives of F(A)) and the Hessian matrix (i.e. the second partial derivatives of F(A)) have to be determined numerically. This asks for a large number of evaluations of the partial differential equation ONEDMOD in order to calculate the first and second derivatives. More important however was the fact that the routine quite often has great trouble finding the appropriate steplength $\alpha^{(k)}$ once the search direction is determined. Notice that the stepsize for this routine to calculate the gradient and the Hessian matrix numerically is about 1.3 10^{-6}. One will have to use appropriate scaling factors to have meaningful results (see section 5.4.4 about scaling of the parameters).
It is opportune to take advantage of the special structure of a sum of squares problem, whereby the Hessian matrix can be approximated by using first partial derivatives only (see 5.4.3). The possibility of introducing constraints is lost. It is hoped that an optimum can be obtained without having to put constraints

116

Selection chart
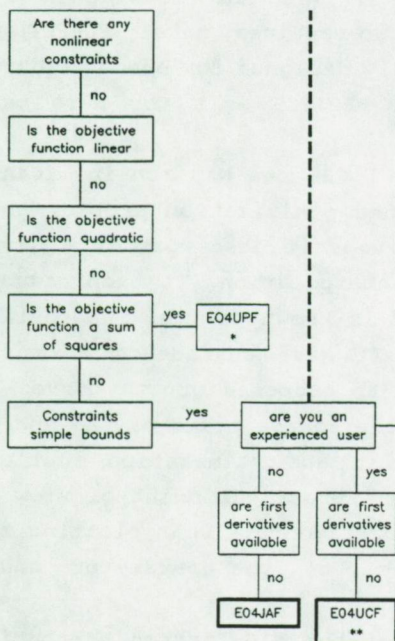
Constrained problems   Unconstrained problems
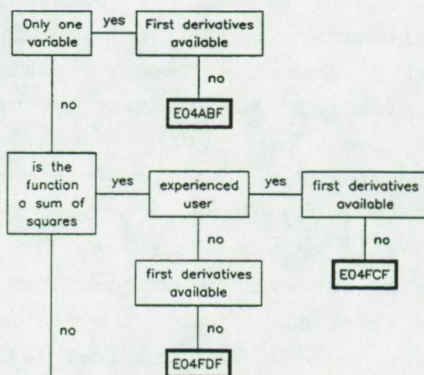
* new in Mark14;
  this version was not
  implemented yet
  (June 24, 1991)

** introduced at Mark 12

Figure 5.22 : Decision free from introductory Guide NAG Fortran Library Mark 14 (1990)

on the parameters. It is believed that parameters far different from those proposed from theories or from those obtained by field experiments, should normally not produce realistic results. If they do produce better results, it can be an indication that one or more of our assumptions, such as source term formulation or accepted growth curve formulation, has or have some shortcomings. The use of the routine E04UCF was not investigated. Since, like E04JAF, it also does not take into account the special structure of a sum of squares problem, it was not considered for implementation. That left us with two routines, namely E04FDF and E04FCF. These routines are specially designed for sum of squares problems. E04FDF is easy in use. E04FCF asks for more user experience (see 5.4.3).

Following the flowchart in Figure 5.22, the NAG routine E04ABF allows for solving an unconstrained minimization problem when there is only one parameter involved. It does work in a given finite interval using quadratic interpolation. It then reduces the interval in which the minimum is known to lie. The routine works without any difficulties. It gave confidence that the approach of obtaining a best fit to proposed growth curves is possible by taking parameters in the source terms of the energy transport equation as variables in an optimization routine. Although it is more elegant, from a practical point of view it is neither much faster nor much more accurate than plotting the cost function value in function of the parameter under consideration (see 5.3).

In the newest release (Mark 14) of the NAG-Fortran subroutine library, the routine E04UPF should be able to handle constraints. Note that the routine E04UPF uses the same sequential quadratic programming (SQP) algorithm as E04UCF (not implemented; see above), and should take advantage of the sum of squares problem structure. In an SQP algorithm the search direction is the solution of a quadratic programming problem. At the time the experiments described in this text were carried out, only the routines E04FDF and E04FCF were available, so that this new routine has not been used.

All routines mentioned above (except E04UCF and E04UPF) have been implemented. They all have the same shell structure (see Figure 5.23). They have been documented with the source code (and necessary Job Controle Language under the IBM-3090 MVS-operating system) in an internal report (Monbaliu, 1992).

5.4.3   Special structure of sum of squares cost function

The cost function (5.1) can be written in the general form of a sum of squares :

$$SUMSQ = F(A) = \sum_{i=1}^{M} f_i^2(A)$$

$$with \ f_i = (\frac{W_{j,i}}{W})^{0.5} (\frac{Y_{i,cal} - Y_{i,meas}}{Y_{i,meas}}) \qquad (5.3)$$

[Y represents E^*, f_p^* or α_P ;

$$f(A) = (f_1(A), \ldots, f_i(A), \ldots, f_M(A))]$$

where $A=(a_1, \ldots, a_n)$ is then the set of parameters to be optimized. Note that :

1. $$E_{i,cal}^* = E_0^* + \frac{g^2}{u_*^4} \{ \int_0^{2\pi} \int_{f_{min}}^{f_{max}} (\int_{x_0}^{x_i} \frac{\partial E(f,\theta)}{\partial x} dx) \ dfd\theta \}$$

    E_0^* is the initial nondimensional energy at x_0

2. $$f_{p \ i,cal}^* = \frac{u_* f_p}{g}$$

    with f_p the frequency where $E_i(f)$, the frequency spectrum at fetch x_i, becomes maximum

3. $\alpha_{p \ i,cal}$: Phillips' constant fitted to the tail of the frequency spectrum at fetch x_i
    Remember that $\partial E(f,\theta)/\partial x$ is given by the energy transport equation (3.2).

4. M corresponds to three times N of the objective function (5.1).

In nonlinear least squares problems one can take advantage of the special structure of the matrix of the second partial derivatives (Hessian matrix) by approximating it. This improves the computational efficiency. The gradient vector g(A) is given by $2 J(A)^T f(A)$ and the Hessian matrix G(A) can be written as :

$$G(A) = 2 [J(A)^T J(A) + \sum_{i=1}^{M} f_i(A) G_i(A)] \qquad (5.4)$$

where   J(A)   :   Jacobian matrix of f(A)

            G_i(A)   :   Hessian matrix of f_i(A)

Two broad classes of specialized algorithms are found in literature (Scales, 1985) : the ones that ignore the second term on the right hand side of equation (5.4) and which are called *small residual algorithms*, and the ones that approximate that term in some way and which are called *large residual algorithms*. The NAG-routines E04FCF and E04FDF, use the Gill-Murray method. This method is a combination of a Gauss-Newton method (small residual algorithm) and a modified Newton method (large residual algorithm). The Jacobian matrix, containing first derivatives of f_i(A) only, has to be calculated. Second derivatives of f_i(A) do not have to be evaluated. For more details, we refer to Gill and Murray (1976), Gill et al. (1981), and Scales (1985). In appendix A, a brief description of the principle behind Newton's method for finding a zero of a function is given. In appendix B, the definitions for Jacobian and Hessian matrices are given. The special case of a function which is the sum of squares of functions, is treated. From the two NAG-routines which provide the possibility of solving an unconstrained minimization problem in the form of equation (5.3) for more than one parameter, E04FDF is easier in use. However, the additional features of E04FCF such as the monitoring routine and the free choice of some tuning parameters, were advantageous in analyzing and understanding the encountered problems. For the computer runs described in Chapter 6, the NAG-routine E04FCF has been used. Note that the routines E04FCF, E04FDF and E04ABF gave virtually the same result when run for a single parameter only.

A flowchart of the structure of the final optimization program is given in Figure 5.23.
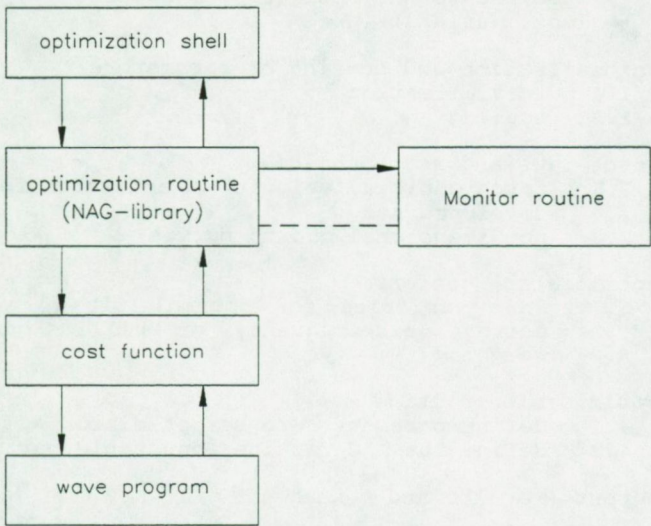
Figure 5.23 :   Structure of the optimization program

The different blocks in this structure are worked out in more detail in Figures 5.24 for the optimization shell, in Figure 5.25 for the non-mandatory monitoring routine and in Figure 5.26 for the cost function. The wave program block has been given in Chapter 4.

```
Optimization shell

variable declaration  -> common variables
       -> specific to NAG optimization routine
       -> local variables

1.   initialisation and scaling of parameters
       1.1   initialisation
       1.2   scaling

2.   fetch laws and fetch choices
       2.1   fetch choices, velocity u. and fetch for fully
             developed sea
       2.2   nondimensional growth curves

3.   optimization options
       3.1   wave variables for optimal fit (i.e. total
             energy, peak frequency, or Phillips'constant)
       3.2   weights

4.   optimization routine
       4.1   define parameters to be optimized
       4.2   define the NAG routine adjustable parameters

5.   output (results and messages)
```

Figure 5.24 :   The optimization shell

```
Monitor routine

print   -   iteration number
        -   Jacobian matrix
        -   residuals
        -   singular values
        -   grade of the matrix
        -   number of times the cost function program is
            called
        -   calculates the gradient (by subroutine)
```

Figure 5.25 :   The monitoring routine

```
Cost Function

1. parameters for input and dissipation source terms

2. calculation of wave variables until maximum fetch

3. cost function calculation

4. intermediate output

5. optional convergence test (user defined)

6. rewind files for wave program
```

Figure 5.26 :   The cost function

The program structure in the Figures 5.23 to 5.26 is general and the details still have to be filled in by the user : choice of NAG-routine (considered as a black-box routine), choice of source terms in the wave program, choice of cost function, choice of weights, choice of growth curves, choice of fetches, etc... The NAG-routine is called by the main program. The NAG optimization routine then calls the subroutine in which the definition of the cost function has been programmed. This subroutine in turn, calls the wave program to calculate the required wave quantities for each set of source function parameters estimated by the optimization routine. Most of the computing time is therefore spent in the wave program.

The time spent in the wave program could be reduced by using an implicit integration scheme instead of the dynamically adjusting first order scheme used here (see Chapter 4). Luo(1991) showed that many of the results of an explicit integration scheme could be reproduced by an implicit integration scheme. The implicit scheme was not used here. The full 2D-WAM model (WAMDI, 1988) also uses the dynamically adjusting first order scheme for the advection term integration. An interesting report comparing different finite difference advection schemes for the advection

equation has been made by Dijkhuis (1990). It is worthwhile to spend more energy in finding a better finite difference scheme than the one used here in order to reduce the numerical errors invariably connected with each iteration scheme. This has not been done in this study.

5.4.4 Scaling of the parameters

For the routine E04FCF and E04FDF scaling of the parameters is required. The variables to be optimized are not necessarily of the same order of magnitude in the region of interest. In particular the overall dissipation level parameter c_1 is considerably different in magnitude from the other parameters. The optimization programs only work properly if the parameters to be optimized are scaled so that they are approximately equal. According to the NAG manual, also the cost function should be scaled in such a way that a unit change in one of the parameters corresponds approximately to a unit change in the cost function. Some test done by the author however showed that scaling of the cost function is neither important for finding the search direction nor for finding an appropriate steplength. It is however crucial in fulfilling the convergence criteria given in section (5.4.6).

Also very important is the magnitude of the scaling factors for the parameters. To find a search direction, the optimization program E04FCF (and also E04FDF) calculates the gradient numerically with a finite forward-difference approximation. To do this, it changes the parameters $A(a_1, \ldots, a_n)$ by a very small absolute step, on the IBM-3090 of the order of 1.10^{-8}. For purposes of curve fitting where the function value can be evaluated accurately after a change in one parameter (i.e., round-off errors are smaller than the changes due to the difference in the parameter value), this does not pose any problems. However, when integrating the energy transport equation (3.2), numerical errors, larger than possible round-off errors, are created. The objective function (5.1) varies randomly and becomes erratic for small changes in the parameters (see also

124

Figure 5.21). The minimization routine produces information which is totally irrelevant for solving the problem. As a possible source for the erratic behaviour of the cost function, the added high frequency tail can be indicated. Also, the dynamically adjusting integration scheme, creates problems. Small differences in the parameter values, often give rise to a different integration step. This phenomenon has been observed. The number of integration steps to reach a particular fetch (starting from the same position) differs depending on the values of the parameters. According to Bard(1974) this can cause severe errors in the calculated gradients. He suggests that all calculations necessary to obtain a complete set of differences to calculate the gradient, should be done with the same integration step size. This is quite impractical. It complicates the choice of wave model. We would loose the advantage of not having to worry about the wave model as such. The option taken here, is to have a reasonably large step for the parameter change to obtain a good search direction. Experience shows that the stepsize for calculating the search direction should be of the order of a few, up to even twenty percent of the parameter value. To obtain this, the parameter a_1 (equal to about 1) in the wind input term according to Snyder (equation (3.24)) should for example be divided by a scaling factor of about 10^6 up to 10^7. In this way an absolute change of 1.10^{-8} represents 1 to 10 percent of the parameter value. Similarly the parameters m and n in the dissipation term (equation (3.27)), should be divided by a factor of the order of 10^6 to 10^7 and the overall dissipation level c_1 should have a scaling factor between 30 and 300.

It is not advisable to work with large scaling factors too close to a minimal solution for the cost function. The change in the parameter to find an initial search direction may then jump over the minimum, giving misleading information to the optimization program. This problem can be overcome by restarting the program with smaller scale factors. The scaling factors should still remain large enough to avoid problems of erratic behaviour mentioned above. If the program jumps to parameter values which are unreasonably far away from the previous iteration step, it

means that no smaller value for the cost function could be found in the search direction. Further improvement of the fit is quite unlikely. Only another initial position may indicate otherwise. Although not tried yet, it may be worthwhile to use negative scaling factors, since the program then calculates the derivatives of the functions in the sum of squares in the other direction. This may overcome local minima problems.

5.4.5 NAG-supplied adjustable parameters

The accuracy of the linear minimization in every iteration step of the optimization routine E04FCF can be adjusted (see equation (5.2)). It should be set to what is called low accuracy linear minimization. More specifically, the best behaviour of the optimization routine was obtained for large values of the ETA parameter (up to 0.99). This forces the optimization program to recalculate the search direction frequently and reduces the number of times the wave program ONEDMOD is called during one iteration step of the optimization routine. Lower values of the parameter ETA force the routine to use most of its energy in finding the best step length.

The parameter MAXCAL should be set to a rather low value (say 20 to 50 times the number of parameters to be optimized) and not the 400 times N as recommended in the NAG manual. Remark that the optimization program always finishes one iteration step, i.e. tries to find a minimum for the current search direction. It is only after the iteration loop, that it compares the number of calls it made to the cost function with the parameter MAXCAL. It is thus possible that the actual number of calls to the cost function exceeds the parameter MAXCAL considerably if it has to spend a lot of time to find the best step length in the case of high accuracy linear minimization. As was mentioned in section (5.4.4) about the scaling of the parameters, the evaluation of the wave characteristics that we want to compare to the measurements is 'erratic'. It is sometimes better to restart the

optimization program at the apparently best solution found up to this point (see above).

The parameter IFAIL can be used to escape out of the optimization process when we feel that the convergence is not good. It is good to keep track of the number of times the cost function is called inside the cost function routine. By setting the error and warning indicator IFAIL to a negative value when the number of calls to the cost function routine exceeds MAXCAL considerably, we avoid getting stuck in a local minimum for too long.

The parameter XTOL will be discussed in section 5.4.6 about the convergence of the optimization routine.

5.4.6   Convergence

For a successful exit from the NAG-optimization routine E04FCF some conditions have to be fulfilled. If one agrees that an average error of a few percent on the fit to the growth curves is acceptable to account for possible deviations from a power law, one could stop at that point. The average error could be defined as the square root of the cost function (equation 5.1). The NAG user's manual for the routine E04FCF gives its own convergence criteria. They are given in Figure 5.27.

$$B1 \equiv \alpha^{(k)} \| p^{(k)} \| < (XTOL + \epsilon) \times (1.0 + \| A^{(k)} \|)$$

$$B2 \equiv |F(A)^{(k)} - F(A)^{(k-1)}| < (XTOL + \epsilon)^2 \times (1.0 + F(A)^{(k)})$$

$$B3 \equiv \| g(A^{(k)}) \| < (\epsilon^{1/3} + XTOL) \times (1.0 + F(A)^{(k)})$$

$$B4 \equiv F(A)^{(k)} < \epsilon^2$$

$$B5 \equiv \| g(A^{(k)}) \| < (\epsilon \times \sqrt{F(A)^{(k)}})^{1/2}$$

Figure 5.27 :   NAG convergence criteria

127

Since the parameters in the differential equation are scaled and are therefore quite small, one will have to make an interpretation of these convergence criteria. Two parameters are important, next to the results obtained from calculation. These parameters are the machine precision ϵ and the NAG adjustable parameter XTOL. The machine precision is the smallest positive real number that gives a result different from 1 when added to or subtracted from 1 and can be obtained with the help of NAG-routine X02JAF and is on the IBM-3090 mainframe equal to $2.22 \ 10^{-16}$. The NAG-parameter XTOL specifies the accuracy to which a solution is required. From section 5.3 concerning the sensitivity of the cost function to the variation in one parameter, we already know that the cost function is quite shallow near the optimum and that small variations in the parameters give rise to erratic behaviour. Therefore the parameter XTOL should ideally be set to about 1 to 10% of the scaled parameter value (typically 10^{-7} to 10^{-9} for the scale factors given in 5.4.4).

In order to have a successful exit from the NAG-routine E04FCF either one of the conditions B4 or B5 in Figure 5.27 should be fulfilled. Another successful exit can be obtained when the condition B1, B2 and B3 are fulfilled simultaneously. It is extremely unlikely that the fourth condition B4 will be met. Such a small cost function value can only be obtained with very large scaling factor for the cost function. The fifth condition B5 is in the current approach harder to fulfil than condition B3 (see below), so that we will have to fulfil the first three conditions simultaneously to have convergence. The first condition (B1 in Figure 5.9), where $\alpha^{(k)}\|p^{(k)}\|$ is the current step in the search direction should not pose any problems. Note that $A^{(k)}$ contains the set of parameters to be estimated. The norm is defined as :

$$\|Y\| = (\sum_{i=1}^{N} Y_i^2)^{\frac{1}{2}}$$

The second condition (B2 in Figure 5.9) is rather difficult to fulfil since the best one can do for the difference between two consecutive estimates of the cost function, is about 10^{-3} (see

Figure 5.21). The only way to circumvent this problem is scaling of the cost function. The recommended value for this scaling is therefore $10^{-3}/(XTOL)^2$. This means that if the difference between two consecutive iterations of the NAG optimization routine becomes smaller than what can be accounted for just on the basis of discontinuities or erratic behaviour, then there is no point in trying to do better.

The third condition (B3 in Figure 5.9) is not really meaningful for large scaling factors for the parameters since the gradient is then calculated with a finite difference approximation which is rather rough near the optimum. This third condition should not be taken too strictly. In practice however, in trying to fulfil condition B2, we will use quite a large scaling factor for the cost function and in this way automatically fulfil condition B3. Once a reasonable cost function value is found, the optimization procedure can be repeated, if we are not pleased with the obtained result. Smaller scaling factors for the parameters should then be used, so that the partial derivatives are calculated with a change in parameter value of only a few percent (maximum 5%). We can then still check whether we are indeed close to a minimum value, by doing a search for every parameter separately. Recommended values for scaling and the procedure to do a search are summarized in Figure 5.28.

5.4.7   Trouble shooting

In a number of occasions the program does not converge or suggests strange parameter values. Although the final parameter values given by the optimization program are ridiculous, it is quite likely that the parameter values suggested in the previous iteration step gave good cost function values. One of the most common cases of strange behaviour of the optimization program is when the cost function value increases from one iteration to the next. Due to our uncommon but necessary choice for scaling, the step in the search direction becomes too large. For some reason the NAG-routine thinks of this as a

A. <u>scaling factors</u>

    wind input   Snyder a_1, a_2 10^7 to 10^6
                     Stewart a_3, a_4 10^7 to 10^6

    dissipation   level c_1 300 to 30
                     steepness   m 10^7 to 10^6
                     frequency   n 10^7 to 10^6

    cost function 10^{12} to 10^{10}

B. <u>NAG parameters</u>

    ETA   0.99
    XTOL 10^{-7}
    STEPMX $5 \cdot 10^{-7}$ to 10^{-7}

C. <u>search procedure</u>

    step 1 : - use rather large scaling factors (high values in A.)
               - do not set convergence criteria very strictly :
                     cost function scaling of 10^{12} to 10^{11}
                     XTOL = 10^{-7}
                     STEPMX = $5 \cdot 10^{-7}$

    step 2 : - use smaller scaling factors but not smaller than minimum values above

    step 3 : - if cost function value is not acceptable, look if anything can be done with a search for one parameter only

    step 4 : - if even step 3 fails, try different starting position and/or different source term

Figure 5.28 :   Recommended search procedure

discontinuity and tries to jump away from that region of parameter values by taking a large step. Large here means one to two orders of magnitude larger than the absolute step it takes to calculate the gradient. Since the problem here is scaled so that the absolute step for the calculation of the gradient is meaningful for the wave program, the 'large' step in the NAG-routine becomes a very large step for the parameter values. The only way to solve this kind of problem, is to restart the optimization program with different scaling factors. One only has to do this, when fit to the growth curve is not satisfactory with the parameters suggested in the previous iteration.

5.5 Summary and conclusions

In this chapter the cost function has been defined as a sum of squares of functions since the practice of nonlinear least squares is known as a powerful approach. The only real need is to be able to calculate the function values.
In a subsequent part, the sensitivity of the cost function to the variation of one parameter only was investigated. Some problems already surfaced: the shallow minimum for certain parameters; the similar influence on the cost function of the different parameters in the source terms, i.e., a change in one parameter can for a great part be compensated by a change in another parameter; and problems of erratic behaviour in the evaluation of the function values.
In the search for a solution procedure, use was made of an existing library of Fortran subroutines, namely the NAG-library. To limit the amount of computer time, the NAG-routine E04FCF was chosen. It takes advantage of the special structure of the sum of squares so that an approximation to the Hessian matrix can be made using first derivatives only. It also has the possibility to adjust convergence criteria.
The chosen finite difference scheme, the added high frequency tail of the energy spectrum, the discrete interaction approximation for the calculation of the nonlinear energy

131

transfer, and the discretization of the frequency-direction energy spectrum, give rise to an erratic behaviour of the cost function for small variations in the parameters. Therefore, the parameters have to be made quite small so that the finite difference approximation for the derivatives gives meaningful results to the optimization routine. The importance of scaling was highlighted and suggestions were given for the magnitude of these scaling factors.

Finally, the convergence criteria were discussed and suggestions were given for the magnitude of the tolerance variables. Scaling of the cost function is hereby necessary since a decrease in the cost function between two consecutive iterations is only significant if it is larger than 10^{-3}, i.e. about the order of magnitude which can be expected for the magnitude of erratic changes in the cost function due to small variations in the parameters.

6 Computer runs

6.1 Introduction

A number of computer runs for fetch limited wind seas were done with the optimization procedure described in the previous chapter (Chapter 5). Details concerning the fetch range, the fetch values for matching measured and calculated wave quantities, and the weights attached to each particular data point will be given for the growing stage, the transition stage and for the fully developed stage. The choice of growth curve for the measured wave variable and the choice of source term formulation for the wave program will be indicated for each set of runs. Upwind boundary conditions, i.e. initial fetch and initial spectrum for the different runs are also described.

6.2 Source terms, measured data and initial conditions

6.2.1 Choice of source terms

The source terms have been formulated in Chapter 3. They are summarized and discussed below in function of the computer simulations to be done.

6.2.1.1 nonlinear interactions :

No attempt has been made to make use of the exact calculations for the nonlinear interactions. It was assumed that the discrete interaction approximation (Hasselmann et al., 1985) is sufficiently accurate and would therefore not appreciably disturb the sensitivity of certain parameters in the wind input term and in the dissipation term. Moreover, the full two-dimensional WAM model also makes use of the discrete interaction approximation. If need arises the computations could be done over

with the exact calculations as given by Van Vledder and Weber (1988).

6.2.1.2 wind input :

Two different types of wind input terms were withheld in Chapter 3 for use in the optimization scheme.

- Snyder type wind input

    The wind input term chosen for a first set of experiments is of the Snyder type, where the parameters, a_1 and a_2 are allowed to vary. The Snyder type wind input term says that the wind input is proportional to the energy in the wave spectrum and that the proportionality factor is a linear function of the ratio between the wind speed and the phase velocity of the wave. It was given in equation (3.24) and is repeated below for convenience:

$$S_{in}(f,\theta) = 0.25 \ a_1 \frac{\rho_a}{\rho_w}(a_2 \frac{28u_*}{c}\cos\theta - 1) \ \omega \ E(f,\theta) \qquad (6.1)$$

    The variation in the parameter a_2 reflects in some ways the lack of knowledge we have in describing the boundary layer above a water surface, i.e. the translation of a velocity measured at a particular height to the friction velocity necessary to drive the numerical model. This ambiguity is also present in the growth curves. Since we do not know exactly from which wave age on we can consider a sea as fully developed, the parameter a_2 gives an additional possibility to tune the wind input term. The parameter a_1 can be seen as determining the overall wind input level. Both parameters will be treated separately.

- Stewart type wind input

    In a second set of experiments the wind input term is of the Stewart type, where only the parameter a_3 and a_4 are allowed to vary. The Stewart type wind input term says that the wind input is proportional to the energy in the wave spectrum and that the proportionality factor is a quadratic

function of the ratio between the wind speed and the phase velocity of the wave. It was given in equation (3.25) and is also repeated below for convenience:

$$S_{in}(f,\theta) = 0.04 \ \frac{\rho_a}{\rho_w} \ a_3 [\ (a_4 \frac{28u_*}{c})^2$$

$$- a_5 (a_4 \frac{28u_*}{c})] \ \cos\theta \ \omega \ E(f,\theta)$$ (6.2)

The parameter a_5 was not considered, see also section 3.4.2. If a_5 would be set to zero, then the waves would not have a reduced growth rate due to wind input although it is clear from measurements (Snyder et al., 1981) that waves travelling at or near the wind speed do not grow much or even do not grow at all.

To have any idea about the behaviour of this type of wind input, a sensitivity run for one parameter only was done and this for the wind input level parameter a_3. The parameter a_4 was set equal to 1. The parameters in the dissipation term had the usual values (as suggested in Komen et al.(1984)). This gave a minimal cost function of 0.091 for a parameter value of 2.2 for a_3 (JONSWAP ; growing stage only). The parameter a_4 is the equivalent of the parameter a_2 in the Snyder type wind input term (see above). Note that the parameters a_3 and a_4 will be treated separately as well (cf. a_1 and a_2 for the Snyder type wind input term).

If there is no other value explicitly mentioned, the parameters a_1, a_2, a_3, a_4 and a_5 have a value 1.

6.2.1.3   the dissipation term :

For the dissipation by whitecapping the expression given by Komen et al.(1984) is used. It was given in equation (3.27) and is also repeated here:

$$S_{diss}(f,\theta) = -c_1 \, \bar{\omega} \, (\frac{\omega}{\omega})^n (\frac{\hat{\alpha}}{\hat{\alpha}_{PM}})^m \, E(f,\theta)$$

(6.3)

The parameters which are allowed to vary are (in view of the sensitivity analysis in 5.3), the parameters c_1 (overall dissipation level), and m (wave steepness dependency) only. The cost function for a variation in the dissipation parameter n has such a shallow behaviour that optimization of this parameter only leads to marginal improvements at a high computational cost and this is not counting on possible numerical problems due to the discontinuity of the cost functions for small changes in the parameters.

The parameter n will always have a value of 2 and if no other values are mentioned, the parameters c_1 and m have a value 3.33 10^{-5} and 2 respectively.

6.2.2 Choice of growth curves

6.2.2.1 JONSWAP

In Chapter 2 the JONSWAP fetch laws (from Hasselmann et al., 1973) were given nondimensionalized with the velocity at 10 m height. Since friction velocity scaling is assumed throughout this work, the JONSWAP relations were transposed with a drag coefficient of 10^{-3} to the relations given in the equations (2.43) and repeated below :

$$E_* = 1.6 \; 10^{-4} \; x_*$$
$$f_p^* = 1.082 \; x_*^{-.33}$$
$$\alpha_p = 0.35 \; x_*^{-.22}$$

(6.4)

$$E_* = \frac{Eg^2}{u_*^4} \qquad f_p^* = \frac{f_p u_*}{g} \qquad x_* = \frac{xg}{u_*^2}$$

136

6.2.2.2 Kahma and Calkoen

The JONSWAP data have been reanalysed since their
original publication of 1973, and compiled together with data
from the Bothnian Sea and from Lake Ontario (Kahma and Calkoen,
1991). This will create the opportunity to look at the influence
of changing the growth curve relations and possibly one will be
able to distinguish between general problems of the optimization
scheme and problems specifically connected to the choice of the
growth curve. In Chapter 2, the Kahma and Calkoen fetch laws were
given nondimensionalized with the velocity at 10 m height but
also in a form nondimensionalized with the friction velocity.
Their findings in terms of the friction velocity were given in
equation (2.50) and are repeated below :

$$E_* = 2.4 \ 10^{-3} \ x_*^{0.78}$$
$$f_p^* = 0.358 \ x_*^{-0.244}$$

(6.5)

6.2.3 Initial spectrum

As initial spectrum, a JONSWAP type spectrum was chosen
with the following characteristics (see Figure 4.3 for a plot of
the frequency spectrum and for a polar contour plot):

- scale parameters : $f_p^* = 0.0193$ and $\alpha_p = 0.0223$
- shape parameters : $\sigma_a = 0.07$; $\sigma_b = 0.09$ and $\gamma = 3.3$

According to the JONSWAP experiments, i.e. the growth curve for
the peak frequency given in equation (6.4), this corresponds to
a spectrum at a nondimensional fetch of $2 \ 10^5$. Note that the
chosen Phillips constant α_p differs from the one given in the
growth curves. This was done to make the total energy consistent
with the energy growth curve (see also Chapter 2). It was
considered more important to have the total energy and the peak
frequency at the right level rather than to have the right
Phillips' constant. For the initial directional distribution a

$\cos^2\theta$ spreading was taken. It is hoped that the initial directional distribution will not have a great influence on the growth curve behaviour. The effect of a different initial directional spreading was however not investigated.

For the Kahma and Calkoen growth curve, the initial spectrum was the same JONSWAP type spectrum as for the runs to fit the JONSWAP growth curves. The starting nondimensional fetch was also chosen at $2 \cdot 10^5$. This results in a slight underestimation of the initial energy (about 2%). This should not affect the optimization procedure. Actually, this deviation of 2% is about the best one would expect as difference between calculated and observed energy levels.

The fetch and weight choices will be chosen identical to the ones used for the JONSWAP growth curves. This makes the interpretation of the results easier, although obtained cost function values can always be compared directly, since the weights are normalized so that the sum of weights equals one (equation 5.2.).

6.3 Fetch choice and weight choice for comparing measured and calculated wave characteristics

6.3.1 Introduction

In view of previous discussions (see Chapter 2 on the growth curves), it is not straightforward to assign weights to the variables one wants to model at the different fetches. For the time being, all the weights will be set equal to 1. This choice is fairly arbitrary and should be changed if there is some evidence that particular data are known with more certainty and therefore should have a relatively higher weight attached to them. In the optimization program (see Chapter 5) there is an option to multiply the individual weights for the energy, the peak frequency or the Phillips' constant α_p with one or zero, as to do an optimization for one of the wave variables only. In fact, all of the experiments described in this chapter were run for an optimal fit to the energy growth curve only. From

Chapter 5 one remembers that the cost function has the largest values for deviations between the observed and calculated total energy levels. Trying to obtain an optimal fit to the energy growth curves, also gives good results for the fit to the peak frequencies, because the source terms tend to keep a self-similar spectrum. The trend of decreasing Phillips' constant α_p with an increasing fetch is also respected. The spread on the measured Phillips' constant α_p values is large however (see JONSWAP growth curves in Chapter 2), so that precise values and even trends are not known with great certainty.

6.3.2 Fetch choice and weight choice in the growing, transition, and fully developed stage

6.3.2.1 The growing stage :

For the growing stage, the fetch values for matching the measured wave variables (growth curves) with the calculated values (wave program ONEDMOD) are given in Table 6.1. This fetch choice is based on a logarithmic scaling where x_i^{i+1} equals 1.2 times x_i^i and covers approximately the fetch range of the JONSWAP experiment. Remember that although all variables discussed here are in nondimensional form, the computer runs were done in dimensional form with a friction velocity of 0.5 m/s as the driving force.
The weights have a value of 1, as mentioned in the introduction (6.3.1).

6.3.2.2 The fully developed stage

Komen et al. (1984) showed that the principal features of the Pierson-Moskowitz spectrum such as the total energy, the peak frequency, and the Phillips' constant α_p can be obtained for large fetches. However, the detailed directional distribution

139

differs from a simple $\cos^2\theta$ or from the more sophisticated
distribution as given by Hasselmann et al.(1980) (see Chapter 2
for the directional distributions). Based on the measurements of
Pierson and Moskowitz (1964), Komen et al.(1984) propose the
following :

$x_*^{PM} = 1.2 \ 10^8$; $E_{PM}^* = 1.1 \ 10^3$; $f_{PM}^* = 5.6 \ 10^{-3}$; $\alpha_p^{PM} = 0.0081$

As mentioned in Chapter 2, there is no real evidence for a fully
developed stage. A strongly reduced growth at large fetches seems
logical. The above values will be used as representative for a
fully developed sea. The fetch values for matching the measured
wave variables with the calculated values are also given in Table
6.1. They are centred around a nondimensional fetch of $1.2 \ 10^8$
and are logaritmically spaced (x_*^{i+1} equals 1.1 times x_*^i). Note
that the first nondimensional fetch is nearly an order of
magnitude larger than what would be expected from the JONSWAP
growth curves. The weights for the variables were again all set
equal to 1, as was the case in trying to fit the growing stage
only.

No experiments were carried out for optimizing parameters for a
fully developed sea alone. It could be done with a Pierson-
Moskowitz spectrum as initial spectrum with, a value for the
Phillips' constant α_p and the peak frequency as suggested above,
and at an initial fetch of for example $0.4 \ 10^8$. This would give
an initial nondimensional energy E. value of 1048 which is close
to the value of 1100 suggested above.

6.3.2.3   Transition stage

In the optimization exercise, no weight, was attached
to calculated values in the transition zone. Only trying to match
the growing part and the fully developed part of the growth
curve, was considered.

Therefore the weights corresponding to the fetches for the
transition stage were set to zero. The fetches are also given in
Table 6.1.

140

Including the transition stage for a weight choice of zero, is a burden for the optimization program because one introduces a number of zeros in the Jacobian and Hessian matrix. No numerical problems which could be related to this weight choice, were encountered however, and since virtually all computer time is spent in the wave program, the advantage of having a very general program structure was considered more important.

growing stage ($* 10^{-6}$)	transition stage ($* 10^{-7}$)	fully developed stage ($* 10^{-8}$)
0.2400	0.6390	0.5089
0.2880	0.7668	0.5598
0.3456	0.9202	0.6158
0.4147	1.104	0.6774
0.4977	1.325	0.7451
0.5972	1.590	0.8196
0.7166	1.908	0.9015
0.8600	2.290	0.9917
1.032	2.748	1.0909
1.238	3.297	1.2000
1.486	3.957	1.3200
1.783	4.748	1.4520
2.140		1.5972
2.568		1.7569
3.081		1.9326
3.698		2.1259
4.437		2.3385
5.325		2.5723

Table 6.1   Nondimensional fetch choice for comparing measured and calculated wave characteristics

6.4   Computer runs

6.4.1   Introduction

The computer runs are designed to obtain optimal
parameter values in the wind input and/or the dissipation source
term, so as to reproduce the chosen growth curves for fetch
limited wind seas. The parameters under consideration are a_1 and
a_2 in the Snyder type wind input term (equation (6.1)) ; a_3 and
a_4 in the Stewart type wind input term (equation (6.2)); and c_1
and m in the Komen dissipation term (equation (6.3)). In each
run, two parameters will be free. The following combinations are
investigated:
- one of the parameters (a_1, a_2, a_3, or a_4) from the wind input
  term, and the overall dissipation level c_1,
- the two parameters from the dissipation term (c_1 and m).
Remember from section (5.3), that the parameter n in the
dissipation term was not considered. The cost function is, for
a fit to the energy growth curve, nearly insensitive to variation
in this parameter.
For the growth curves either the JONSWAP (equation (6.4)) or the
Kahma and Calkoen (equation (6.5)) energy growth curve is chosen.

6.4.2   Illustration of the effect of scaling and of the NAG-
adjustable parameters

In Table 6.2, a summary is given of the runs done to
assign optimal values to the parameters in the Snyder type wind
input term and in the Komen dissipation term. The fit considered
is the fit to the JONSWAP energy growth curve. This first set of
runs is quite large. It is used to demonstrate the effect of
scaling and the influence of the NAG-routine adjustable
parameters.
The effect of scaling factors is well illustrated in the runs 2e
and 2f, and the runs 2g and 2h.   Run 2f and run 2g have

142

relatively small scaling factors for the adjustable parameters a_2 and c_1. If the gradient is calculated using small scaling factors, the optimization program is not able to escape from the starting region of parameter values. If one forces the program to calculate a gradient with a relatively large difference in parameter values (runs 2e and 2h), it is possible to find a route in this shallow region of the cost function.

The effect of the different adjustable NAG-parameters can be observed from runs 2a and 2e. Run 2a has values for the NAG parameters as were recommended in Chapter 5, while 2e has other values. Although run 2e has a slightly better final cost function value (but not better than what can be accounted for due to the erratic behaviour of the cost function for a small variation in one parameter, see 5.3), it did not satisfy the convergence criteria imposed by the optimization routine. In run 2a on the other hand, convergence has been reached after 2 iterations only. The cost function is still larger than in some of the other runs. The trend is similar. There is an increase in the wind input and in the damping level.

It is clear that the scaling factors for the parameters to be optimized, mainly determine the ability and the speed to get away from the starting position and/or from some local minima, therefore they should be relatively large. The adjustable NAG-parameters together with the scaling factor for the cost function on the other hand, mainly influence the strictness of the convergence criteria. The values recommended in Chapter 5, most often avoid that one spends too much calculational power to obtain only marginal improvements in the calculated cost function.

	source term parameters (initial → final)				(initial → final)	scaling factors					NAG parameters		
run	a_1	a_2	c_1 (* 10^5)	m	cost function	a_1 *10^{-6}	a_2 *10^{-6}	c_1	m 10^{-6}	cost *10^{-10}	XTOL *10^7	STEPMX *10^7	remarks
growing stage													
1a	1.28 → 1.08	1.	4.4 → 3.47	2.	0.032 → 0.0275	10	-	200	-	50	1	5	1 iteration
1b	0.64 → 0.56	1.	1.19 → 0.536	2.	0.023 → 0.018	10	-	200	-	50	1	5	2 iterations
1c	0.56 → 0.40	1.	0.54 → 0.018	2.	0.019 → 0.019	10	-	100	-	50	1	5	2 iterations
2a	1.	1. → 1.37	3.33 → 7.21	2.	0.0297 → 0.00965	-	10	200	-	50	1	5	2 iterations
2b	1.	0.5 → 1.66	1. → 11.0	2.	0.433 → 0.00522	-	10	200	-	10^{-4}	5 10^3	5 10^3	4 iter. (NC)
2c	1.	0.5 → 1.66	1 → 11.4	2.	0.0297 → 0.00539	-	10	200	-	10^{-2}	5 10^3	5 10^3	4 iterations
2d	1.	0.5 → 1.61	4.5 → 10.2	2.	0.629 → 0.0062	-	5	100	-	10	1	5	4 iterations
2e	1.	1. → 1.45	3.33 → 8.25	2.	0.0297 → 0.008	-	10	200	-	10^{-2}	5 10^3	5 10^3	4 iter. (NC)
2f	1.	1. → 1.07	3.33 → 3.55	2.	0.0297 → 0.0224	-	1	20	-	10^{-2}	5 10^3	5 10^3	2 iterations
2g	1.	0.5 → 1.06	1. → 3.62	2.	0.433 → 0.0229	-	5	100	-	100	1	1	3 iterations
2h	1.	0.5 → 1.52	1. → 9.36	2.	0.433 → 0.00713	-	10	200	-	100	1	1.1	5 iterations
2i	1.	1.66 → 1.66	1.11 → 11.0	2.	13.09 → 0.00578	-	10	200	-	10^{-2}	5 10^3	5 10^3	7 iterations
3a	1.	1.	3.33 → -	2. → -	0.0297 → -	-	-	200	10	50	1	5.	neg. c_1 1st iter.
3b	1.	1.	3.33 → -	2. → -	0.0297 → -	-	-	100	5	50	1	5.	neg. c^1 after a few iterations
3c	1.	1.	3.33 → 0.361	2. → -	0.0297 → 0.00285	-	-	100	5	50	1	1.5	5 iterations
3d	1.	1.52	7.0 → 5.95	2. → 2.49	0.0744 → 0.00233	-	-	200	5	50	1	3.	2 iterations
3e	1.	1.52	6.93 → 4.52	2.83 → 2.82	0.0721 → 0.0016	-	-	100	1	50	1	1.1	4 iterations

run	source term parameters (initial → final)				cost function	scaling factors					NAG parameters		remarks
	a_1	a_2	c_1 (* 10^5)	m		a_1 *10^{-6}	a_2 *10^{-6}	c_1	m 10^{-6}	cost *10^{-10}	XTOL *10^7	STEPMX *10^7	
	growing + fully developed stage												
4a	1. → 1.01	1.	3.33 → 3.074	2.	0.0177 → 0.0145	5	-	100	-	5	1	5	1 iteration
4b	2. → 1.02	1.	4.5 → 3.182	2.	0.2 → 0.0145	5	-	100	-	10	1	5	2 iterations
5a	1.	1. → 1.05	3.33 → 3.89	2.	0.0177 → 0.0128	-	5	100	-	100	1	5	1 iteration
5b	1.	1.24 → 1.21	6.62 → 5.91	2.	0.0157 → 0.0129	-	2.5	50	-	10	1	5	2 iter. (NC)
5c	1.	2 → 1.17	4.5 → 5.66	2.	43.72 → 0.0128	-	5	100	-	10	1	5	6 iterations
6a	1.	1.	3.33 → 3.05	2. → 2.04	0.0177 → 0.014	-	-	50	2.5	20	1	3	2 iterations
6b	1.	1.	3.33 → 3.09	3. → 2.014	0.107 → 0.014	-	-	100	5	20	1	3	3 iterations
6c	1.	1.	1. → 3.04	3. → 2.023	0.803 → 0.014	-	-	100	5	20	1	3	3 iterations
6d	1.	1.52	5. → 15.5	3. → 1.458	1.44 → 0.0126	-	-	100	5	20	1	3	4 iter. (NC)
6e	1.	1.52	5. → 15.5	1. → 1.484	6.79 → 0.0123	-	-	100	5	20	1	3	5 iter. (NC)

NC : did not satisfy NAG convergence criteria after number of iterations given (cause : cost function in next iteration larger than in the one given)

Table 6.2 Runs for fitting the JONSWAP energy growth curve using a Snyder type wind input source term

6.4.3   JONSWAP growth curve - Snyder type wind input

As mentioned in the previous section (6.4.2), an extensive summary of the runs done can be found in Table 6.2.

6.4.3.1 wind input and overall dissipation level were allowed to vary

When we tried to fit the growing stage, the optimization program had great difficulty finding an optimal value for the parameter a_1 (runs 1a to 1c). One can visualize the solution surface as trough shaped with no clear minimum and with slightly better cost function values for low or even physically unrealistic negative damping levels combined with low wind input levels. It became clear that the reason for this is that changes in the overall dissipation level can be compensated by changes in the wind input level, leading to nearly identical cost function values for widely varying coefficients. Indeed the parameters a_1 and c_1 are part of the proportionality factor to the energy level of their respective source term at that moment or place. The other part of the proportionality factor is only slowly varying with frequency. An optimization program cannot deal with this kind of minimum behaviour. We shall have to impose additional constraints and/or additional requirements.

Another set of runs was done to investigate the combined behaviour of the wind input parameter a_2 and the overall dissipation level c_1 (runs 2a to 2i). All parameter combinations overestimate the energy at short fetches and underestimate the energy at larger fetches. The best combination for fitting the growing stage only, seems to be a value of about 1.65 for the wind input parameter a_2 and a value of about 11. 10^{-5} for the overall damping level c_1.

When we also try to fit the fully developed stage, the results are the following. The optimization exercise for the parameters a_1 in the wind input term and c_1 in the dissipation term gave, for two quite different starting positions, a nearly identical final cost function value (runs 4a and 4b). The final parameter values

146

found do not differ much and are in fact very close to what Komen et al.(1984) recommended as good values for reproducing fully developed wind sea conditions.

In the runs 5a, 5b and 5c, the parameters a_2 and c_1 were allowed to vary. In run 5a, the initial values for the parameters are again the ones from Komen et al. (1984). The optimization program converged after only one iteration. As many as nine calls to the wave program were made in that one iteration. That means that even a low accuracy linear minimization in the search direction (high ETA-value, see 5.4.5), has a considerable amount of trouble, indicating that in this search direction the minimum is not clearly defined. Reducing the scaling factors for the parameters to be optimized may help to have less function calls in one iteration. However, it would not necessarily give a smaller final cost function value. As can be seen from run 5b and run 5c, a similar final cost function value can be obtained starting at other initial values. Notice that run 5c, although having a very large initial cost function value, converged to a solution not far from the one found in run 5b. The resulting optimal parameter values differ from the ones found in run 5a. For a final cost function in the different runs, which differs less than what can be accounted for by discontinuities in calculating the cost function (of the order 10^{-3}), the final combinations for the parameter values differ more than 10 % for a_2 and more than 50 % for c_1. One can thus conclude that the problem is not so well posed. Different combinations of the parameters a_2 and c_1, can give about the same cost function value. For the combination of the parameter a_2 in the wind input term and c_1 in the dissipation term, the additional requirement of also matching the energy in the fully developed stage is not sufficient to produce a unique solution.

6.4.3.2 *dissipation level and wave steepness dependency were allowed to vary*

At first, it was tried to fit the growing stage only. In a first run, the Snyder type wind input term as used in Komen et al.(1984), i.e. a_1 equal to 1 and a_2 equal to 1, was chosen as the correct wind input. In the dissipation term the overall dissipation level c_1 and the wave steepness dependency parameter m are allowed to vary. When started from the original proposed values ($c = 3.33 \ 10^{-5}$ and $m = 2$), the optimization program reduces the overall damping level and increases the parameter m for the wave steepness dependency. After run 3a it was necessary to reduce the rather large scaling factors for the parameters in order to avoid obtaining negative overall dissipation levels. As can be seen from run 3b, reducing the scaling factors only was not enough and also different measures for the convergence criteria had to be taken. The stepsize STEPMX was therefore reduced (run 3c). The cost function value becomes low (less than 0.005). Although this is a good cost function value, it is clear that the obtained parameter values are of limited significance because of the low overall dissipation level. Low levels for overall damping will not give rise to severely reduced growth rates at large fetches (fully developed stage), as was found by Komen et al. (1984).

Higher values for the wind input parameter a_2 (set equal to 1.52), made the optimization program produce results with parameter values for m between 2.5 and 2.8. The damping levels are fairly high. The cost function values are less than 0.003, i.e., barely above values that can be expected due to noise in the calculation of the cost function. Two runs with a higher wind input parameter a_2 are given in Table 6.2. Although these runs (3d and 3e) do not produce exactly the same final optimal parameter values, they move towards similar parameter values.

Different runs were done with the additional requirement of including the fully developed sea state in the cost function. The optimal parameters found are nearly identical, independent of the starting positions. The runs 6a, 6b and 6c had a wind input

parameters a_1 and a_2 equal to 1, as proposed by Komen et al.(1984). The obtained solution for the parameters c_1 and m in the dissipation term, differ only little from their suggested values. The small differences are probably entirely due to assumptions in the wave program ONEDMOD (such as the arbitrary high frequency tail..), and to the fact that the wave program was probably run with a different friction velocity in their experiments.

In runs 6d and 6e, a higher wind input level was chosen (compare with run 3d and 3e. Whereas in the growing stage, the wave steepness dependency parameter m remained rather high (2.5 to 2.7), we notice that when we also try to fit the fully developed stage, this parameter is reduced and even becomes less than 2. The problem in the 5th iteration in run 6d and the 6th iteration in run 6e was due to the fact that the first step in the new search direction did not give a smaller cost function than the minimum obtained in the previous iteration step. The optimization program does not continue with a linear search along the search direction in the neighbourhood of the current parameter values. It jumps to totally different parameter values. For problems where one does not have to deal with such large scaling factors, this feature helps to disregard noise in the cost function calculation. Here, these sometimes 'ridiculous' values for the parameters make it possible for the wave program to produce 'ridiculous' results and therefore execution is abandoned. Since the optimization program is a black box routine, one cannot do much to avoid this problem.

In Figures 6.1 to 6.3, the energy growth curves for some of the found optimal parameter values are drawn. The runs indicated on these figures, correspond with the run specifications given in Table 6.2. We see that the fit to the energy growth curve is quite good for all of the parameter combinations. Only run 2c produces too high energy values. This is not surprising, since only a fit to the growing stage was considered important.

In Figure 6.2 and Figure 6.3 the resulting growth curves for the peak frequency and the Phillips' constant α_p are drawn. The main difference is in the asymptotic level. There is little difference

in the fetch range where there is still a considerable decrease in these two wave quantities.

In Figures 6.4 to 6.7, it is shown how the cost function varies when changing one parameter. The x-axis indicates the value of the parameters relative to the suggested optimal solution. Figure 6.4 (run 4b in Table 6.2) and Figure 6.5 (run 6b) both display a clear but shallow minimum. In Figure 6.6 (run 5a) and Figure 6.7 (run 5b), one sees that for variations in the parameter c_1, the resulting cost function barely differs. For variations in the parameter a_2, the minimum is defined more sharply. Nevertheless, the optimal parameter values are quite different in the Figures 6.6 and 6.7. This corresponds to what is written in section (6.4.2.2). The region where the minimum cost function for the combined parameter set is to be found, is indeed very shallow.
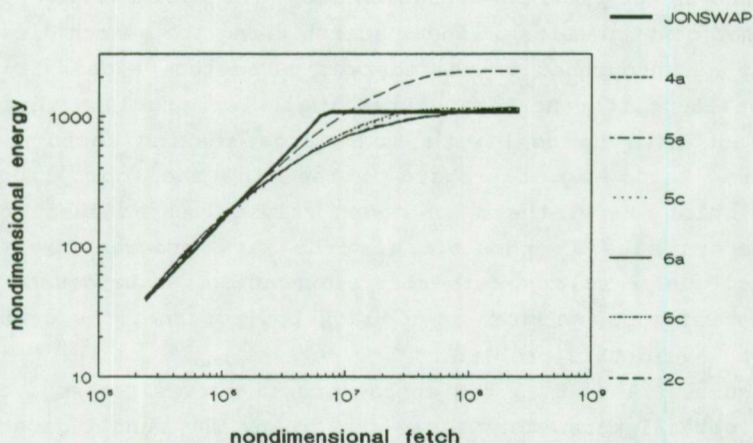
Figure 6.1 : Energy growth curves for sets of optimal parameter values (fit to energy; Snyder type wind input term ; Table 6.2)
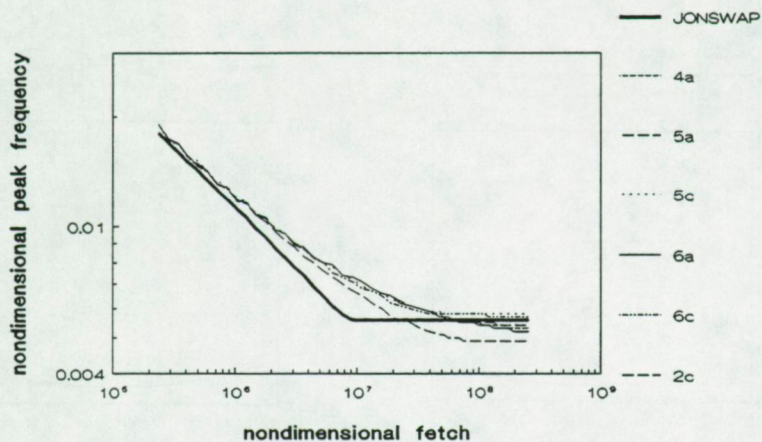
Figure 6.2 : Peak frequency growth curves for sets of optimal parameter values (fit to energy ; Snyder wind input term ; Table 6.2)
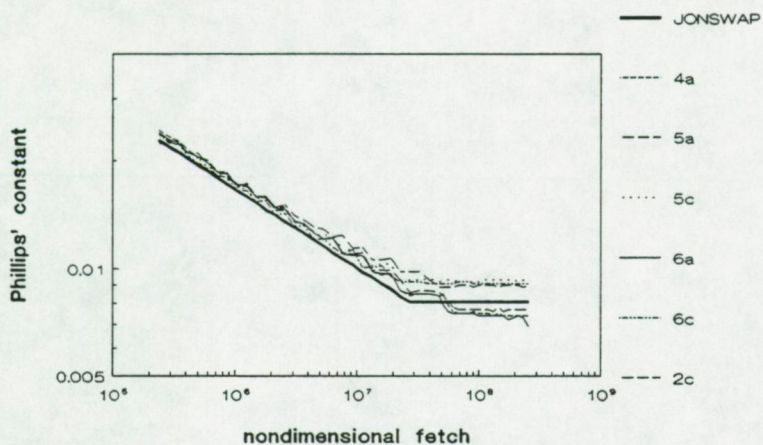
Figure 6.3 : Phillips' constant growth curves for sets of optimal parameter values (fit to energy ; Snyder wind input term; Table 6.2)
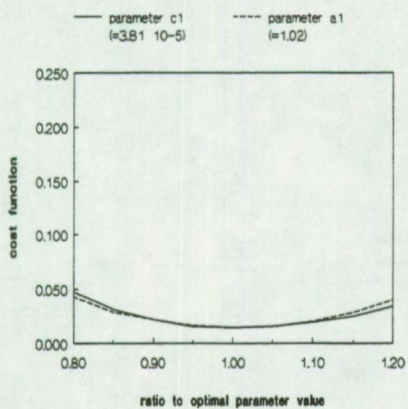
Figure 6.4 : Sensitivity analysis for run 4b of Table 6.2
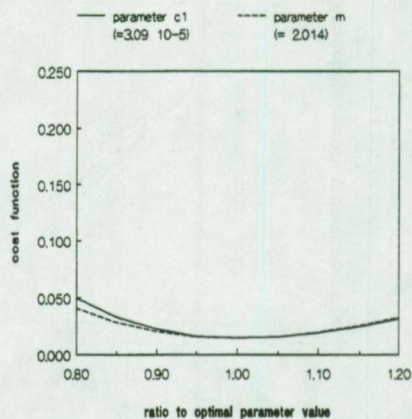
Figure 6.5 : Sensitivity analysis for run 6b of Table 6.2
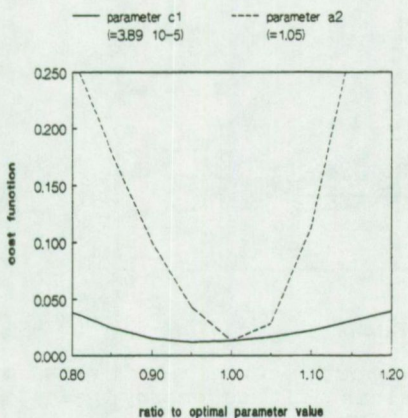
Figure 6.6 : Sensitivity analysis for run 5a of Table 6.2
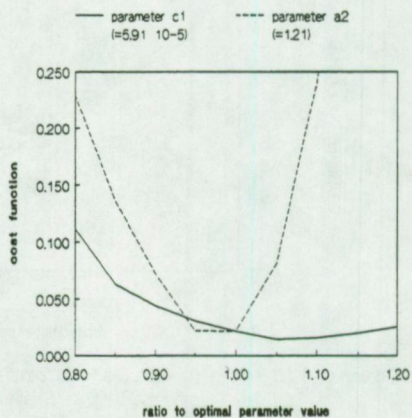
Figure 6.7 : Sensitivity analysis for run 5b of Table 6.2

6.4.4   JONSWAP growth curve - Stewart type wind input

        The different runs for trying to fit the JONSWAP energy
growth curve (equation 6.4) using a Stewart type wind input term
and the Komen dissipation term, are summarized in Table 6.3.

*6.4.4.1   wind input and overall dissipation level were allowed
           to vary*

        For the growing stage, several runs (see 1a and 1b)
were done trying to obtain optimal values for the wind input
parameter a_3 and the overall dissipation level parameter c_1.
Giving the parameter a_3 a starting value of one, the optimization
program was not capable of finding a minimum cost function for
a positive overall dissipation level c_1. Since negative damping
levels are not at all realistic, we have to disregard these
results. In fact, we have the same problem as with the parameter
a_1 in the Snyder type wind input term, see above. Starting at a
position where the cost function is approximately minimum for one
parameter only (in this case a_3), we notice that it is not
possible to get away from this position (runs 1c and 1d). With
small scaling factors (run 1d), the program had great trouble to
find a minimum during its linear search in the search direction
(needing 7 function calls to the wave program), indicating that
there is at least a local minimum. In a last run (1e), still
another starting position did not result in a reduction of the
cost function. We should also remark that all solutions produced
by the optimization program have a cost function which is only
marginally better than the minimum cost function obtained for
changing the parameter a_3 only (see 6.2.1.2).
When using the parameters a_4 and c_1 for tuning, we obtain for an
overall wind input level a_3 of 1 (runs 2a and 2b), nearly the
same cost function starting from two different initial positions.
The minimum value is almost equal to the one found from the
sensitivity run for the parameter a_4 only (about 0.065 for an a_4
value of 1.4), for parameter values differing by as much as 20
% for a_4 in the wind input and nearly 100 % for the c_1 in the

153

dissipation term (compared to $a_4 = 1.4$ and $c_1 = 3.33 \ 10^{-5}$). This indicates a shallow region in the optimal zone of the posed problem. Additional requirements will be necessary to come to a unique answer. The same can be said when the overall wind input level a_3 is equal to 2.2 (runs 2c and 2d).

Matching the growing stage and the asymptotic stage, we see from the runs 4a and 4b (using the parameters a_3 and c_1), that the obtained cost function from two different starting positions is nearly equal although the parameters are still quite different. We could say however that the trend of the parameters is similar, it moves towards a_3 values around 1.45 and c_1 values around 1.85. The combination of the parameters a_4 and c_1, also does not have a clearly defined minimum, as was the case for the combination of a_2 and c_1 (see above).

6.4.4.2 overall dissipation level and wave steepness dependency were allowed to vary

The runs with the high overall wind input level ($a_3 = 2.2$), lead to the same final parameter values, when we try to fit the growing stage only and using the parameters m and c_1 as tuning parameters.

When the overall wind input level is lower ($a_3 = 1$), the optimization program tries to find optimal solutions in the region of negative damping levels, as was the case for variation of the wind input level a_3 combined with a variation in the overall dissipation level. Again this is not realistic.

When including the requirements of a fully developed stage, we find a relatively clearly defined minimum. A difference in the overall wind input level a_3, compare runs 6a and 6b with runs 6c and 6d, leads to different final values for the parameters m and c_1. A higher wind input level not only increases the overall damping level, it also increases the wave steepness dependency parameter m.

For some of the optimal combinations of parameters, the resulting growth curves are drawn in the Figures 6.8 to 6.10. All

154

combinations tend to overestimate the energy for short fetch values and underestimate it for large fetch values of the growing stage. In the fully developed stage, all optimal parameter combinations (except run 5c) have a tendency of increasing energy with increasing fetch.

The behaviour of the growth curve for the peak frequency and for the Phillips' constant α_p, differs substantially from the case where the Snyder wind input term was used (section 6.4.3). The peak frequency decreases more slowly with fetch, compare Figure 6.2 and Figure 6.9. The Phillips' constant α_p displays a much wider spread for the different 'optimal' parameter combinations, compare Figures 6.3 and 6.10.

In the Figures 6.11 to 6.15, a sensitivity analysis for the parameters around the suggested optimal solutions is done. Especially the final combination of the wind input parameter a_3 and the dissipation parameter c_1 (Figure 6.11), and the final combinations of the dissipation parameters c_1 and m (Figures 6.14 and 6.15), are situated in a shallow to very shallow region. The cost function seems to be only rather sensitive to variations in the parameter a_4 (Figure 6.12 and 6.13). However, as can be found in Table 6.3, different combinations of final parameter values for c_1 and a_4, result in nearly identical final cost function values.

run	source term parameters (initial → final)				(initial → final) cost function	scaling factors					NAG parameters		remarks
	a_3	a_4	c_1 (* 10^5)	m	cost function	a_3 *10^{-6}	a_4 *10^{-6}	c_1	m 10^{-6}	cost *10^{-10}	XTOL *10^7	STEPMX *10^7	
growing stage													
1a	1. → -	1.	2.5 → -	2.	0.222 → -	5	-	200	-	50	1	3	neg. c_1 in first iteration
1b	1. → -	1.	2.5 → -	2.	0.222 → -	1	-	50	-	50	1	1.1	neg. c_1 in third iteration
1c	2.2 → 2.2	1.	3.33 → 3.33	2.	0.091 → 0.091	2.6	-	100	-	50	1	5	no reduction in first search
1d	2.2 → 2.25	1.	3.33 → 3.331	2.	0.091 → 0.0906	1.	-	20	-	10	1	10	1 iteration 7 fc
1e	1.8 → 1.846	1.	2.5 → 2.6	2.	0.084 → 0.084	5.	-	200	-	50	1	5	1 iteration
2a	1.	1. → 1.76	3.33 → 6.09	2.	0.305 → 0.064	-	5	200	-	50	1	5	5 iterations
2b	1.	1.5 → 1.59	2. → 4.847	2.	0.571 → 0.063	-	5	200	-	50	1	5	3 iterations
2c	2.2	1. → 1.18	3.33 → 5.02	2.	0.091 → 0.087	-	5	100	-	10	1	5	3 iterations
2d	2.2	0.5 → 1.32	4.5 → 5.47	2.	0.674 → 0.087	-	5	100	-	10	1	5	2 iter. (NC)
3a	1.	1.	3.33 → -	2. → -	0.305 → -	-	-	100	5	10	1	5	neg. c_1 value in first search
3b	2.2	1.	3.33 → 2.79	2. → 2.18	0.091 → 0.0755	-	-	100	5	10	1	5	1 iter. (NC)
3c	2.2	1.	3.33 → 2.68	3. → 2.23	0.621 → 0.0764	-	-	100	5	10	1	5	2 iter. (NC)

run	source term parameters (initial → final)				(initial → final) cost function	scaling factors					NAG parameters		remarks
	a_3	a_4	c_1 (* 10^5)	m		a_3 $*10^{-6}$	a_4 $*10^{-6}$	c_1	m 10^{-6}	cost $*10^{-10}$	XTOL $*10^7$	STEPMX $*10^7$	
growing + fully developed stage													
4a	1. → 1.39	1.	3.33 → 1.69	2.	0.308 → 0.043	5	-	100	-	10	1	5	3 iterations
4b	2.2 → 1.53	1.	3.33 → 1.93	2.	0.0878 → 0.044	5	-	200	-	50	1	5	3 iter. (NC); result from first iteration
5a	1.	1. → 1.11	3.33 → 1.86	2.	0.308 → 0.0495	-	5	100	-	10	1	5	3 iterations
5b	1.	1.35 → 1.044	2. → 1.425	2.	0.0707 → 0.0499	-	2.5	100	-	50	1	5	2 iterations
5c	2.2	1 → 1.19	3.33 → 4.52	2.	0.0878 → 0.0545	-	0.5	100	-	10	1	5	3 iterations
5d	2.2	1 → 1.11	3.33 → 3.781	2.	0.0878 → 0.0571	-	5	100	-	10	1	5	3 iterations
6a	1.	1.	3.33 → 1.11	3. → 1.6	0.41 → 0.044	-	-	100	2.5	50	1	5	4 iterations
6b	1.	1.	4.5 → 1.118	2. → 1.686	0.446 → 0.0445	-	-	100	5	10	1	5	3 iterations
6c	2.2	1.	3.33 → 2.37	2. → 2.28	0.0879 → 0.0387	-	-	200	10	50	1	5	2 iterations
6d	2.2	1.	2. → 2.413	2. → 2.265	0.156 → 0.0387	-	-	100	50	10	1	5	3 iterations

NC : did not satisfy NAG convergence criteria after number of iterations given (cause : cost function in next iteration larger than in the one given)

TABLE 6.3 Runs for fitting the JONSWAP energy growth curve using a Stewart type wind input source term
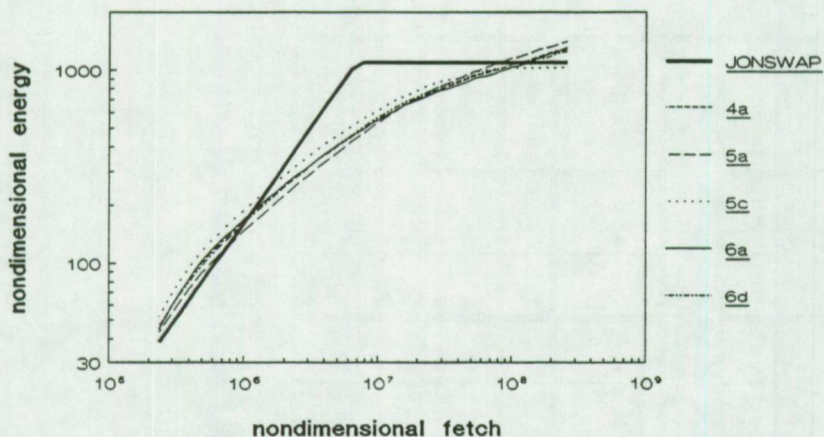
Figure 6.8 : Energy growth curves for sets of optimal parameter values (fit to energy ; Stewart type wind input term ; Table 6.3)
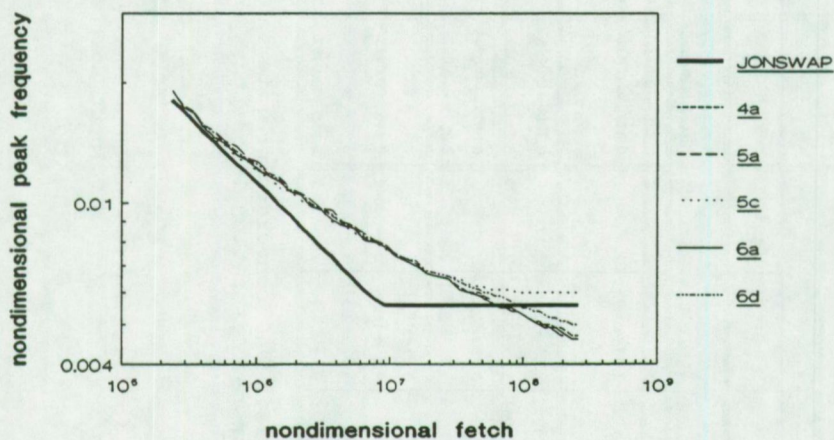
Figure 6.9 : Peak frequency growth curves for sets of optimal parameter values (fit to energy ; Stewart type wind input term ; Table 6.3)
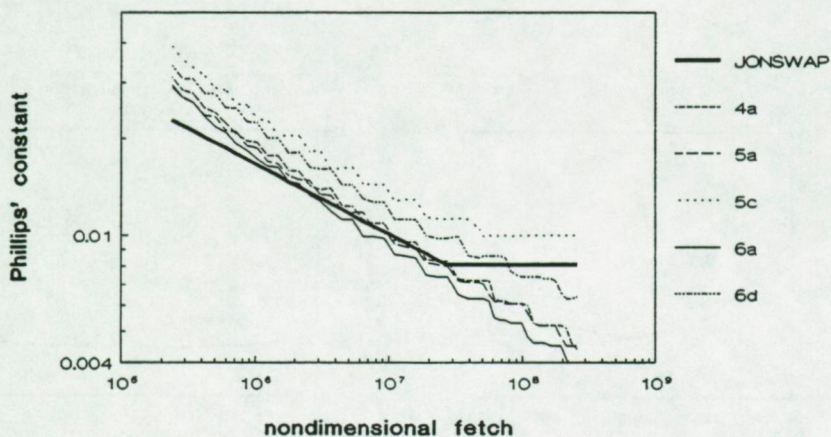
Figure 6.10 : Phillips' constant growth curves for sets of
optimal parameter values (fit to energy ;
Stewart type wind input term ; Table 6.3)
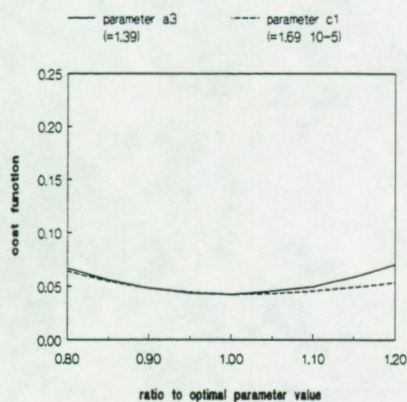
Figure 6.11 : Sensitivity
analysis for
run 4a of
Table 6.3
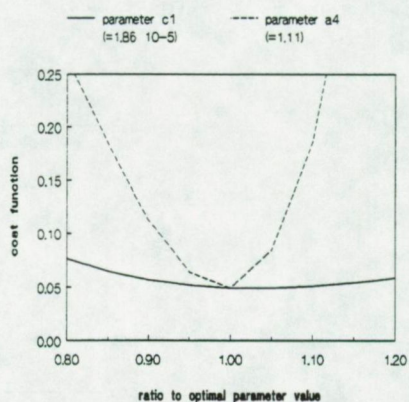
Figure 6.12 : Sensitivity
analysis for
run 5a of
Table 6.11
($a_3 = 1$)
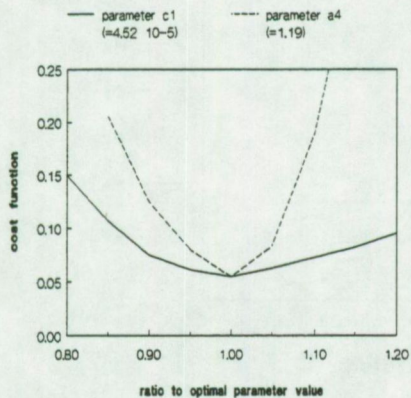
Figure 6.13 : Sensitivity analysis for run 5c of Table 6.3 ($a_3 = 2.2$)
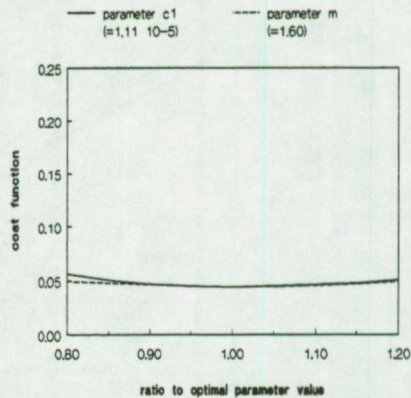
Figure 6.14 : Sensitivity analysis for run 6a of Table 6.3 ($a_3 = 1$)
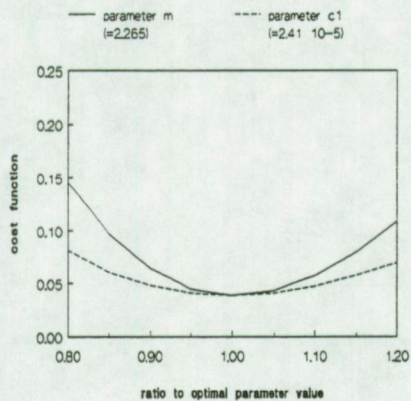
Figure 6.15 : Sensitivity analysis for run 6d of Table 6.3 ($a_3 = 2.2$)

6.4.5   Kahma and Calkoen growth curve - Snyder type wind input

The different runs for trying to fit the Kahma and
Calkoen growth curves (equation 6.5) using the Snyder type wind
input term and the Komen dissipation term, are summarized in
Table 6.4.

6.4.5.1   wind input and overall dissipation level were allowed
to vary

For the growing stage, two runs were done for the
variation in the parameters a_1 of the wind input and c_1 of the
dissipation term. The obtained final cost function values are
quite good. The resulting parameters differ a bit. Also for the
variation in the parameters a_2 and c_1, the final cost function
values are quite good. The resulting parameter values differ now
substantially. Only additional requirements (asymptotic stage)
may limit the amount of possible combinations of the parameters.
Comparing this to what was obtained trying to fit the JONSWAP
growth curves in the growing stage, one notices first of all that
there is no trend to go to low (or even negative) damping values.
The obtained cost function values are also better.
When trying to fit the fully developed sea state, as well as the
growing stage, the resulting cost function values are very good
and barely above expected numerical noise. The combination of
parameters a_1 for the wind input and c_1 for the dissipation term,
gave however rather low c_1 values. On the other hand the
combination of a_2 and c_1 gives rather high c_1 values. The
asymptotic behaviour for the growth curves is different. Indeed
in Figure 6.16, we can see that for the low overall damping level
c_1 combined with a smaller a_1 value (run 4b), the energy is still
growing in the fully developed stage. Also the peak frequency is
still decreasing, see Figure 6.10. The high overall damping level
combined with a higher value for the wind input parameter a_2,
displays a very nice asymptotic behaviour, both for the energy
growth curve and for the peak frequency growth curve.

161

6.4.5.2 *dissipation level and wave steepness dependency were allowed to vary*

For fitting the growing stage, two runs were done. The end result is comparable to changing the wind input parameter a_1 or a_2, and the overall dissipation level c_1. A higher damping level with only a slight increase in the wave steepness dependency parameter m, results in a nearly perfect fit to the energy growth curve.

Fitting the fully developed stage as well as the growing stage, also results in very good final cost function values. The value found is similar to the ones obtained for a variation of the wind input and overall dissipation level. The value found for m is higher than suggested by Hasselmann's whitecapping theory (Hasselmann, 1974). It is close to the value of 3 as used by Janssen (1991).

In Figure 6.16, the energy growth curve for selected sets of parameters are drawn. The indications refer to the runs as given in Table 6.4. Run 1a does not have the right asymptotic level because the set of parameters corresponds to a fit to the growing stage only. The still increasing energy level in run 4b has been discussed above. In the Figures 6.17 and 6.18, the growth curves for the peak frequency and for the Phillips' constant α_p are drawn. The difference between the different growth curves is mainly visible in the stage of fully developed wind waves.

In the Figures 6.19 to 6.21, the variation of the cost function due to a relative change in one parameter, is shown. The term 'relative' refers to the ratio between the parameter value used and the optimal parameter value suggested from the optimization runs (Table 6.4). As was the case for the fitting exercise to the JONSWAP energy growth curve (compare the Figures 6.19 and 6.21 with the Figures 6.4 and 6.5), the combination of the overall wind input level a_1 with the overall damping level c_1, and the combination of c_1 with the wave steepness dependency parameter m, have a shallow minimum. The sensitivity of the cost function to variations in the wind input parameter a_2 is more distinct, see Figure 6.20 and compare with Figure 6.6 and 6.7.

	source term parameters (initial → final)				(initial → final)	scaling factors					NAG parameters		
run	a_1	a_2	c_1 (* 10^5)	m	cost function	a_1 *10^{-6}	a_2 *10^{-6}	c_1	m 10^{-6}	cost *10^{-10}	XTOL *10^7	STEPMX *10^7	remarks
					growing stage								
1a	1. → 0.796	1	3.33 → 3.622	2	0.114 → 0.0022	5	-	100	-	50	1	5	2 iterations
1b	0.5 → 0.85	1	4.5 → 4.06	2	0.1872 → 0.0021	5	-	100	-	10	1	5	3 iterations
2a	1.	1. → 0.99	3.33 → 5.04	2	0.114 → 0.0032	-	2	200	-	50	1	5	2 iterations
2b	1.	0.5 → 1.19	4.5 → 8.27	2	0.538 → 0.00225	-	5	100	-	10	1	5	2 iterations
3a	1.	1	3.33 → 4.44	2. → 2.2	0.114 → 0.0026	-	-	200	10	50	1	5	2 iterations
3b	1.	1	3.33 → 4.03	3. → 2.3	0.0374 → 0.0023	-	-	100	5	10	1	5	3 iterations
					growing + fully developed stage								
4a	1. → 0.627	1.	3.33 → 2.25	2.	0.06 → 0.0054	5	-	100	-	50	1	5	2 iterations
4b	0.5 → 0.607	1.	4.5 → 2.13	2.	0.228 → 0.0053	5	-	100	-	10	1	5	3 iterations
5a	1	1. → 1.42	3.33 → 12.2	2.	0.06 → 0.00215	-	2	200	-	50	1	5	4 iterations
5b	1	2. → 1.36	4.5 → 10.68	2.	47.34 → 0.00321	-	5	100	-	10	1	5	6 iterations
6a	1.	1.	3.33 → 3.02	2. → 2.673	0.06 → 0.004	-	-	200	10	50	1	5	2 iterations
6b	1.	1.	3.33 → 3.2	3 → 2.65	0.0298 → 0.004	-	-	100	5	10	1	5	2 iterations

NC : did not satisfy NAG convergence criteria after number of iterations given (cause : cost function in next iteration larger than in the one given)

TABLE 6.4 Runs for fitting the Kahma and Calkoen energy growth curve using a Snyder type wind input source term
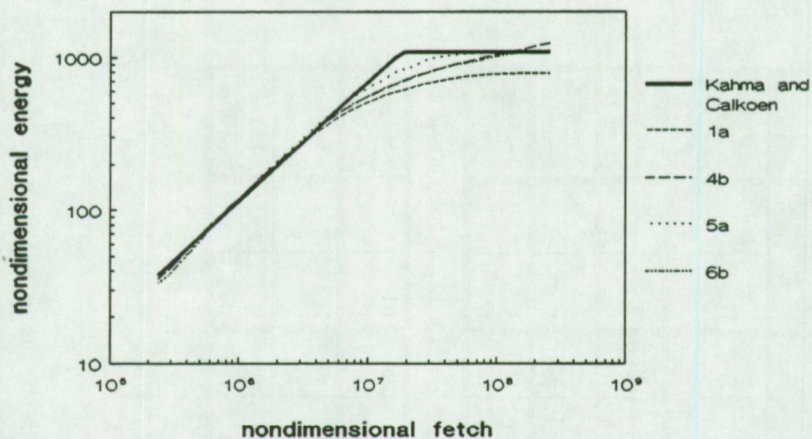
Figure 6.16 : Energy growth curve for sets of optimal parameter values (fit to energy ; Snyder type wind input term; Table 6.4)
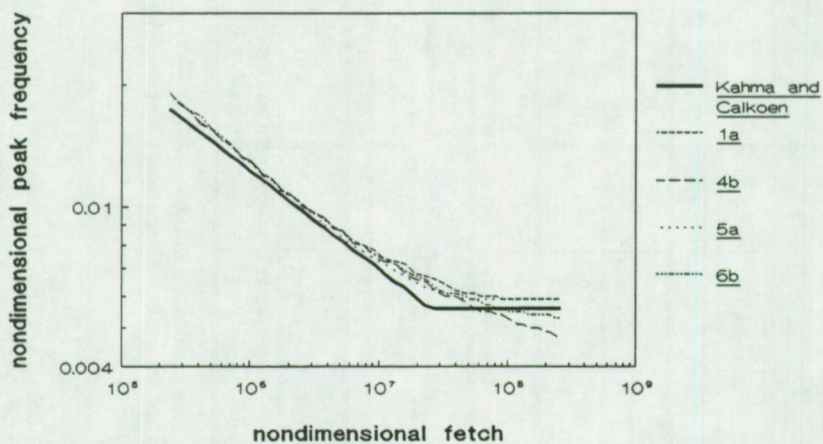
Figure 6.17 : Peak frequency growth curves for sets of optimal parameter values (fit to energy ; Snyder type wind input term ; Table 6.4)
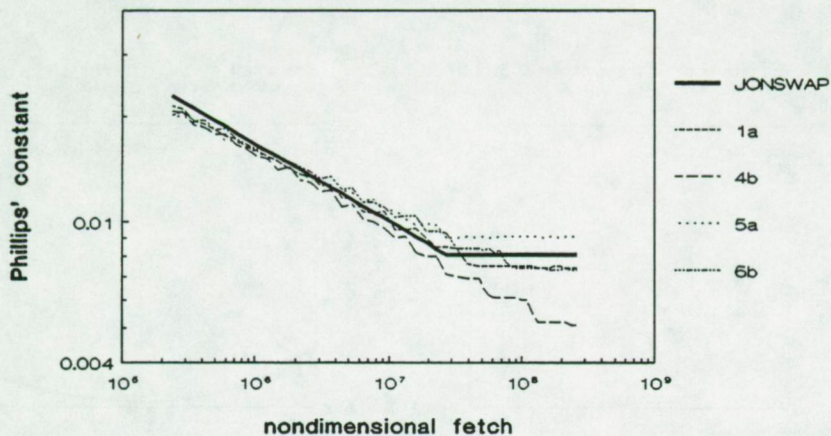
Figure 6.18 : Phillips' constant growth curve for sets of optimal parameter values (fit to energy ; Snyder type wind input term; Table 6.4)
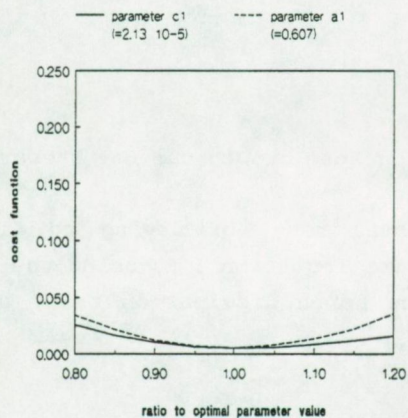
Figure 6.19 : Sensitivity analysis for run 4b of Table 6.4
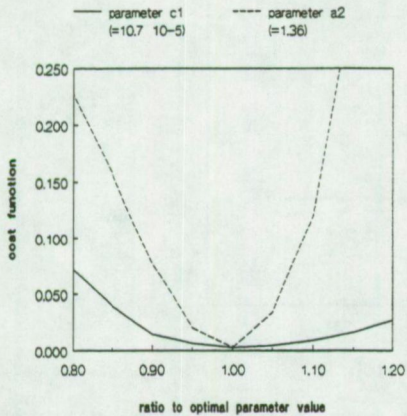
Figure 6.20 : Sensitivity analysis for run 5b of Table 6.4
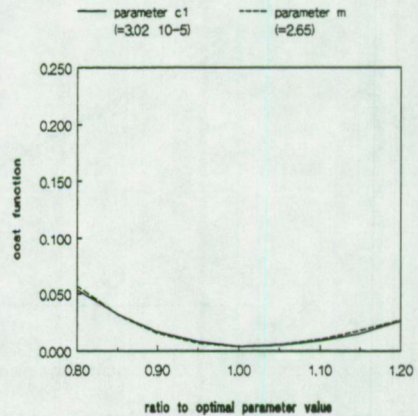
Figure 6.21 : Sensitivity analysis for run 6b of Table 6.4

6.4.6   Kahma and Calkoen growth curve - Stewart type wind input

The different runs for trying to fit the Kahma and Calkoen growth curves (equation 6.5) using the Stewart type wind input term and the Komen dissipation term, are summarized in Table 6.5.

6.4.6.1   wind input and overall dissipation level were allowed to vary

The combination of the parameters a_3 and c_1, results in unrealistic negative damping levels, when only the growing stage is to be matched. The combination of the parameters a_4 and c_1,

166

again for fitting the growing stage only, results in a fairly large variation in the final parameter values. However, the final cost function values are nearly equal.

Adding the requirement of also fitting the fully developed stage, results in a stable estimate for the combination of optimal values for the parameters a_3 for the wind input and c_1 for the dissipation. The combination of the parameter a_4 and c_1 on the other hand, does not yield a very clear minimum, although the final cost function values for the runs (5a and 5b) are nearly the same.

Comparing the final cost function values to the ones that were found by using a Snyder type wind input term instead of the Stewart type wind input, we see that they are considerably higher.

6.4.6.2 *overall dissipation level and were steepness dependency are allowed to vary*

Fitting the growing stage only, yields low final cost function values when tuning the parameters c_1 and m in the dissipation term. We can also see that a higher value for the wind input parameter a_4, increases the overall damping level considerably.

Fitting the growing stage and the fully developed stage simultaneously, results in a stable estimate for the parameters considered. The final cost function value however, is considerably higher than when a Snyder type wind input term is used (see Table 6.4).

	source term parameters (initial → final)				(initial → final)	scaling factors					NAG parameters		
run	a_3	a_4	c_1 (* 10^5)	m	cost function	a_3 *10^{-6}	a_4 *10^{-6}	c_1	m 10^{-6}	cost *10^{-10}	XTOL *10^7	STEPMX *10^7	remarks
growing stage													
1a	1. → -	1	3.33 → -	2	0.142 → -	5	-	100	-	10	1	5	neg. c_1 after first iteration
1b	0.5 → -	1	4.5 → -	2	0.467 → -	5	-	100	-	10	1	5	neg. c_1 after 6 iterations
2a	1.	1. → 1.63	3.33 → 6.73	2	0.142 → 0.016	-	5	200	-	50	1	5	3 iterations
2b	1.	1.5 → 1.245	2.0 → 3.63	2	1.89 → 0.015	-	5	200	-	50	1	5	2 iter. (NC)
2c	1.	1.4 → 1.35	4.0 → 4.38	2	0.049 → 0.014	-	1	50	-	50	1	5	2 iterations
2d	1.	0.5 → 1.37	4.5 → 4.523	2	0.676 → 0.014	-	5	100	-	10	1	5	4 iterations
3a	1.	1.	3.33 → 0.642	2. → 2.98	0.142 → 0.003	-	-	50	1	50	1	5	5 iterations
3b	1.	1.35	4.38 → 2.33	2 → 2.59	0.0144 → 0.001	-	-	50	1	50	1	5	4 iterations
3c	1.	1.35	3.33 → 1.89	3 → 2.787	0.339 → 0.0002	-	-	100	5	10	1	5	3 iterations

run	source term parameters (initial → final)				(initial → final)	scaling factors					NAG parameters		
	a_3	a_4	c_1 $(* 10^5)$	m	cost function	a_3 $*10^{-6}$	a_4 $*10^{-6}$	c_1	m 10^{-6}	cost $*10^{-10}$	XTOL $*10^7$	STEPMX $*10^7$	remarks
growing + fully developed stage													
4a	$2.2 \to 0.890$	1.	$3.33 \to 1.15$	2.	$0.098 \to 0.020$	2.5	-	200	-	50	1	5	4 iterations
4b	$0.5 \to 0.874$	1.	$4.5 \to 1.12$	2.	$0.558 \to 0.021$	5	-	100	-	10	1	5	2 iterations
5a	1.	$1.35 \to 1.37$	$4.5 \to 4.47$	2.	$0.013 \to 0.010$	-	2.5	100	-	50	1	5	1 iteration
5b	1	$2. \to 1.55$	$4.5 \to 5.89$	2.	$5.05 \to 0.011$	-	5	100	-	10	1	5	4 iterations
6a	1.	1.	$3.33 \to 1.36$	$3. \to 2.2$	$0.36 \to 0.018$	-	-	100	2.5	50	1	5	2 iterations
6b	1.	1.	$2.5 \to 1.316$	$2. \to 2.212$	$0.118 \to 0.017$	-	-	100	5	10	1	5	3 iterations

NC : did not satisfy NAG convergence criteria after number of iterations given (cause : cost function in next iteration larger than in the one given)

TABLE 6.5 Runs for fitting the Kahma and Calkoen energy growth curve using a Stewart type wind input source term

In the Figures 6.22 to 6.24, the growth curves are drawn. We notice that only run 5a, optimizing the parameters c_1 in the dissipation source term and a_4 in the wind input source term, results in severely reduced growth rates for fully developed seas. The difference in the calculated peak frequencies for different final parameters combinations, are only visible in the fully developed range. The difference between the growth curves for the Phillips' constant for the different final parameter combinations, is clearly larger compared to the difference in the growth curves for the energy and for the peak frequency.

In the Figures 6.25 to 6.27, a sensitivity analysis for the parameters around the optimal values is performed. For the parameter combination a_3 (wind input) and c_1 (dissipation), the region of minimum cost function values is very shallow, see Figure 6.25. This is also the case for the parameter combination c_1 and m (dissipation source term), see Figure 6.27. The cost function is more sensitive in the parameter a_4, see Figure 6.26.
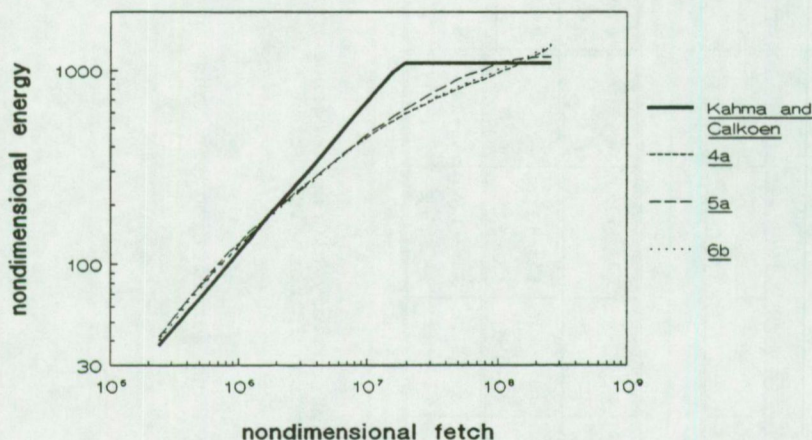
Figure 6.22 : Energy growth curve for sets of optimal parameter values (fit to energy ; Stewart type wind input term ; Table 6.5)

170
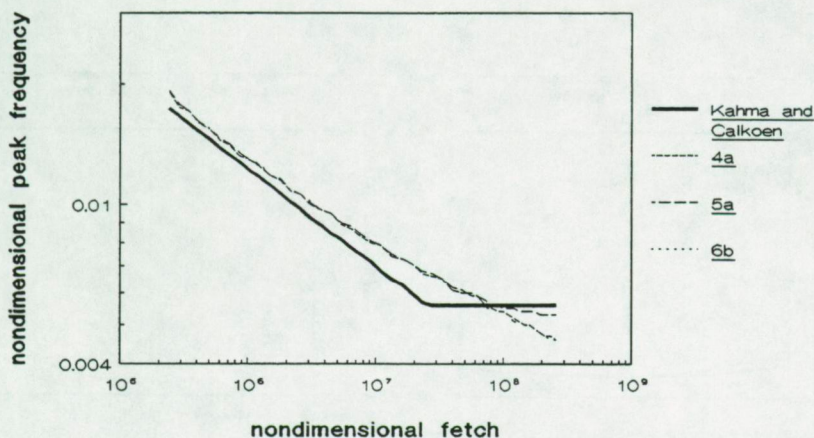
Figure 6.23 :   Peak frequency growth curves for sets of optimal parameter values (fit to energy ; Stewart type wind input term; Table 6.5)
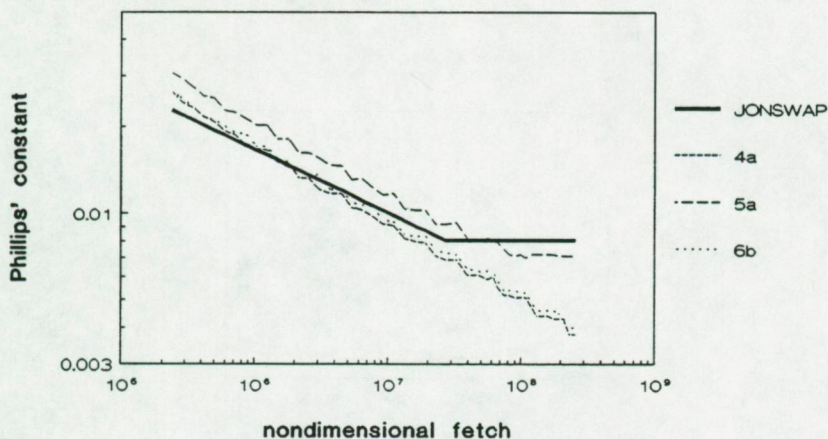
Figure 6.24 :   Phillips' constant growth curves for sets of optimal parameter values (fit to energy ; Stewart type wind input term ; Table 6.5)
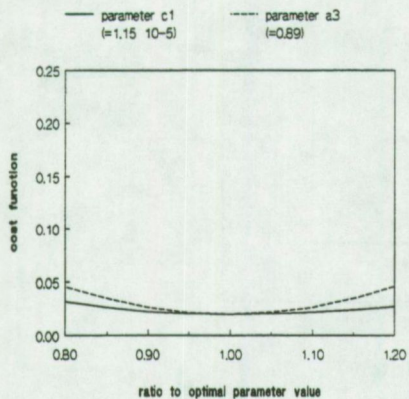
Figure 6.25 : Sensitivity analysis for run 4a of Table 6.5
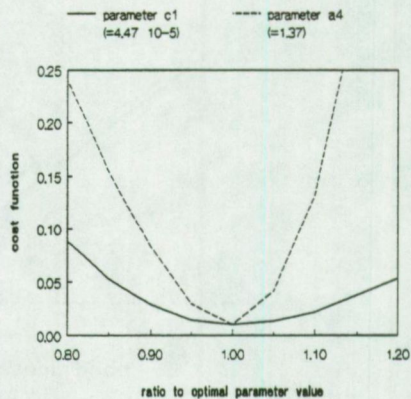
Figure 6.26 : Sensitivity analysis for run 5a of Table 6.5
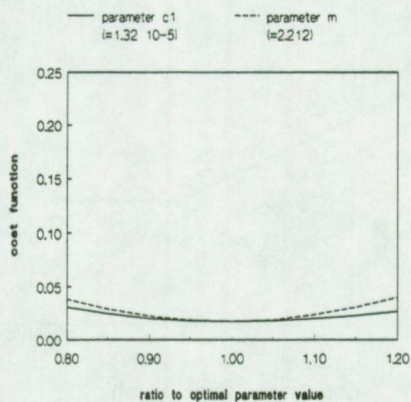
Figure 6.27 : Sensitivity analysis for run 6b of Table 6.5

6.5   Discussion

Obtaining a successful termination of the optimization program, may depend on starting values, scaling factors and/or NAG adjustable parameters.

The numerical scheme used (adjustable step size), the added high frequency tail and the limitation of the energy growth in a bin,.., lead to numerical noise and disturb the optimization program in taking decisions. We had to make the decision of using large scaling factors and compromise on the convergence criteria by adjusting the NAG-supplied parameters. The optimization program is capable of reducing the cost function considerably, no matter what the starting position is, as long as the scaling factors are properly chosen. The choice of adjustable NAG-subroutine parameters thereby determines the speed and/or the ability to convergence. Tight limits on the convergence criteria force the optimization routine to spend a lot of computer time with only marginal or no improvement in the final cost function value, compared to looser limits. The suggested values in Chapter 5 proved to work quite well.

The additional requirement of fitting an asymptotic stage is needed to reach the desired energy level for fully developed wind seas. It also avoids obtaining unrealistic (negative) overall damping levels. Komen et al.(1984) already demonstrated the need for a minimum level of overall damping in order to have severely reduced growth at large fetches.

The possibility of obtaining different parameter values for nearly equal cost function values, indicates that the problem is ill-determined for certain combinations of parameters. More specifically, the combination of the parameter a_2 (or a_4) in the wind input term with the parameter c_1 for the overall damping level, displays a region where the cost function is very shallow. This finding is especially true for the cases where we tried to fit the JONSWAP energy growth curve. Although still there, it is less noticable when we try to fit the Kahma and Calkoen energy growth curve. In section (6.2.1.2), we indicated that the parameters a_2 and a_4 in fact reflect our doubts as to when we can

say that a wind sea is fully developed. The parameter tuning exercise did not resolve this problem completely. We found that shifting the notion of a fully developed sea to older wind seas, asked for an increase in the overall damping level. The growth rates for fully developed seas are severely reduced.

It is remarkable that, for a given energy growth curve and a given wind input term, the different combinations of tunable parameters, led to nearly identical final cost function values. It is impossible to conclude which set of parameters is the best. For the runs with a Snyder type wind input term, the fit to the JONSWAP growth curves (growing + fully developed stage) resulted in final parameter values nearly equal to the ones suggested by Komen et al. (1984) in their exercise to obtain fully developed wind sea conditions. Shifting the notion of a fully developed sea to a higher wave age (increasing parameter a_2, a parameter not considered by Komen et al. (1984)), increased the overall damping level.

For the runs with a Snyder type wind input term, the fit to the Kahma and Calkoen growth curves is definitely better than the fit to the JONSWAP growth curves. That does not mean that a linear relationship between energy and fetch should be disregarded, it only means that mathematically it is not easy or even impossible to obtain linear growth of the energy with fetch with the proposed expression of the Snyder type wind input term. Further research concerning the growth curves (wave age dependent conversion of the velocity at 10 m to the friction velocity), should decide whether or not the energy grows less fast than linear with fetch.

For the Kahma and Calkoen growth curve, the Snyder type wind input term can be tuned together with the overall dissipation level to give a nearly perfect fit, both in the growing stage and the fully developed stage. The wind input level a_2 and the overall dissipation level c_1 are larger however than suggested by Komen et al. (1984). Nearly the same effect can be obtained by tuning the dissipation term only. This gives a wave steepness dependency parameter m which is larger than suggested by the whitecapping theory of Hasselmann (1974).

174

From the two proposed formulations for the wind input term, the Snyder type is better for reproducing the energy growth curve. Since the solutions found by the optimization program are not unique, additional criteria should be imposed.

6.6   Conclusion

The optimization program is capable of improving the fit to a proposed energy growth curve considerably. The scaling factors and convergence criteria parameters proposed in Chapter 5 are a good compromise between the computational cost, i.e. the number of calls to the wave program where virtually all computer time is spent, and the accuracy which can possibly be obtained for the relevant parameters in the chosen wind input term and dissipation term.

Trying to fit the energy growing stage only, sometimes led to unrealistically low or even negative dissipation levels. Additional restrictions in terms of formulating an appropriate energy level for a fully developed sea, avoids this trend in the solutions obtained by the optimization program.

The Snyder type wind input term is easier to tune than the Stewart type wind input term and the resulting cost function values are also better. This was so for fits to either one of the energy growth curves considered.

The parameter choice of Komen et al. (1984) ($a_1 = 1$, $a_2 = 1$, $c_1 = 3.33 \ 10^{-5}$, $m = 2$, $n = 2$) for the Snyder type wind input term is a good one. Fitting the JONSWAP energy growth curve leads to nearly identical values when we use either the combination (a_1, c_1) or the combination (c_1, m) as free parameters in the optimization exercise.

When using the Snyder type wind input term, the Kahma and Calkoen energy growth curve could be fitted nearly perfectly, both in the fully developed and in the growing stage. The following combination of parameters gave good results : (a_1 = 1, a_2 = 1.42, c_1 = 12.2, m = 2) and (a_1 = 1, a_2 = 1, c_1 = 3.2, m = 2.65).

The optimal region for the parameters is very shallow, so that various combinations of certain parameters may result in nearly identical cost function values. In the research work done here, only two parameters were allowed to vary at one time. It should be possible to tune more than two parameters simultaneously, as to obtain a better fit to the growth curves. However, it is felt that the problem of uniqueness of the solution has to be solved first, before proceeding with more parameters to tune. In the first place, we would suggest additional criteria (peak frequency, Phillips' constant) in the fully developed stage.

Shifting the definition of a fully developed sea to older waves (parameter a_2 in the Snyder type and parameter a_4 in the Stewart type wind input source term), increases the overall dissipation level (parameter c_1 in the dissipation source term). This leads to severely reduced growth rates for the energy in fully developed wind sea conditions.

7 Conclusions and recommendations for further research

7.1 Introduction

At the end of each chapter a summary was given together with the conclusions for that chapter. Below, the important findings from this study are highlighted.
Finally some suggestions for further work are noted.

7.2 Conclusions

The Toba spectrum, in combination with a peak width parameter σ as defined for the Donelan spectrum, combines the merits of a strongly peaked spectrum for young wind seas and a broader spectrum for a fully developed sea without the need to define a wave age dependent peak enhancement factor γ.

To obtain wave parameters which are nondimensionalized with the friction velocity, the currently available wave data should be reanalysed using a wave age dependent drag coefficient.

High frequeny waves are mainly responsible for the form drag. This can be seen from the fact that the nondimensional roughness length z_0^* is closely related to the Donelan constant α_D, which in turn is solely determined by the equilibrium frequency range of the spectrum. When equaling the Donelan spectrum to the Toba spectrum in the equilibrium frequency range, the Donelan constant α_D and the nondimensional roughness length z_0^* show the same wave age dependency. This means that the description of the water surface and of the atmospheric boundary layer, have one common nondimensional parameter.

The wave age dependency of the roughness length in the form of a power law as suggested by Maat et al. (1991) cannot be extended

177

to very young wind seas. For young wind seas or for short fetches (especially laboratory conditions) there appears to be a limit to the exerted shear stress. This may be an indication that when exceeding this limit, the waves break, thereby reducing the form drag and also reducing the exerted shear stress.

When the wave program ONEDMOD used in this study was run with different friction velocities, the resulting growth curves did not scale perfectly. It was argued that only a finer resolution at a higher computational cost or an adjustable frequency grid may resolve this problem.

Using the WAM model (WAMDI, 1988) source terms, the net momentum transfer obtained with the program ONEDMOD is higher than what would be expected from measurements. Numerical damping in the advection scheme and possibly the added high frequency tail, produce additional damping which is not accounted for in the source term momentum balance.

A cost function defined as a sum of squares of functions was shown to be an adequate practical choice. The power of the approach is that the only real need is to be able to calculate the function values. It is possible to take advantage of the special structure of the sum of squares so that an approximation to the Hessian matrix for the Newton search can be made using first derivatives only. Standard routines were found in the NAG-subroutine library. The NAG-routine E04FCF appeared to be the best one suited for the purpose.

The chosen finite difference scheme, the cut-off frequency for attaching the high frequency tail of the energy spectrum and probably also the discrete interaction approximation for the calculation of the nonlinear energy transfer, give rise to some erratic behaviour in the cost function for small variations in the parameters.

There is need for scaling of the parameters and for being able to manipulate the convergence criteria. By scaling, the parameters to be tuned should be made quite small, so that the finite difference approximation for the derivatives to the parameters (calculated in the NAG-subroutines by means of an absolute step in the parameter value), gives meaningful results to the optimization routine. Scaling of the cost function, as to interpret the convergence criteria, is necessary to have convergence after a limited number of iterations.

The optimization program is capable of improving the fit to a given growth curve considerably. The proposed scaling factors and convergence criteria parameters appear to be a good compromise between the computational cost (the number of calls to the wave program where virtually all computer time is spent) and the accuracy possibly achievable of the relevant parameters in the chosen wind input and dissipation term.

The optimal region for the parameters is very shallow, so that various combinations of certain parameters may result in nearly identical cost function values. A change in one parameter can be greatly compensated by a change in another parameter. Although the optimization program may improve the fit to a proposed energy growth curve considerably, it is impossible to prove that the obtained solution is indeed the absolute minimum. We can only say that the found solution most probably is one of the better choices to be made for the parameters.

Trying to fit the energy growing stage only, sometimes led to unrealistically low or even negative dissipation levels. Additional restrictions in terms of formulating an appropriate energy level for a fully developed sea, avoids this trend in the solutions obtained.

In this study, only two parameters were allowed to be tuned simultaneously. It should be possible to tune more than two parameters at once as to obtain an even better fit to the energy

growth curve. However, it is felt that the problem of uniqueness of the solution has to be solved first, before proceeding with more adjustable parameters. This could be done by imposing additional criteria to be met. In the first place, we would suggest additional criteria (peak frequency, Phillips' constant) in the fully developed stage.

From the two formulations used in this study for the wind input term, the Snyder type wind input term is easier to tune than the Stewart type wind input term. The resulting cost function values are also better.

When using the Snyder type wind input and the Komen dissipation source term, the optimal parameter values found in this study for reproducing the JONSWAP energy growth curve simultaneously in the growing and in the fully developed region, differ little from the ones proposed by Komen et al. (1984) after their study on the existence of a fully developed sea. Only shifting the definition of a fully developed sea to older waves (parameter a_2 in the Snyder type and parameter a_4 in the Stewart type wind input source term), increases the overall dissipation level (parameter c_1 in the dissipation source term). This leads to severely reduced growth rates for the energy in fully developed wind sea conditions.

The Kahma and Calkoen energy growth curve could be fitted nearly perfectly with a Snyder type wind input source term. This is simultaneously so in the fully developed and in the growing stage.

7.3 Applications and recommendations for further research

The suggestion that the Donelan constant α_D is a direct measure for the roughness at sea has to be further investigated. Once the full HEXMAX data set is made publicly available, the data fitting exercise has to be repeated. Its validity for

180

laboratory wave data should also be checked thoroughly. If we can confirm the hypothesis, it could be used in the reanalysis of existing data to obtain better nondimensional growth curves based on friction velocity scaling.

On the fundamental level there is still a lot to do in improving our understanding of the source terms. First of all there is the extension of the model to shallow water which would bring in an additional source term for bottom friction. Most work done for the shallow water zone has been limited to constant water depth and sloping beach. Bathymetries as found in the Belgian coastal zone with parallel sand banks and continuously varying water depth have not been studied extensively. The calculation of the nonlinear transfer could be studied in more detail, again with particular interest in the shallow water zone. Exact computations are very time consuming and computer efficient algorithms are needed.

The coupling with an atmospheric model shows great promise in increasing our knowledge of many different aspects of the air-sea interaction ranging from improved wind input for wave models, and consequently improved weather models, to an improvement in our understanding of the modelling of fluxes of momentum, heat, and trace gases in coupled ocean/atmosphere carbon cycle climate models.

In all of the more theoretical aspects, the optimization framework worked out in this study can be used for tuning unknown coefficients. More parameters (than 2) can readily be tuned as long as we can formulate a cost function which will produce unique results. Extension of the growth curves to the usage of a full dataset instead of a proposed regression line, may prove to give valuable additional information. However, the problem of the current approach remains. One has to exploit field conditions in which the energy transport equation assumes a simple form (e.g. fetch limited). The formulation of a cost function for individual source terms, could be done if those measurements

181

become available. Another way of looking at the problem, is the approach Snyder et al. (1990) are taking. They examine the integral consequences of the transport equation and assume that 'a sufficiently complete record of the evolution of a wavefield and of those influences driving this field contains all the information necessary to determine the interactions which played a significant role in this evolution'. It remains to be seen if the smaller scale field experiment by Snyder et al. (1991) in the Bight of Abaco and the large scale surface wave dynamics experiment (SWADE) described by Donelan (1987) will provide this sufficiently complete record of data.

A practial application is the implemention (and partial development) and testing of a regional third generation wave model for the Southern North Sea, with special emphasis on the Belgian coastal waters. It was not considered as being part of the scope of this study, not because the task in itself is impossible. It would require, next to an extended access to powerful computer facilities, a team of 2 or 3 persons with some experience in wave modelling to tackle this most complicated part of the North Sea as to be able to do the job within a reasonable amount of time. In the long run this model should replace the current second generation model in use for the Belgian coastal area. Together with improved wind input, a third generation model is capable of doing better forecasts. The experience obtained from comparing measurements and forecasts by the Belgian HYPAS version, will reveal this model's strong points but also weaknesses. It will form a good basis for extended comparison and evaluation of the enhanced performance of a regional third generation model. Data assimilation techniques can be used to give additional input to an operational model. Data could be obtained from satellite, but also from buoys. In how far this would improve the forecast on regional level should be investigated.

The coupling of a wave forecast model to a hydrodynamic model as to forecast currents and water levels, has to be investigated

further. Not only do water depth and currents have an influence
on the wave characteristic (difference in dispersion relation,
breaking of waves, ...), also the waves have an influence on
currents and water levels (storm surge).

REFERENCES

1   Al-Zanaidi, M.A. and Hui, W.H., *Turbulent air flow over water waves*, J. Fluid Mech., 148, 225-246, 1984.

2   Amorocho, J. and De Vries, J.J., *A new evaluation of the wind stress coefficient over water surfaces*, J. Geoph. Res., 85, C1, 433-442, 1980.

3   Bard, Y., *Nonlinear parameter estimation*, Academic Press, 1974.

4   Barnett, T.P., *On the generation, dissipation and prediction of ocean wind waves*, J. Geoph. Res., 73, 2, 513-529, 1968.

5   Battjes, J.A., Zitman T.J. and Holthuysen L.H., *A reanalysis of the spectra observed in JONSWAP*, J. Phys. Ocean., 17, 1288-1295, 1987.

6   Blake, R.A., *The Dependence of Wind Stress on Wave Height and Wind Speed*, J. Geoph. Res., 96, C11, 20,531-20,545, 1991.

7   Cavaleri, L., Bertotti, L. and Lionello, P., *Shallow Water Application of the Third-Generation WAM Wave Model*, J. Geoph. Res., 94, C6, 8111-8124, 1989.

8   Charnock, H., *Wind stress on a water surface*, Quart. J. of Meteor. Soc., 81, 639-640, 1955.

9   Chavent, G., *On the theory and practice of non-linear least squares*, Adv. Water Resources, 14, 2, 55-63, 1991.

10 DeLeonibus, P.S. and Simpson, L.S., *Near-neutral drag coefficients over open-ocean waves*, IEEE Journal of Oceanic Engineering, OE-11, 4, 480-484, 1986.

11 DeLeonibus, P.S. and Simpson, L.S., *Dissipation observations of drag coefficients over the open ocean*, IEEE Journal of Oceanic Engineering, OE-12, 1, 296-300, 1987.

12 Dijkhuis, B., *A comparison of finite difference schemes for the advection equation*, 30 p., Department of Oceanography, KNMI, the Netherlands, 1990.

13 Donelan, M.A., *On the fraction of wind momentum retained by waves*, Marine Forecasting, ed. J.C.J. Nihoul, Elsevier, 141-159, 1979.

14 **Donelan, M.**, *The dependence of the aerodynamic drag coefficient on wave parameters*, Proc. of the first intern. conf. on meteorology and the air/sea interaction of the coastal zone, The Hague, The Netherlands, 381-387, American Meteorological Society, Boston, Mass., 1982.

15 **Donelan, M.A., Hamilton, J.A. and Hui, W.H.**, *Directional spectra of wind generated waves*, Phil. Trans. R. Soc. Lond., A.315, 509-562, 1985.

16 **Donelan, M.A. and Pierson, W.J.**, *Radar scattering and equilibrium ranges in wind-generated waves with application to scatterometry*, J. Geophys. Res., 92, C5, 4971-5029, 1987.

17 **Donelan, M.A.**, *The Surface Wave Dynamics Experiment (SWADE) overview and preliminary plans*, National Water Research Institute, Canada Center for Inland Waters, Burlington, Ontario, 1987.

18 **Donelan, M.A. and Hui, W.H.**, *Mechanics of ocean surface waves*, in Surface waves and fluxes, Geernaert, G.L and Plant, W.J. eds., Vol. I, 209-246, Kluwer Academic Publishers, 1990.

19 **Donelan, M.A.**, *Air-Sea Interaction*, from The Sea : Ocean Engineering Science, Volume 9 (two volume set), John Wiley & Sons, 1990.

20 **Garratt, J.R.**, *Review of drag coefficients over oceans and continents*, Monthly Weather Review, 105, American Meteorological Society, 915-929, 1977.

21 **Geernaert, G.L, Larsen, S.E. and Hansen, F.**, *Measurements of the wind stress, heat flux, and turbulent intensity during storm conditions over the North Sea*, J. Geophys. Res., 92, C12, 13127-13139, 1987.

22 **Geernaert, G.L and Plant, W.J.** eds., *Surface waves and fluxes*, Vol. I, 209-246, Kluwer Akademic Publishers, 1990.

23 **Gill, P.E. and Murray, W.**, *Algorithms for the solution of the non-linear least-squares problem*, NPL report NAC 71, National Physical Laboratory, 38 p., 1976.

24 **Gill, P.E., Murray, W. and Wright, M.H.**, *Practical Optimization*, Academic Press, 1981.

25 **Günther, H.**, *A parametric surface wave model and the statistics of the prediction parameters*, Hamburger Geophysikalische Einzelschriften, Heft 55, 90 p., Hamburg, 1981.

26 **Hasse, L.**, *On Charnock's relation for the roughness at sea*, E.C. Monahan and G.Mac Niocaill (eds.), Oceanic Whitecaps, 49-56, 1986.

27   **Hasselmann, D.E., Dunckel, M. and Ewing, J.A.**, *Directional Wave Spectra observed during JONSWAP 1973*, J. Phys. Ocean., 10, 1264-1280, 1980.

28   **Hasselmann, K.**, *On the non-linear energy transfer in a gravity-wave spectrum. Part 1. General Theory*, J. Fluid Mech. 12, 481-500, 1962.

29   **Hasselmann, K.**, *On the non-linear energy transfer in a gravity-wave spectrum. Part 2. Conservation Theorems ; wave-particle analogy ; irreversibility*, J. Fluid Mech., 15, 273-281, 1963.

30   **Hasselmann, K.**, *On the non-linear energy transfer in a gravity-wave spectrum. Part 3. Evaluation of the energy flux and swell-sea interaction for a Neumann spetrum*, J. Fluid Mech., 15, 385-398, 1963.

31   **Hasselmann, K., Barnett, T.P., Bouws, E., Carlson, H., Cartwright, D.E., Ewing, J.A., Gienapp, H., Hasselmann, D.E., Kruseman, P., Meerburg, A., Müller, P., Olbers, D.J., Richter, K. Sell, W. and Walden, H.**, *Measurements of wind-wave growth and swell decay during the Joint North Sea Wave Project (JONSWAP)*, Dtsch. Hydrogr. Z., A8, 12, 95 p., 1973.

32   **Hasselmann, K.**, *On the spectral dissipation of ocean waves due to whitecapping*, Boundary Layer Meteorology, 6, 107-127, 1974.

33   **Hasselmann   S.,   Hasselmann,   K.**,   *Computations   and parametrizations of the nonlinear energy transfer in a gravity-wave spectrum, Part I : A new method for Efficient computations of the exact nonlinear transfer integral*, J. Phys. Ocean., 15, 1369-1377, 1985.

34   **Hasselmann S., Hasselmann, K., Allender, J.H. and Barnett, T.P.**, *Computations and parametrizations of the nonlinear energy transfer in a gravity-wave spectrum, Part II : Parametrizations of the nonlinear energy transfer for the application in wave models*, J. Phys. Ocean., 15, 1378-1391, 1985.

35   **Hasselmann, S.**, *The WAM wave model system*, Max Planck Institut für Meteorologie, Report No. 9, Hamburg, 43 p. + App., 1987.

36   **Hermans, I.**, *Wave Modelling at the Belgian Coast by means of the HYPAS Model*, Progress in Belgian Oceanographic Research, ed. G. Pichot, 75-111, 1989.

37   **Hsiao, S.V. and Shemdin, O.H.**, *Measurements of wind velocity and pressure with a wave follower during MARSEN*, J. Geophys. Res., 88(C14), 9841-9849, 1983.

38 **Hsu, S.A.**, *A dynamical roughness equation and its application to wind stress determination at the air-sea interface*, J. Phys. Ocean., 4, 116-120, 1974.

39 **Janssen, P.A.E.M., Komen, G.J. and de Voogt, W.J.P.**, *An operational coupled hybrid wave prediction model*, J. Geoph. Res., 89, C3, 3635-3654, 1984.

40 **Janssen, P.A.E.M. and Komen, G.J.**, *Effect of atmospheric stability on the growth of surface gravity waves*, Boundary Layer Meteorology, 32, 85-96, 1985.

41 **Janssen, P.A.E.M., Komen, G.J. and De Voogt, W.J.P.**, *Friction velocity scaling in wind wave generation*, Boundary Layer Meteorology, 38, 29-35, 1987.

42 **Janssen, P.A.E.M.**, *Wave induced stress and the drag of air flow over sea waves*, J. Phys. Ocean., 19, 6, 745-754, 1989.

43 **Janssen, P.A.E.M., Lionello, P. and Zambresky L.**, *On the interaction of wind and waves*, Department of Oceanography, KNMI, de Bilt, The Netherlands, 17 p. + Fig., prelimenary report, 1990.

44 **Janssen, P.A.E.M.**, *Quasi-linear theory of wind wave generation applied to wave forecasting*, J. Phys. Ocean., 21, 1631-1642, 1991.

45 **Jeffreys, H.**, *On the formation of waves by wind*, Proc. R. Soc. London, A.107, 189-206, 1924.

46 **Jeffreys, H.**, *On the formation of waves by wind II*, Proc. R. Soc. London, A.110, 341-347, 1925.

47 **Kahma, K.K.**, *A study of the growth of the wave spectrum with fetch*, J. Phys. Ocean., 11, 1503-1515, 1981.

48 **Kahma, K.K. and Calkoen, C.J.**, *Reconciling discrepancies in the observed growth of wind-generated waves*, submitted to the J. Phys. Ocean., The contents are subject to revision, april 1991.

49 **Katsaros, K.B., Smith, S.D. and Oost, W.A.**, *HEXOS-Humidity Exchange Over the Sea. A program for research on water-vapor and droplet fluxes from sea to air at moderate to high wind speeds*, Bull. American Meteorological Society, 68, 5, 466-476, 1987.

50 **Kawai, S. Okada,K. and Toba, Y.**, *Field data support of three-seconds power law and $gu_*\sigma^{-4}$-spectral form for growing wind waves*, J. of the Geographical Society of Japan, 33, 137-150, 1977.

51 **Kitaigorodskii, S.A.,** *Applications of the theory of similarity to the analysis of wind-generated motion as a stochastic process,* Izv. Akad. Nauk SSSR, Geophys. Ser. 1, 105-117, 1962.

52 **Komen, G.J., Hasselmann, S., Hasselmann, K.,** *On the Existence of a Fully Developed Wind-Sea Spectrum,* J. Phys. Oceanogr., 14, 8, 1984.

53 **Komen, G.J.,** *summary of the 9th WAM meeting in Sylt,* Germany, 1991.

54 **Large, W.G. and Pond, S.,** *Open Ocean Momentum Flux Measurements in Moderate to Strong Winds,* J. Phys. Ocean., 11, 324-336, 1981.

55 **Larson, T.R. and Wright, J.W.,** *Wind generated gravity-capillary waves: Laboratory measurements of temporal growth rates using microwave backscatter,* J. Fluid Mech., 70, 417-436, 1975.

56 **Lamb, H.,** *Hydrodynamics,* Dover, New York, 1930.

57 **Luo, W.,** *A third generation wave model: investigation of an implicit scheme to simulate the evolution of fetch limited wind wave,* master thesis, department of civil engineering, K.U.Leuven, Belgium, 1991.

58 **LeBlond, P.H. and Mysak, L.A.,** *Waves in the ocean,* Elsevier, 1978.

59 **Maat, N. , Kraan, C. and Oost, W.A.,** *The roughness of wind waves,* Boundary Layer Meteorology, 54, 89-103, 1991.

60 **Monbaliu, J.,** *Wind driven seas: Optimal parameter choice for the wind input term,* 8th International Conference on Wind Engineering, London, Ontario, Canada, Proc. to be Publ. in J. Wind Engin. Industr. Aerodyn., 1991.

61 **Monbaliu, J.,** *The use of nonlinear least squares to estimate parameters in the source terms of the wind wave energy transport equation,* K.U.Leuven, Laboratory for Hydraulics, Internal Report, 1992 (in preparation).

62 **MUMM,** *Activity Report No. 5,* Project Deiningsprediktiemodel, Ministry of Public Health and Environment, 1990.

63 **NAG** (Numerical Algorithm Group), *Introductory guide to NAG Fortran Library Mark 14,* Oxford, United Kingdom, 1990.

64 **Oost, W.A.,** *The wind profile in a wave flume,* J. of Wind Engineering and Industrial Aerodynamics 37, 113-121, 1991.

65 **Oost, W.A.,** *Flow Distortion by an Ellipsoid and Its Application to the Analysis of Atmospheric Measurements,* J. Atmos. Oceanic Tech. 8, 331-340, 1991.

66 **Panofsky, H.A. and Dutton, J.A.**, *Atmospheric turbulence. Models and methods for engineering applications*, John Wiley & Sons, 1984.

67 **Phillips, O.M.**, *On the generation of waves by turbulent wind*, J. Fluid Mech., 2, 417-448, 1957.

68 **Phillips, O.M.**, *The equilibrium range in the spectrum of wind-generated waves*, J. Fluid Mech., 4, 426-434, 1958.

69 **Phillips, O.M.**, *The dynamics of the upper ocean*, second edition, 1977.

70 **Phillips, O.M.**, *Spectral and statistical properties of the equilibrium range in wind-generated gravity waves*, J. Fluid Mech., 156, 505-531, 1985.

71 **Plant,W.J.**, *A relation between wind stress and wave slope*, J. Geoph. Res., 87, C3, 1961-1967, 1982.

72 **Pierson, W.J. and Moskowitz, L.**, *A Proposed Spectral Form for Fully Developed Wind Seas Based on the Similarity Theory of S.A. Kitaigorodskii*, J. Geoph. Res., 69, 24, 5181-5190, 1964.

73 **Riley, D.S., Donelan M.A. and Hui, W.H.**, *An extended Miles' theory for wave generation by wind*, Boundary Layer Meteorology, 22, 209-225, 1982.

74 **Rosenthal, W.**, *Derivation of Phillips α-parameter from turbulent diffusion as a damping mechanism*, GKSS-report 89/E/33, GKSS Hamburg, 1989.

75 **Scales, L.E.**, *Introduction to non-linear optimization*, Springer Verlag, New York, 1985.

76 **Smith, S.D. and Banke, E.G.**, *Variation of the sea surface drag coefficient with wind speed*, Quart. J. R. Met. Soc., 101, 665-673, 1975.

77 **Smith, S.D., Katsaros, K.B., Oost, W.A. and Mestayer, P.G.**, *Two major experiments in the Humidity Exchange Over the Sea (HEXOS) program*, Bull. American Meteorological Society, 71, 2, 161-172, 1990.

78 **Snyder, R.L., Dobson F.W., Elliot J.A. and Long R.B.**, *Array measurements of atmospheric pressure fluctuations above surface gravity waves*, J. Fluid Mech., 102, 1-59, 1981.

79 **Snyder, R.L., Neu W.L., Long R.B. and de Voogt W.J.P.**, *A long range program to parametrize the two-dimensional evolution of the surface-gravity-wave field*, Nova University Technical Report, 37 pp., 1990.

80 **Sobey, R.J.**, *Wind-wave prediction*, Annual Review of Fluid Mechanics, 18, 149-172, 1986.

81 **Stewart, R.W.**, *The air-sea momentum exchange*, Boundary Layer Meteorology, 6, 151-167, 1974.

82 **Toba, Y.**, *Local balance in the air-sea boundary process, Part I, On the growth process of wind waves*, J. of the Oceanographical Society of Japan, 28, 109-121, 1972.

83 **Toba, Y.**, *Local balance in the air-sea boundary process, Part II, Partition of wind strss to waves and currents*, J. of the Oceanographical Society of Japan, 29, 70-75, 1973.

84 **Toba, Y.**, *Local balance in the air-sea boundary process, Part III, On the spectrum of wind waves*, J. of the Oceanographical Society of Japan, v. 29, 209-220, 1973.

85 **Tolman, H.L.**, *The numerical model WAVEWATCH : a third generation model for hindcasting wind waves on tides in shelf seas*, Communications on hydraulic and geotechnical engineering, TU Delft, Faculty of Civil Engineering, April 1989.

86 **Tolman, H.L.**, *Wind wave propagation in tidal seas*, Delft University of Technology, Faculty of Civil Engineering, Fluid Mechanics Group, Report 90-1, 1990.

87 **Van den Eynde, D. and Monbaliu, J.**, *On the introduction of refraction effects in a wave prediction model*, Progress in Belgian Oceanographic Research, ed. G. Pichot, 111-128, 1989.

88 **Van den Eynde, D. and De Wolf, P.**, *Deiningsprediktie aan de Belgische kust*, Water 52, 163-167, 1990 a. (in Dutch)

89 **Van den Eynde, D., Berlamont, J. and Monbaliu, J.**, *Refraktie van deiningsspectra*, Water 52, 168-172, 1990 b (in Dutch).

90 **Van Vledder, G. Ph. and Weber, S.L.**, *Guide for the program EXACT-NL*, Report No. 20, 27 p., Max-Planck-Institut für Meteorologie, Hamburg, 1988.

91 **Van Vledder, G. Ph.**, *CERES Interactive Graphics Program*, Version 1.0, September, 1991.

92 **WAMDI** (the WAMDI group), *The WAM model - A third generation ocean wave prediction model*, J. Phys. Ocean., Vol. 18, 1775-1810, dec. 1988.

93 **Wu, J.**, *Wind stress and surface roughness at air-sea interface*, J. Geoph. Res., 74, 2, 444-455, 1969 + correction in 74, 13, 3450, 1969.

94 **Wu, J.**, *Anemometer height in Froude scaling of wind stress*, ASCE J. of the waterways, harbors and coastal engineering division waves, 131-137, 1971.

95 **Wu, J.**, *Physical and dynamical scales for generation of wind*, ASCE J. of the waterways, harbors and coastal engineering division, 163-175, 1972.

96 **Wu, J.**, *Wind-stress coefficients over sea surface near neutral conditions - A revisit -*, J. Phys. Ocean., 10, 727-740, 1980.

97 **Wu, J.**, *'Wind-Stress Coefficients Over Sea Surface From Breeze to Hurricane'*, J. Geoph. Res., 87, C12, 9704-9706, 1982.

98 **Wu, J.**, *Parameterization of wind-stress coefficients over water surfaces*, J. Geoph. Res., 90, C5, 9069-9072, 1985.

99 **Wu, J.**, *Roughness elements of the sea surface - their spectral composition*, Tellus 38 A, 2, 178-188, 1986.

100 **Young, I.R.**, *A shallow water spectral wave model*, J. Geoph. Res., 93, C5, 5113-5129, 1988.

APPENDIX A Note on Newton's method for finding a zero of a function
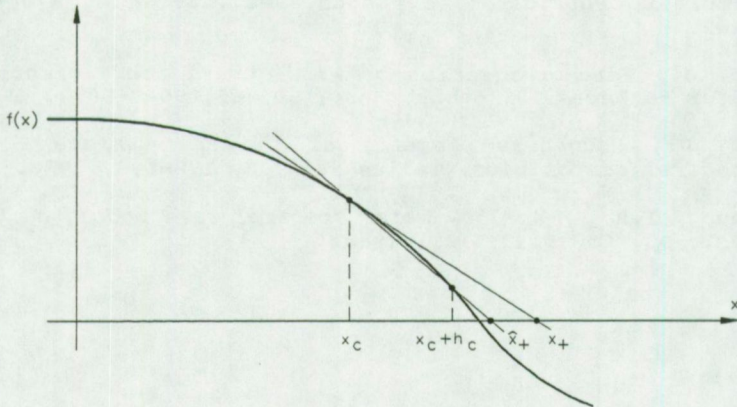
Figure A.1

When the derivative in a particular point x_c is known analytically, one can write (see Figure A.1)

$$x_+ = x_c - \frac{f(x_c)}{f'(x_c)} \tag{A.1}$$

When the derivative is not available, one can approximate the derivative by

$$\hat{x}_+ = x_c - \frac{f(x_c)}{a_c} \tag{A.2}$$

where $a_c = \dfrac{f(x_c + h_c) - f(x_c)}{h_c}$.

Several problems can be encountered in evaluating a_c:

- $|h_c|$ has to be large enough so that there is a difference between $f(x_c + h_c)$ and $f(x_c)$, i.e. the computer has to be able to see the difference or has to be able to compute the difference

- the accuracy in evaluating $f(x_c)$ has to be such that round-off errors have to be small

- the function should not contain discontinuities

The step from finding the zero of a function to finding the minimum of a function is straightforward. A function that reaches a minimum has a derivative which is zero :

$$f'(x) = 0$$

so that in analogy with equation (A.1), one can write

$$x_+ = x_c - \frac{f'(x)}{f''(x)} \tag{A.3}$$

One has to make sure however that a minimum but not a maximum is obtained. This is checked by the condition :

$$f''(x) > 0$$

The method can be generalized if the variable x is not a scalar but a vector $\overline{x}$.

$$\overline{x_{k+1}} = \begin{bmatrix} x_1 \\ \vdots \\ x_n \end{bmatrix}_{k+1} = \overline{x}_k + \overline{s}_k \tag{A.4}$$

where $\overline{s}_k$ is the solution of

$$\nabla^2 f(\overline{x}_k) \cdot \overline{s}_k = - \nabla f(\overline{x}_k)$$

193

$\nabla f\ (\overline{x})$ is the gradient of $f(\ \overline{x}\ ) \equiv \begin{bmatrix} \dfrac{\partial\ f(\overline{x})}{\partial x_1} \\ \cdot \\ \cdot \\ \cdot \\ \dfrac{\partial\ f(\overline{x})}{\partial x_n} \end{bmatrix}$

$\nabla^2 f(\overline{x})$ is the Hessian matrix and is given by

$$\begin{bmatrix} \dfrac{\partial^2 f(\overline{x})}{\partial^2 x_1} & \dfrac{\partial^2 f(\overline{x})}{\partial x_1 \partial x_2} & \cdots & \dfrac{\partial^2 f(\overline{x})}{\partial x_1 \partial x_n} \\ \dfrac{\partial^2 f(\overline{x})}{\partial x_2 \partial x_1} & \cdot\cdot & \cdot\cdot & \cdot\cdot \\ \cdot\cdot & \cdot\cdot & \cdot\cdot & \cdot\cdot \\ \dfrac{\partial^2 f(\overline{x})}{\partial x_n \partial x_1} & \cdot\cdot & \cdot\cdot & \dfrac{\partial^2 f(\overline{x})}{\partial^2 x_n} \end{bmatrix}$$

Note that the Hessian matrix is a symmetric matrix.

APPENDIX B   The special case of the sum of squares of functions

Given : $F(A) = \sum_{i=1}^{m} f_i^2(A)$ where $A = \begin{bmatrix} a_1 \\ \cdot \\ \cdot \\ a_n \end{bmatrix}$

Define the Jacobian matrix as :

$$J(A) = \begin{bmatrix} \dfrac{\partial f_1(A)}{\partial a_1} & \dfrac{\partial f_1(A)}{\partial a_2} & \cdots & \dfrac{\partial f_1(A)}{\partial a_n} \\ \dfrac{\partial f_2(A)}{\partial a_1} & \cdot\cdot & \cdot\cdot & \cdot\cdot \\ \cdot\cdot & \cdot\cdot & \cdot\cdot & \cdot\cdot \\ \dfrac{\partial f_m(A)}{\partial a_1} & \cdot\cdot & \cdot\cdot & \dfrac{\partial f_m(A)}{\partial a_n} \end{bmatrix}_{m \times n}$$

The gradient of F(A) becomes :

$$g(A) = \begin{bmatrix} \dfrac{\partial F(A)}{\partial a_1} \\ \cdot \\ \cdot \\ \dfrac{\partial F(A)}{\partial a_n} \end{bmatrix}_{n \times 1} = 2\ J(A)_{n \times m}^{T} \begin{bmatrix} f_1(A) \\ \cdot \\ \cdot \\ f_m(A) \end{bmatrix}_{m \times 1} = 2\ J(A)^{T}\ f(A)$$

(the superscript T denotes the transpose of a matrix)

The above indicates that the gradient is defined through the Jacobian matrix which contains the first derivatives of the individual functions in the sum of squares of functions.

Define $G_i(A)$ as the Hessian matrix of $f_i(A)$:

$$G_i(A) = \begin{bmatrix} \dfrac{\partial^2 f_i(A)}{\partial^2 a_1} & \dfrac{\partial^2 f_i(A)}{\partial a_1 \partial a_2} & \cdots & \dfrac{\partial^2 f_i(A)}{\partial a_1 \partial a_n} \\[2ex] \dfrac{\partial^2 f_i(A)}{\partial a_2 \partial a_1} & \cdot\cdot & \cdot\cdot & \cdot\cdot \\[2ex] \cdot\cdot & \cdot\cdot & \cdot\cdot & \cdot\cdot \\[1ex] \dfrac{\partial^2 f_i(A)}{\partial a_n \partial a_1} & \cdot\cdot & \cdot\cdot & \dfrac{\partial^2 f_i(A)}{\partial^2 a_n} \end{bmatrix}_{n \times n}$$

$G(A)$ is the Hessian matrix of the function $F(A)$ or :

$$G(A) = \begin{bmatrix} \dfrac{\partial^2 F(A)}{\partial^2 a_1} & \dfrac{\partial^2 F(A)}{\partial a_1 \partial a_2} & \cdots & \dfrac{\partial^2 F(A)}{\partial a_1 \partial a_n} \\[2ex] \dfrac{\partial^2 F(A)}{\partial a_2 \partial a_1} & \cdot\cdot & \cdot\cdot & \cdot\cdot \\[2ex] \cdot\cdot & \cdot\cdot & \cdot\cdot & \cdot\cdot \\[1ex] \dfrac{\partial^2 F(A)}{\partial a_n \partial a_1} & \cdot\cdot & \cdot\cdot & \dfrac{\partial^2 F(A)}{\partial^2 a_n} \end{bmatrix}_{n \times n}$$
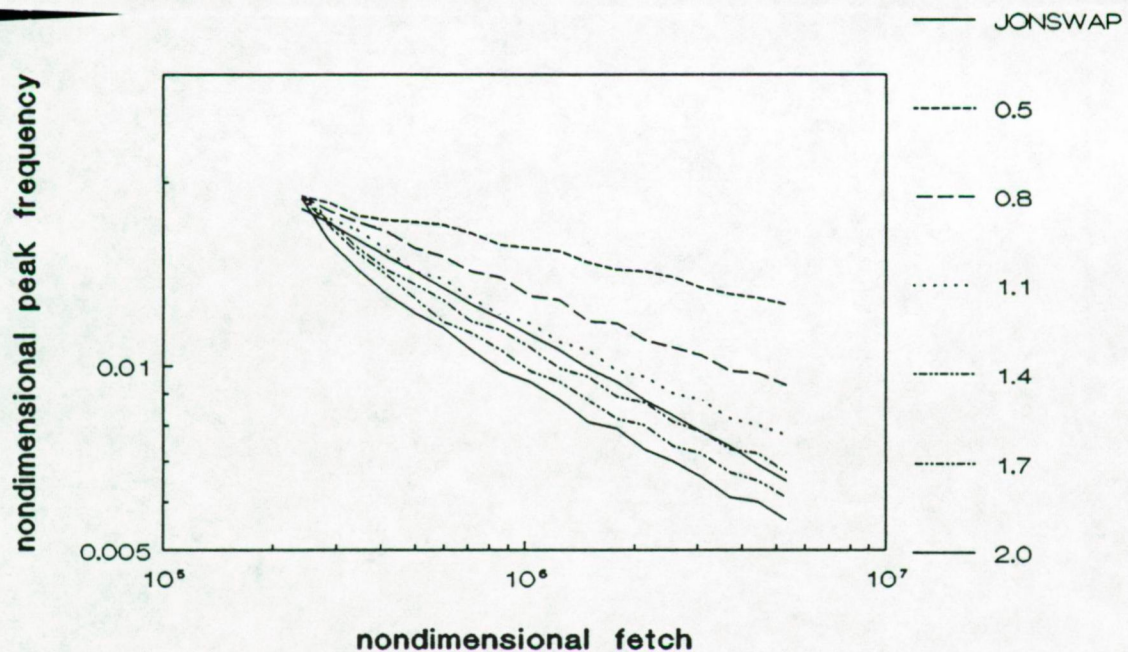
This can also be written as :

$$G(A)_{n \times n} = 2\, J(A)^T_{n \times m}\, J(A)_{m \times n} + 2 \sum_{i=1}^{m} f_i(A)\, G_i(A)$$

Close to a minimum the second term on the right hand side can be neglected, so that the Hessian marix can be approximated by an expression in the Jacobian matrix (containing only first derivatives).

196

ERRATA

page	at present	must be
XIII	verhoogde druk (stroomlijnen dichter bij elkaar)	verhoogde druk (stroomlijnen verder uit elkaar)
XIII	verminderde druk (stroomlijnen verder uit elkaar)	verhoogde druk (stroomlijnen dichter bij elkaar)
41 (Figure 2.7) 42 (Figure 2.8) 43 (Figure 2.9)	$x_* = \dfrac{x_g}{u_*^2}$	$x_* = \dfrac{xg}{u_*^2}$
77	$\dfrac{\partial E}{\partial x} = 0$: fetch limited	$\dfrac{\partial E}{\partial t} = 0$: fetch limited
152 (Figure 6.4)	parameter c_1 (=3.81 10^{-5})	parameter c_1 (=3.18 10^{-5})

Figure 5.12 : Variation of the peak frequency growth curve with wind input parameter a_2